Analysis of Doppler Experiments (II)

(SEFOR)

February 15, 1972

TOKYO SHIBAURA ELECTRIC CO. LTD.

〒319-1184　茨城県那珂郡東海村村松4番地49
核燃料サイクル開発機構
技術展開部 技術協力課

電話:029-282-1122(代表)
ファックス　:029-282-7980
電子メール:jserv@jnc.go.jp

Analysis of Doppler Experiments (II)

—— SEFOR ——

Abstract

Many fast critical assemblies have been built in many countries in the world in order to accumulate valuable data about the nuclear characteristics and safety of the fast breeder reactor. The experiments on the Doppler reactivity effect are also not the exceptional case and hence are performed energetically at every research laboratory. However, almost all the measuring method so far employed have been the sample Doppler reactivity methods, namely, those to determine the reactivity worth difference of a hot sample located at the center of a core from the same sample at the same location but in cold situation.

SEFOR (Southwest Experimental Fast Oxide Reactor) is an experimental fast reactor, one of the main purposes of which is the study of the whole core Doppler reactivity effect which has not been enough studied up to now on the fast critical assemblies, and a lot of data obtained from the experiments performed on SEFOR have been published.

The main purpose of the present work is to establish the method of analysis for Doppler experiments by comparing the calculated results with the measured values. The objects of the present analysis are criticality, various reaction rate traverse, sample reactivity worth traverse, temperature coefficient and Doppler reactivity effect

which were obtained in the static experiments on the first core of the SEFOR (SEFOR-I) and were compiled in "Analysis of Doppler Experiments (1)" (J201 72-15).

In addition, analysis of ZPR -3-47, the SEFOR mockup assembly, was also carried out to investigate the parallelism of the C/E's of mockup assembly and the SEFOR itself. Further, the relations between C/E's of the FCA (JOYO mockup assembly) and JOYO itself will be discussed and predicted based on knowledges obtained from the present analysis.

To Mr. Higashihara and Mr. Kinjo of PNC we owe valuable discussions about the method of analysis.

February 15, 1973

Y. Matsuno
T. Yoshida
S. Iijima
T. Kamei

NAIG Nuclear Research Laboratory,
Nippon Atomic Industry Group Co., Ltd.

Analysis of Doppler Experiments (II)

Contents

I. Preface

As is well known, intensive research efforts have been devoted to the fast breeder reactor physics in many countries in recent years. One of the most important of such studies is that of the safety of the fast reactor. As a result, efforts have begun to be made to establish the method for calculations by analyzing the extensive measurements of the Doppler reactivity effect which is closely related to the safety and performing characteristics of the fast reactor and it was for this purpose that SEFOR (Southwest Experimental Fast Oxide Reactor) was designed and built.

The measurements of the Doppler reactivity effect itself have been carried out also before the measurements on SEFOR by the research institutes of various countries, using their fast critical equipment. However, most of such experiments employed a method in which a sample is placed in the center of the fuel assembly and heated and the reactivity change due to temperature rise is measured.[1], [2] This method, needless to say, has its own significance but it does not make direct measurements of the changes taking place in the Doppler reactivity with the rise of the temperature of the whole reactor core.

SEFOR is a fast experimental reactor which has been built mainly for the purpose of making investigations of the Doppler reactivity effect of the whole system, which had not sufficiently been studied by the

previously used method on critical assemblies. There have been published a great deal of data obtained from the experiments which have been carried out up to this time on the SEFOR since it reached criticality in April 1969.

The experiments carried out at SEFOR can be broadly divided into two types, i.e. static measurements and dynamic measurements. The former are the measurements of the material reactivity worth, fission rate traverses, temperature coefficients, etc. and the latter are aim at obtaining information on the nuclear characteristics including the Doppler reactivity effect from the responses of the system when its power is caused to fluctuate by the sudden reactivity insertion into the system. The methods for analyzing the results of the above two different types of experiments are considerably different in nature from one another. The present analysis will deal with only the static measurements.

There are 8 versions of the SEFOR cores, i.e. I-A, I-B, I-C, I-D, I-E, I-F, I-I and I-J for the necessity of making measurements.[3] I-A is the initial critical core in which measurements are made not only of the criticality but also of the effect of the spontaneous fission neutrons, which are emitted from P_u240, on the reactivity. I-B consists of I-A with some added fuel rods around it to have some excess reactivity so that the reflector can be calibrated (this reactor is controlled by moving the nickel reflector up and down) and the reactivity worth of other substances can be measured.

During the measurements of the fuel rod reactivity worth on the I-B, several of the fuel rods loaded in the core showed a reactivity worth about 40% lower than the standard one. The defective fuel rods were replaced by normal ones and the clean minimum critical mass was determined thus obtaining I-C core.

In I-D and other cores, some B_4C rods are inserted at various locations of core to reduce the reactivity so that the fuel rods are fully loaded throughout the entire range of the fuel channels.

In the analytical study on the cores containing B_4C rods, we used the model in which B_4C is dispersed homogeneously throughout the core.

The analytical calculations were made using mainly the two-dimensional diffusion approximation. As for the nuclear constants set, we used the set of 13 groups reduced from 25-group NNS-5 and JAERI-FAST (version II).

In group reduction the energy division was made relatively finely on the low energy side in order to prevent the inclusion of the effects of group reduction.

The calculations are made on a homogeneous model. However, since the actual core is heterogeneous, it is necessary to make proper correction. This correction calculation was made only for I-C, assuming that thus obtained amount of correction was also applicable to

other cores. As for the correction for the transport theory, the calculation was also made only for I-C and thus obtained result was applied to other cores.

II. An Outline of SEFOR Calculation Model

2.1 Core

SEFOR is a sodium-cooled fast experimental reactor with a thermal power of 20MW and uses PuO_2-UO_2 (Pu enrichment: 18.7%) for fuel. A hexagonal fuel element consists of 6 fuel rods (2.22cmØ) arranged around a BeO rod (1.97cmØ) in the center. The BeO rod is used to soften the neutron spectrum, thereby the SEFOR spectrum simulates a large reactor spectrum so well that the physical and engineering characteristics of the reactor can be better understood.

The fully loaded core consists of 108 hexagonal fuel elements (core volume: approx. 560 ℓ), which are surrounded by 10 control nickel reflectors. In the static experiments, no fuel is put in the channel in the center of the core but only liquid sodium is flown through it.

The sectional views of the fuel element are shown in Fig. 2.1.1 and Fig. 2.1.2. The core loaded with the fuel elements is shown in Fig. 2.1.3. The main specifications are given in Table 2.1.1.

2.2 Calculation Model

2.2.1 Homogeneous model

The calculations are based on the two-dimensional calculations. As for the calculation model for the fully loaded core, we used the one described in GEAP-13588, p. 169.[4] As for the

calculation model for the not fully loaded core (I-C), we provided a region corresponding to the not fully loaded region (peripheral region of the core). The latter is shown in Fig. 2.2.1 and the former in Fig. 2.2.2.

Tab. 2.1.1 SEFOR Elemental Dimensions

Items	Dimensions	
Core dimensions	Equivalent diameter	88,135 cm
	Cumulative fuel Length	85,879 cm
	Core height (incl. axial gap and UO_2)	92,865 cm
Core element	Maximum number in core	109
	Fuel rods in core element	6
	Tightener rod per core element	1
	Rod pitch	2,781 cm
Fuel channel	Material	Type 304 SS
	Shape	Hexagonal
	Outside dimension across flats	8.0007 cm
	Wall thickness	0.1524 cm
	Side rod diameter	0.6350 cm
Fuel rod	Overall length	126,0425 cm
	Diameter	2.4688 cm
	Fuel Length	85.8791 cm
	Cladding material	Type 316 SS
	Cladding inner diameter	2.2605 cm
	Cladding wall thickness	0.1041 cm

Tab. 2.1.1 SEFOR Elemental Dimensions (cont'd)

Items	Dimensions	
Fuel pellet	Material	PuO_2-UO_2
	Diameter	2.2224 cm
	Length	1.5874 cm
Fuel pellet (cont'd)	Density	10.2 g/cc
	Composition: Pu(239+241)/(Pu+U)	18.7% (standard)
		25.0% (special)
Tightening rod	Diameter (outer)	2.2224 cm
	Cladding material	Type 316 SS
	Cladding wall thickness	0.1016 cm
	BeO rod	Sintered BeO
	BeO diameter	1.9735 cm
	Density	2.9 g/cc
Tightener Sleeve	Material	Type 304 SS

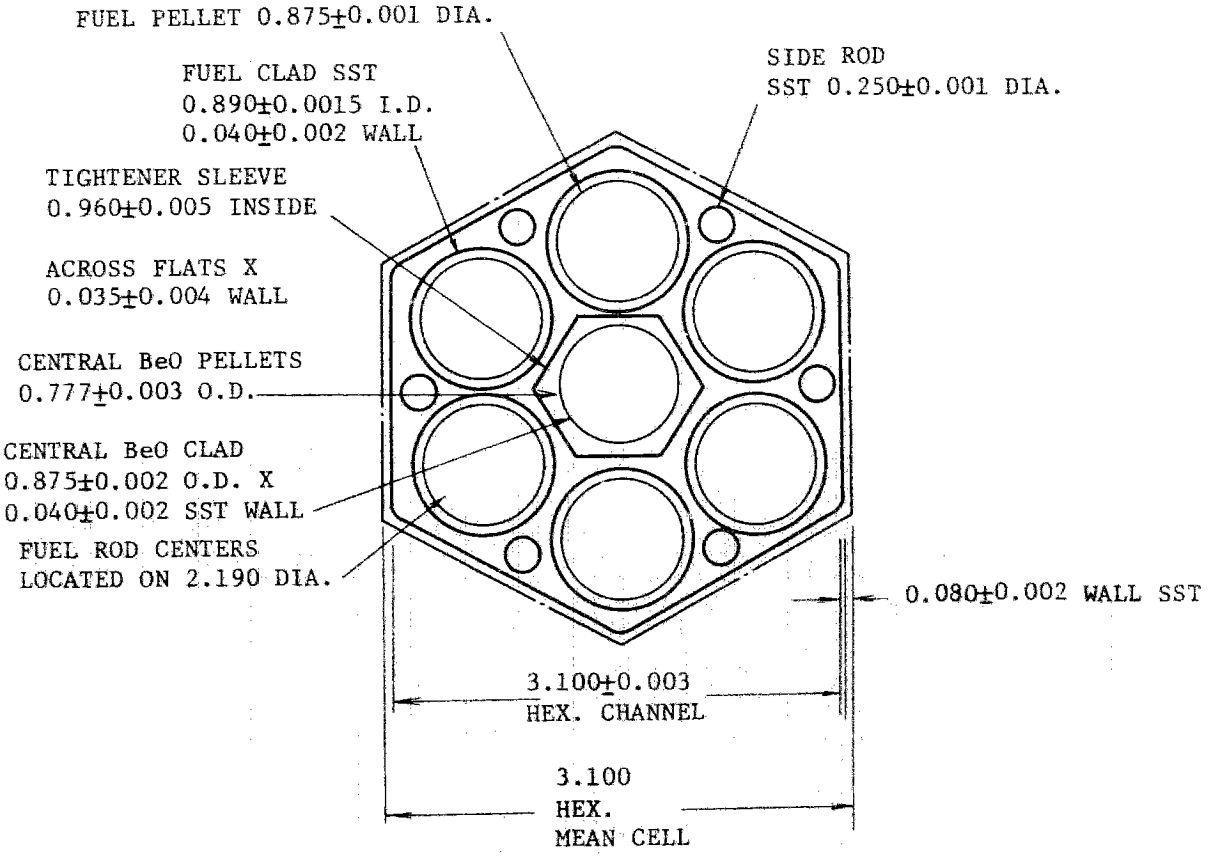

(unit: inch)

Fig. 2.1.1 SEFOR Fuel Channel

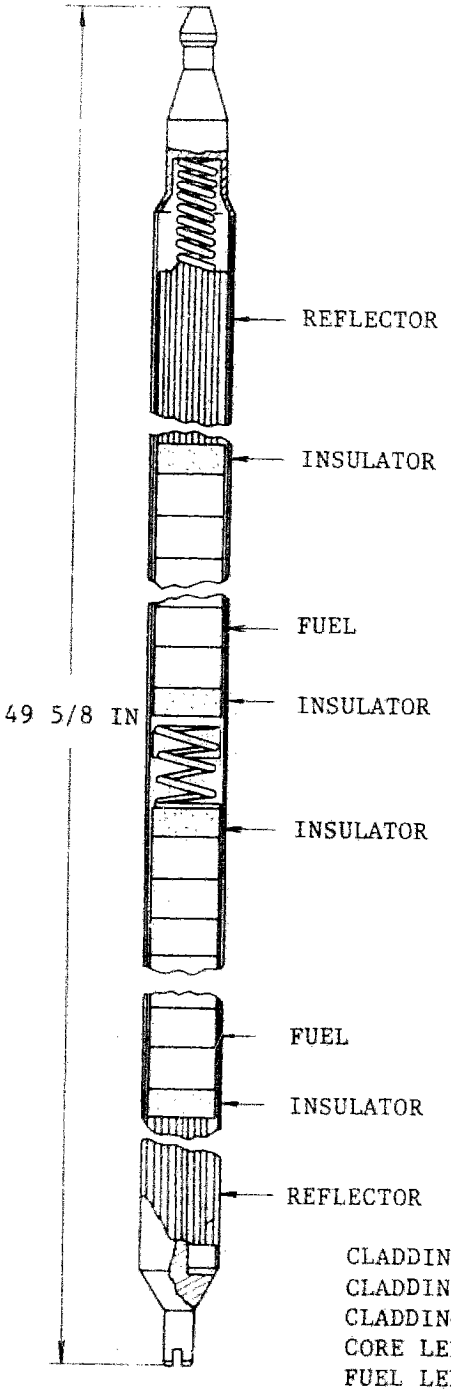

CLADDING O.D.	0.970
CLADDING MATL	STN.STL
CLADDING THICKNESS	0.040
CORE LENGTH	36.56
FUEL LENGTH	33.81

Fig. 2.1.2 SEFOR Fuel Rod

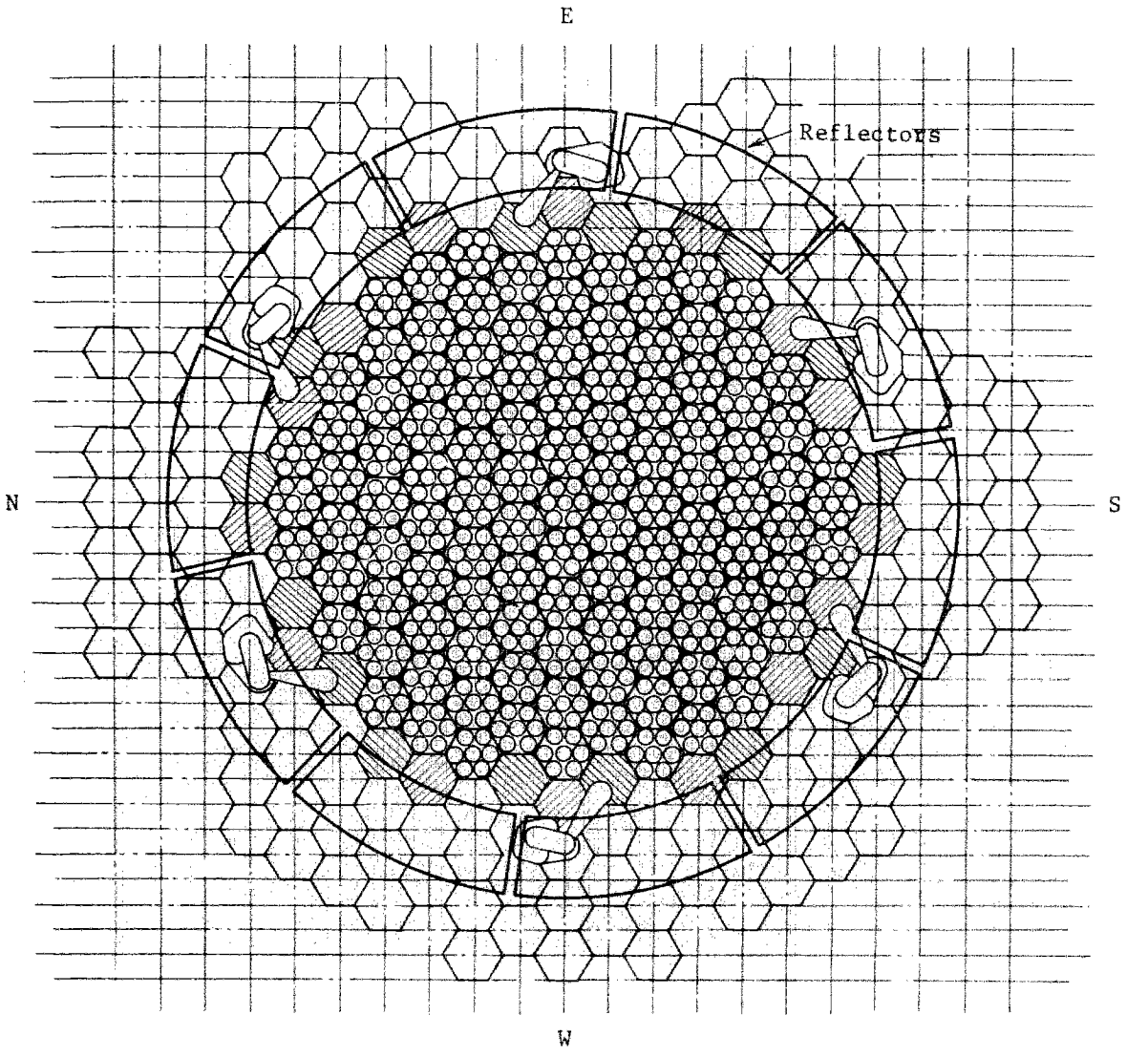

Fig. 2.1.3 Core Loading Location

2.2.2 Heterogeneous model

The heterogeneous calculations were made by use of the collision probability method. The calculation model was constructed as follows due to the restrictions of the calculation code (HETRO-CR[5]).

i) The hexagonal fuel channel was transformed into a ring with its area being preserved and the sodium layer outside the channel wall was homogeneously mixed into the ring.

ii) The outside diameter of the BeO rod in the center of the cluster was equalized to that of other fuel rods and the density of BeO was reduced accordingly.

iii) The gap between the fuel pellet and the inner surface of the cladding was homogeneously mixed into the inside of the cladding and the density of the cladding was adjusted accordingly.

iv) The tightener sleeve outside the BeO rod and the side rod inside the channel wall were homogeneously mixed into the sodium.

This model is shown in Fig. 2.2.3.

2.3 Atomic Number Densities

2.3.1 Atomic number densities for homogeneous calculations

The atomic number densities were calculated from the list of the volume ratios of core components given in GEAP-13588 pp. 173 - 174 and the list of densities of material on p. 175. As for the not fully loaded section, the atomic number densities were calculated so that the substances may be homogeneously distributed in the ring equal in area to the said section. The atomic number densities of the not fully loaded system and the fully loaded system are shown in Table 2.3.1 and Table 2.3.2, respectively. The region numbers correspond to those which are given in Fig. 2.2.1 and Fig. 2.2.2, respectively. I-D core contains the poison rod of B_4C but the composition of the poison rod is not precisely described. So, we considered three different models, i.e. a model in which the presence of the poison rod was utterly ignored, a model in which the B_4C was exactly of the same size with the fuel rod, and a model in which about 50% of the fuel rod volume was assumed to be that of B_4C on the basis of the insufficient description of the poison rod in GEAP-13588. The atomic number densities corresponding to the above-mentioned three models are marked with *, **, and *** in Table 2.3.2.

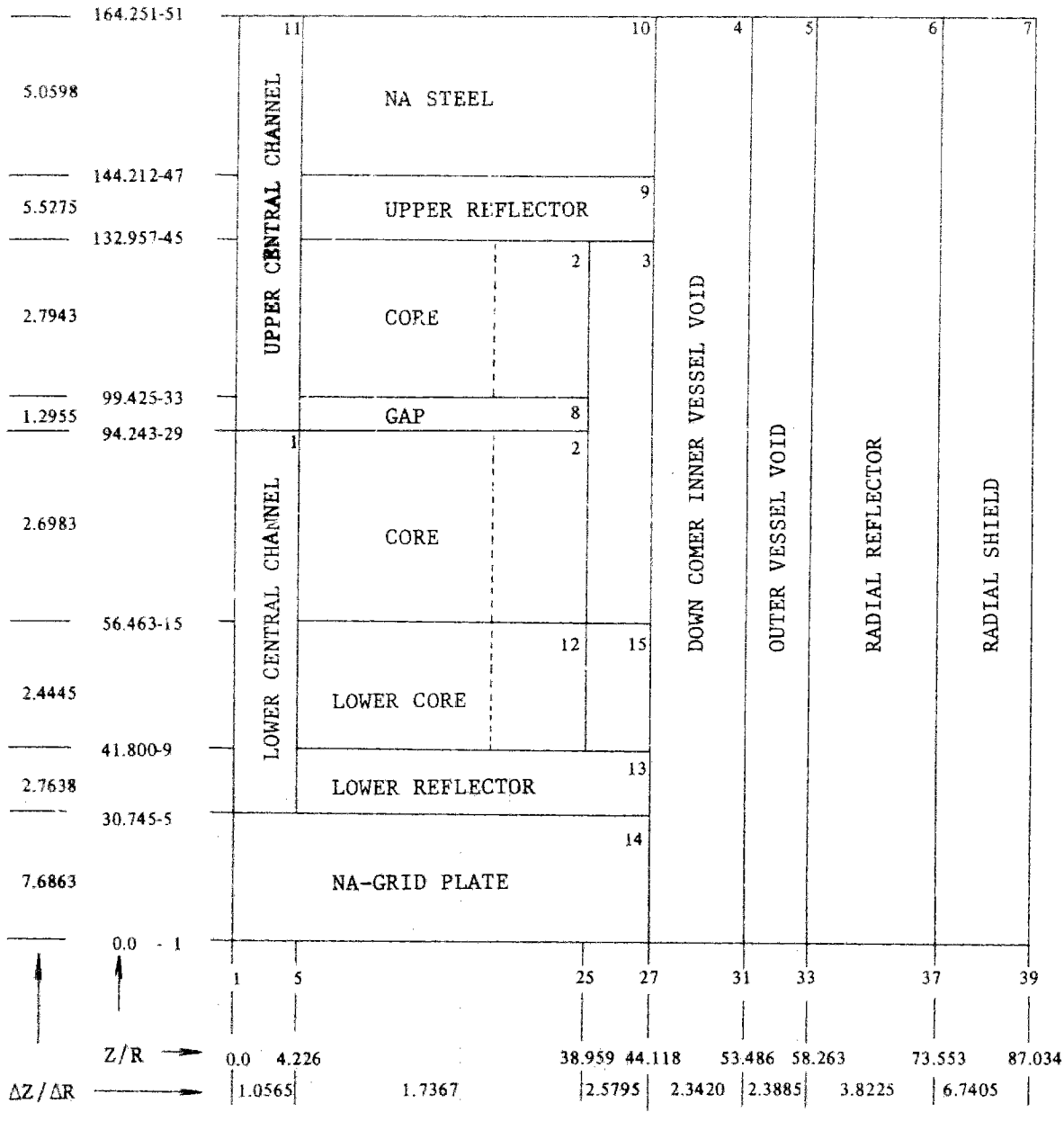

Fig. 2.2.1 SEFOR I-C Core Geometry for Homogeneous Calculation (350°F)

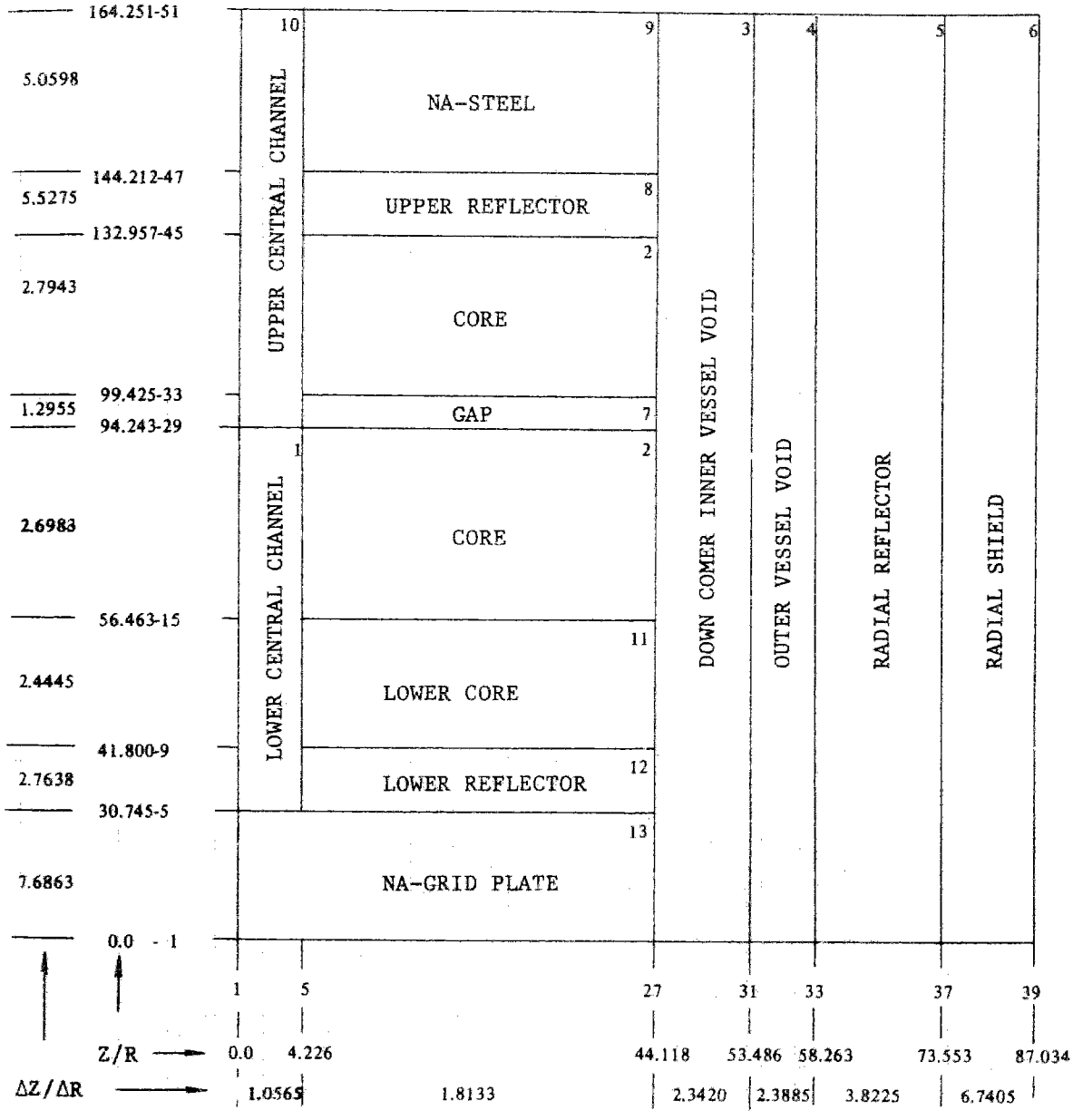

Fig. 2.2.2 SEFOR Full Loaded Core Geometry

for Homogeneous Calculation (350°F)

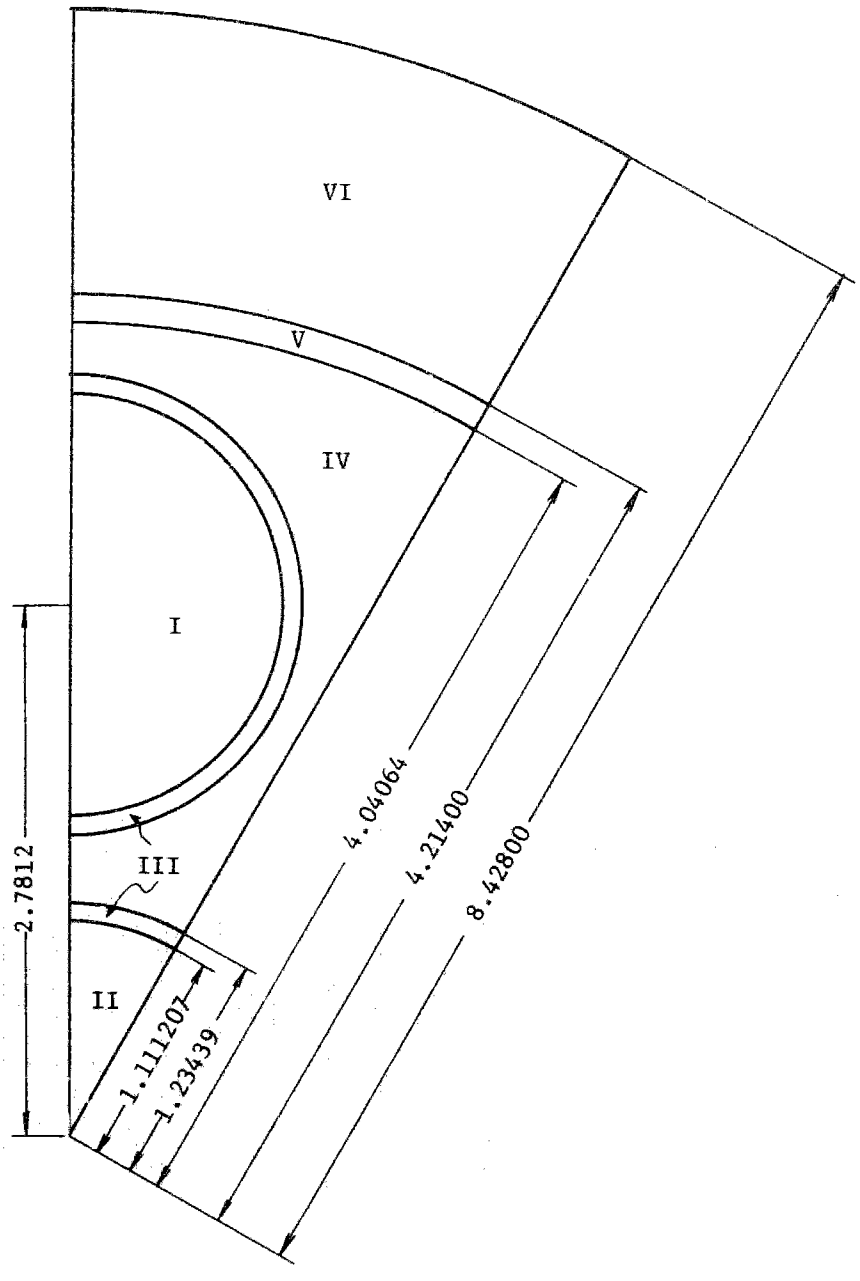

Unit of Length: cm

Fig. 2.2.3 Unit Cell Geometry for Heterogeneous Calculation

2.3.2 Atomic number densities for heterogeneous calculations

The atomic number densities of the respective regions were calculated in the same manner as descrived in Section 2.2.2. Thus calculated values are given in Table 2.3.3.

Tab. 2.3.1 Atomic Number Densities for I-C Core (1)

(10^{22} atoms/cc)

Region / Element	1	2	3	4	5	6
Pu-239		0.17110	0.02139			
Pu-240		0.01549	0.00194			
Pu-241		0.00144	0.00018			
U -235		0.00162	0.00020			
U -238		0.73296	0.09162			
Be		0.37753	0.25168			
B -10						
B -11						
C						
O		2.21360	0.48119			
Na	1.66100	0.68076	1.81362	1.48375		
Mg					0.05286	0.00955
Aℓ					1.14279	0.20646
Cr	0.53540	0.37907	0.25863	0.50019	0.27383	0.05922
Mn				0.00046		
Fe	1.86276	1.34319	0.90454	1.74051	0.95271	0.20602
Ni	0.24957	0.21602	0.12817	0.40386	0.12764	7.34702
Mo		0.01190	0.00231			

Tab. 2.3.1 Atomic Number Densities for I-C Core (2)

(10^{22} atoms/cc)

Region / Element	7	8	9	10	11	12
Pu-239						0.17110
Pu-240						0.01549
Pu-241						0.00144
U -235		0.00078	0.00018			0.00162
U -238		0.35237	0.08118			0.73296
Be		0.37753	0.03223			0.26835
B -10	0.54137					
B -11	2.17912					
C	0.68010					
O		1.08737	0.19577			2.10441
Na		0.68076	0.68674	1.35147	1.66100	0.68076
Mg	0.03478					
Aℓ	0.75183					
Cr	0.21024	0.49313	0.39027	0.56939	0.20621	0.39522
Mn		0.00030				
Fe	0.73145	1.74017	1.38193	1.98101	0.71743	1.40199
Ni	0.09800	0.38158	3.80150	0.26541	0.09612	0.22779
Mo		0.01191	0.01179			0.01319

Tab. 2.3.1 Atomic Number Densities for I-C Core (3)

(10^{22} atoms/cc)

Region / Element	13	14	15
Pu-239			0.02139
Pu-240			0.00194
Pu-241			0.00018
U -235	0.00018		0.00020
U -238	0.08118		0.09162
Be	0.02302		0.17890
B -10		0.06941	
B -11		0.27937	
C		0.08719	
O	0.18656		0.40841
Na	0.69559	1.68874	1.81362
Mg			
Aℓ			
Cr	0.36366	0.42748	0.26939
Mn			
Fe	1.28981	1.48728	0.94374
Ni	3.90561	0.19926	0.13602
Mo	0.01202		0.00317

Tab. 2.3.2 Atomic Number Densities for I-D Core (1)

(10^{22} atoms/cc)

Region / Element	1	2*	2**	2***	3	4
Pu-239		0.17112	0.16739	0.16739		
Pu-240		0.01549	0.01516	0.01516		
Pu-241		0.00144	0.00142	0.00142		
U -235		0.00162	0.00158	0.00158		
U -238		0.73296	0.71717	0.71717		
Be		0.37753	0.37753	0.37753		
B -10			0.01142	0.00570		
B -11			0.04596	0.02295		
C			0.01434	0.00716		
O		2.21360	2.17371	2.17371		
Na	1.66100	0.68076	0.68076	0.68076	1.48375	
Mg						0.05286
Al						1.14279
Cr	0.53540	0.37907	0.37907	0.38730	0.50019	0.27383
Mn					0.00046	
Fe	1.86276	1.34319	1.34319	1.37183	1.74051	0.95271
Ni	0.24957	0.21602	0.21602	0.21986	0.40386	0.12764
Mo		0.01191	0.01191	0.01191		

* Number densities for the model without B_4C rod

** Number densities for the model with B_4C rod having the same volume as that of fuel rod and the given density for B_4C rod.

*** Number densities for the model with B_4C rod having the volume of 49.82% of a rod (cf GEAP-13588 p.171)

Tab. 2.3.2 Atomic Number Densities for I-D Core (2)

(10^{22} atoms/cc)

Region / Element	5	6	7	8	9	10
Pu-239						
Pu-240						
Pu-241						
U -235			0.00078	0.00018		
U -238			0.35237	0.08118		
Be			0.37753	0.03223		
B -10		0.54137				
B -11		2.17912				
C		0.68010				
O			1.08737	0.19577		
Na			0.68076	0.68674	1.35147	1.66100
Mg	0.00095	0.03478				
Aℓ	0.20646	0.75183				
Cr	0.05922	0.21024	0.49312	0.39027	0.56939	0.20621
Mn			0.00030			
Fe	0.20602	0.73145	1.74017	1.38193	1.98101	0.71743
Ni	7.34702	0.09800	0.38158	3.80150	0.26541	0.09612
Mo			0.01191	0.01179		

Tab. 2.3.2 Atomic Number Densities for I-D Core (3)

(10^{22} atoms/cc)

Region / Element	11*	11**	11***	12	13
Pu-239	0.17112	0.16739	0.16739		
Pu-240	0.01549	0.01516	0.01516		
Pu-241	0.00144	0.00142	0.00142		
U -235	0.00162	0.00158	0.00158	0.00018	
U -238	0.73296	0.71717	0.71717	0.08118	
Be	0.26835	0.26835	0.26835	0.02302	
B -10		0.01142	0.00570		0.06941
B -11		0.04596	0.02295		0.27937
C		0.01434	0.00716		0.08719
O	2.10441	2.06485	2.06485	0.18656	
Na	0.68076	0.68076	0.68076	0.69559	1.68874
Mg					
Aℓ					
Cr	0.39522	0.39522	0.40380	0.36366	0.42748
Mn					
Fe	1.40199	1.40199	1.42967	1.28981	1.48728
Ni	0.22779	0.22779	0.23184	3.90561	0.19926
Mo	0.01319	0.01319	0.01319	0.01201	

Tab. 2.3.3 Atomic Number Densities for Heterogeneous Calculation

($\times 10^{22}$ atoms/cc)

Region / Element	I	II	III	IV	V	VI
Pu-239	0.39644					0.17112
Pu-240	0.03589					0.01549
Pu-241	0.00333					0.00144
U -235	0.00376					0.00162
U -238	1.69824					0.73296
Be		5.18632				0.37753
O	4.25409	5.18632				2.21360
Na				2.15384	0.18749	0.68076
Cr			1.31207	0.26385	1.61463	0.37907
Fe			4.77860	0.91798	5.61759	1.34320
Ni			0.95696	0.12299	0.75260	0.21602
Mo			0.10457			0.01191

III. Criticality

3.1 Diffusion Calculations

Calculations were made only for I-C and I-D. The I-C core is what is called the "clean system" which contains no other material than the standard fuel but its peripheral section is not fully loaded. (Fig. 3.1.1) On the other hand, I-D has B_4C rods for adjusting the reactivity as shown in Fig. 3.1.2. If the calculations are made with these B_4C rods in positions as such, it would be inevitable to make the X-Y two-dimensional calculations and this will make it necessary to calculate the transverse buckling in each region of the core. However, since a high degree of accuracy cannot be expected for such calculations, we decided to make the R-Z two-dimensional calculations on a model in which B_4C was homogeneously mixed in the core in order to avoid the uncertainties of the X-Y calculations due to the transverse buckling. Therefore, it is considered appropriate to evaluate the criticality on the I-C core involving less uncertainties than I-D.

In this analytical study, we used mainly the NNS-5 set (NAIG Nuclear Set 5) and occasionally the JAERI-FAST (Version II) set to make R-Z two-dimensional calculations on the basis of the 13-group diffusion approximation method. The 13-group contraction was carried out as 2/4/6/8/10/11/12/13/14/15/16/17/25/. The energy division points were as shown in Table 3.1.1. The temperature of the reference system at the calculations was 450°K in all the regions.

We used a fission spectrum corresponding to ν =2.9. (Table 3.1.2)

The eigenvalues obtained for I-C and I-D under the above conditions were 0.98197 and 0.98293, respectively.

Fig. 3.1.3 and Fig. 3.1.4 show the neutron spectrum of the various regions in the radial direction of I-C and I-D which were calculated by use of the NNS-5 set. The spectra of I-C showed a slight hardening as compared with I-D due to the B_4C homogeneously mixed in it. The spectra have peak at about 200 KeV and trailed long toward the low energy side.

The neutron flux distributions in R direction of I-C and I-D are shown in Fig. 3.1.7 and Fig. 3.1.8, respectively, and the distributions in Z direction in Fig. 3.1.9 and Fig. 3.1.10, respectively.

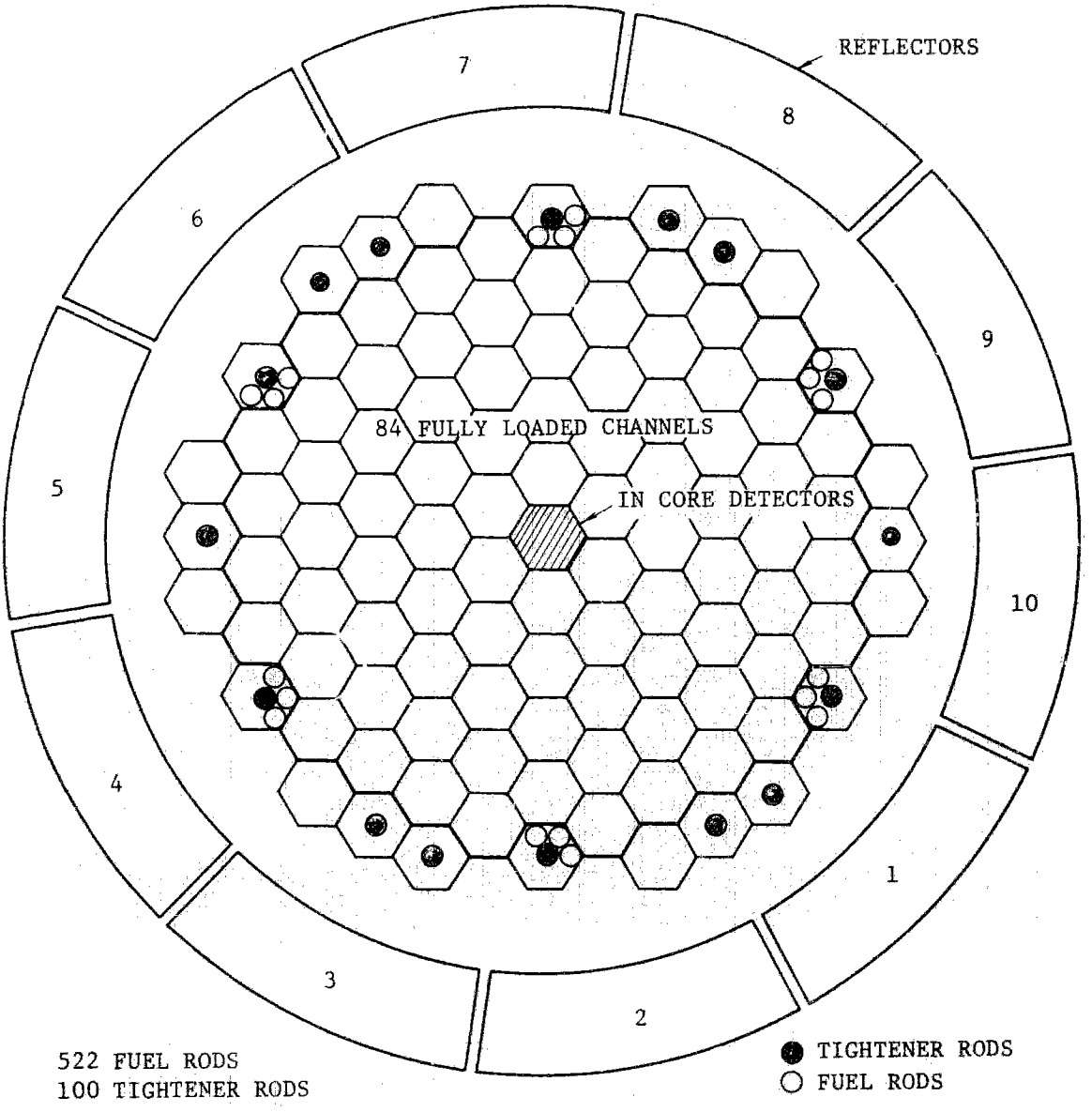

Fig. 3.1.1 Assembly I-C

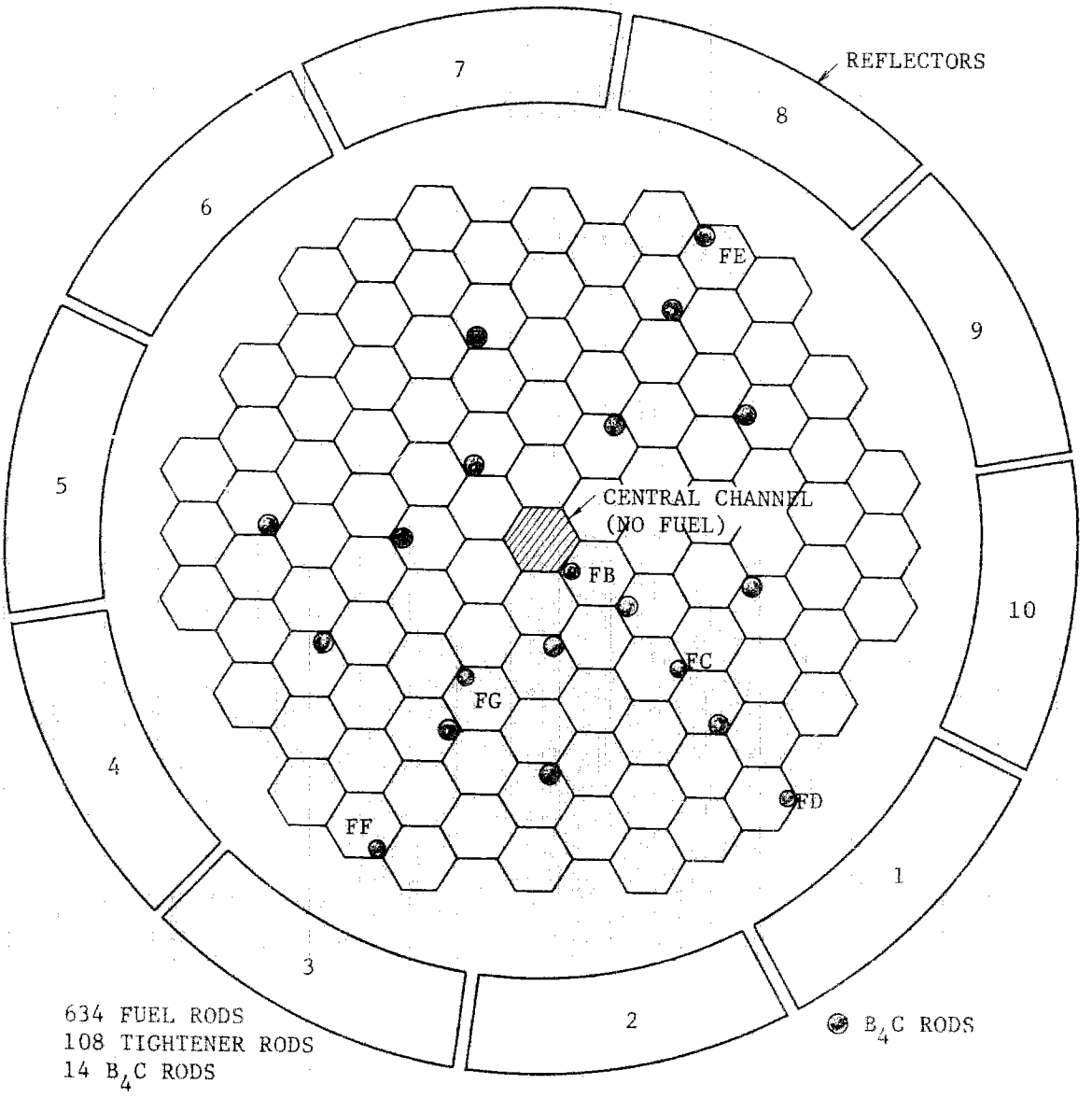

Fig. 3.1.2 Assembly I-D

3.2 Heterogeneous Effect

The heterogeneous calculations were made on a lattice system in which unit cells shown in Fig. 2.2.3 were infinitely arranged. Fuel was mixed in Region I, BeO in Region II, fuel and BeO cladding in Region III, and Region IV is sodium mixed with SUS of tightener sleeve and slide rod, Region V is the wrapper tube, and Region VI outside Region V is a homogeneous core region. The size of Region VI was determined by transforming into a ring the sum of one-halves of the areas of the six hexagonal regions adjacent to the heterogeneous region under consideration.

We calculated the effective macroscopic cross sections of the heterogeneous region by use of the mean neutron flux obtained in each region on the basis of the collision probability method. Using thus obtained effective macroscopic cross sections, we obtained the eigenvalue of 1.02262 by one-dimensional diffusion calculation.

On the other hand, the eigenvalue obtained by the homogeneous calculations was 1.015549.

Therefore, the correction factor by the heterogeneous effect becomes as follows.

$$(K^{Hetero} - K^{Homo}) / K^{Homo} = 0.702\%$$

3.3 Transport Theory Correction

We made the transport theory calculations by DTF-IV[6] on one-dimensional spherical models for I-C core. The approximations were S_4 and P_0.

We contructed two spherical models; one had the axial material compositions outside the core and the other had the radial material compositions, and we carried out the diffusion calculation and S_4 approximation on these two models, respectively. The results are shown in Table 3.3.1.

Tab. 3.3.1 Comparison of Eigenvalues by Diffusion and S_4 Approximations

Approximation	Surrounded by axial compositions	Surrounded by radial compositions
S_4	1.14987	1.10907
Diff.	1.13652	1.11886

The differences between diffusion approximation and S_4 approximation when the core is surrounded by the axial and radial compositions are 1.175% and 0.913%, respectively. The correction factor was obtained by averaging these two values with weight of surface areas of the core contacting the axial and radial material.

3.4 Calculations of kinetic parameters

The value of β_{eff} to be used as a scale factor for the reactivity was calculated in I-D from the following equations, using ϕ and ϕ^* obtained by RZ 13-group diffusion approximation.

$$\beta_{eff} = \sum_{m=1}^{6} \frac{1}{F} \int_{reactor} d\vec{r} \sum_j \chi_j^{(m)} \phi_j^* \sum_i \nu_i \Sigma_{fi} \beta^{(m)} \phi_i / k$$

$$F = \int_{reactor} d\vec{r} \sum_j \chi_j \phi_j^* \sum_i \frac{1}{k} \nu_i \Sigma_{fi} \phi_i$$

where m(= 1, ..., 6) represents the six delayed neutron groups. Since the value of β_{eff} varies somewhat according to the element-wise delayed neutron data and becomes uncertain for the scale factor, here we used the β data of Keepin,[7] Tomlinson[8] and Krick & Evans[9] to investigate the variations of β_{eff}. These data are shown in Table 3.4.1. The β_{eff} values obtained for I-D, using the data of Table 3.4.1 are shown in the following table.

Tab. β_{eff} Values for SEFOR I-D Core

Keepin	Tomlinson	Krick+Evans
0.00309	0.00330	0.00350
(0.00311)	(0.00332)	(0.00351)

Note: Values in parentheses represent β_{eff}'s for core with no B_4C.

Tab. 3.4.1 Comparison of Elementwise β-data

Nuclide	m / Data	1	2	3	4	5	6
	K	7.752(-5)	5.712(-4)	4.406(-4)	6.691(-4)	2.101(-4)	7.140(-5)
Pu-239	T	8.216(-5)	6.054(-4)	4.670(-4)	7.091(-4)	2.227(-4)	7.567(-5)
	KE	8.360(-5)	6.160(-4)	4.752(-4)	7.216(-4)	2.266(-4)	7.700(-5)
	K	7.448(-5)	7.262(-4)	5.107(-4)	9.310(-4)	3.405(-4)	7.714(-5)
Pu-240	T	8.078(-5)	7.876(-4)	5.539(-4)	1.010(-3)	3.693(-4)	8.367(-5)
	KE	8.078(-5)	7.876(-4)	5.539(-4)	1.010(-3)	3.693(-4)	8.367(-5)
	K	1.862(-4)	1.044(-3)	9.215(-4)	1.994(-3)	6.272(-4)	1.274(-4)
Pu-241	T	2.014(-4)	1.129(-3)	9.967(-4)	2.157(-3)	6.784(-4)	1.378(-4)
	KE	2.014(-4)	1.129(-3)	9.967(-4)	2.157(-3)	6.784(-4)	1.378(-4)
	K	2.451(-4)	1.374(-3)	1.213(-3)	2.625(-3)	8.256(-4)	1.677(-4)
U -235	T	2.538(-4)	1.423(-3)	1.256(-3)	2.719(-3)	8.550(-4)	1.737(-4)
	KE	2.630(-4)	1.474(-3)	1.301(-3)	2.816(-3)	8.858(-4)	1.799(-4)
	K	1.911(-4)	2.014(-3)	2.381(-3)	5.704(-3)	3.308(-3)	1.103(-3)
U -238	T	2.058(-4)	2.169(-3)	2.564(-3)	6.143(-3)	3.562(-3)	1.188(-3)
	KE	2.288(-4)	2.411(-3)	2.851(-3)	6.829(-3)	3.961(-3)	1.321(-3)

Note: K : Keepin
T : Tomlinson
KE: Krick & Evans

The prompt neutron generation time (ℓ_p) in I-D is

$$\ell_p = 5.4938 \cdot 10^{-7} \text{ sec } (6.0606 \cdot 10^{-7} \text{ sec})$$

(Value in parenthesis is for K-D with no B_4C.)

The reactivity conversion factor is

$$1\%\ \Delta K/K = \begin{cases} 1002.7 \text{ Ih (Keepin)} \\ 941.6 \text{ Ih (Tomlinson)} \\ 900.2 \text{ Ih (Krick \& Evans)} \end{cases}$$

Hence ℓ_p/β_{eff} becomes

$$\frac{\ell_p}{\beta_{eff}} = \begin{cases} 1.78 \cdot 10^{-4} (1.95 \cdot 10^{-4}) \text{sec (Keepin)} \\ 1.67 \cdot 10^{-4} (1.83 \cdot 10^{-4}) \text{sec (Tomlinson)} \\ 1.57 \cdot 10^{-4} (1.73 \cdot 10^{-4}) \text{sec (Krick \& Evans)} \end{cases}$$

(Value in parenthesis is for I-D with no B_4C.)

Tab. 3.1.1 13 Group Structure

Group	Energy Range
1	10.5 - 4.0 MeV
2	4.0 - 1.4 MeV
3	1.4 - 0.4 MeV
4	0.4 - 0.1 MeV
5	100.0 - 21.5 KeV
6	21.5 - 10.0 KeV
7	10.0 - 4.65 KeV
8	4.65 - 2.15 KeV
9	2.15 - 1.0 KeV
10	1000.0 - 465.0 eV
11	465.0 - 215.0 eV
12	215.0 - 100.0 eV
13	100.0 - Th

Tab. 3.1.2 Fission Spectrum for 13 Energy Groups

Gr. No.	1	2	3	4	5	6	7 - 13
χ_i	.113	.457	.335	.082	.012	.001	0. 0

Fig. 3.1.7 Neutron Flux Radial Distribution (I-C)

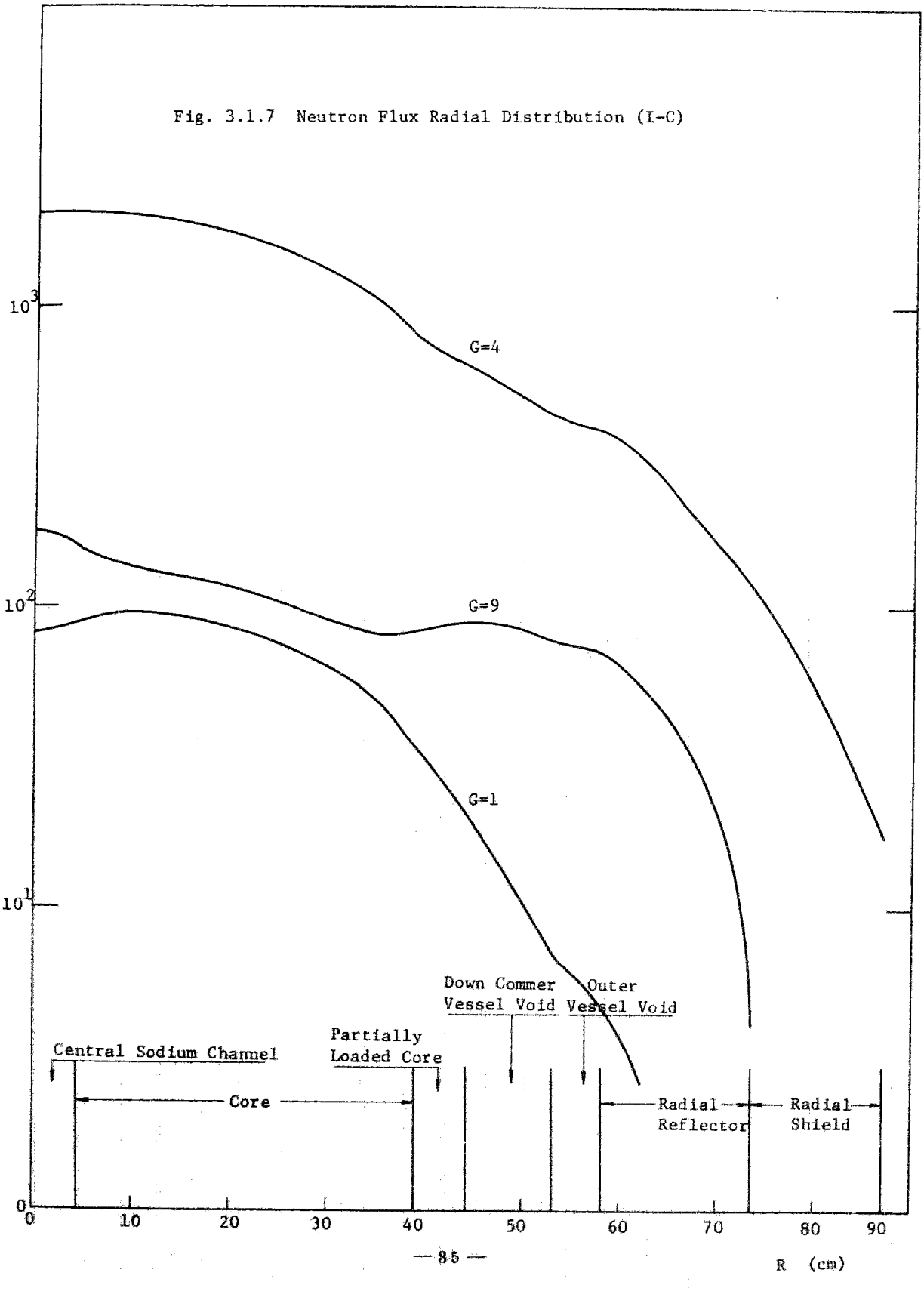

Fig. 3.1.8 Neutron Flux Radial Distribution (I-D)

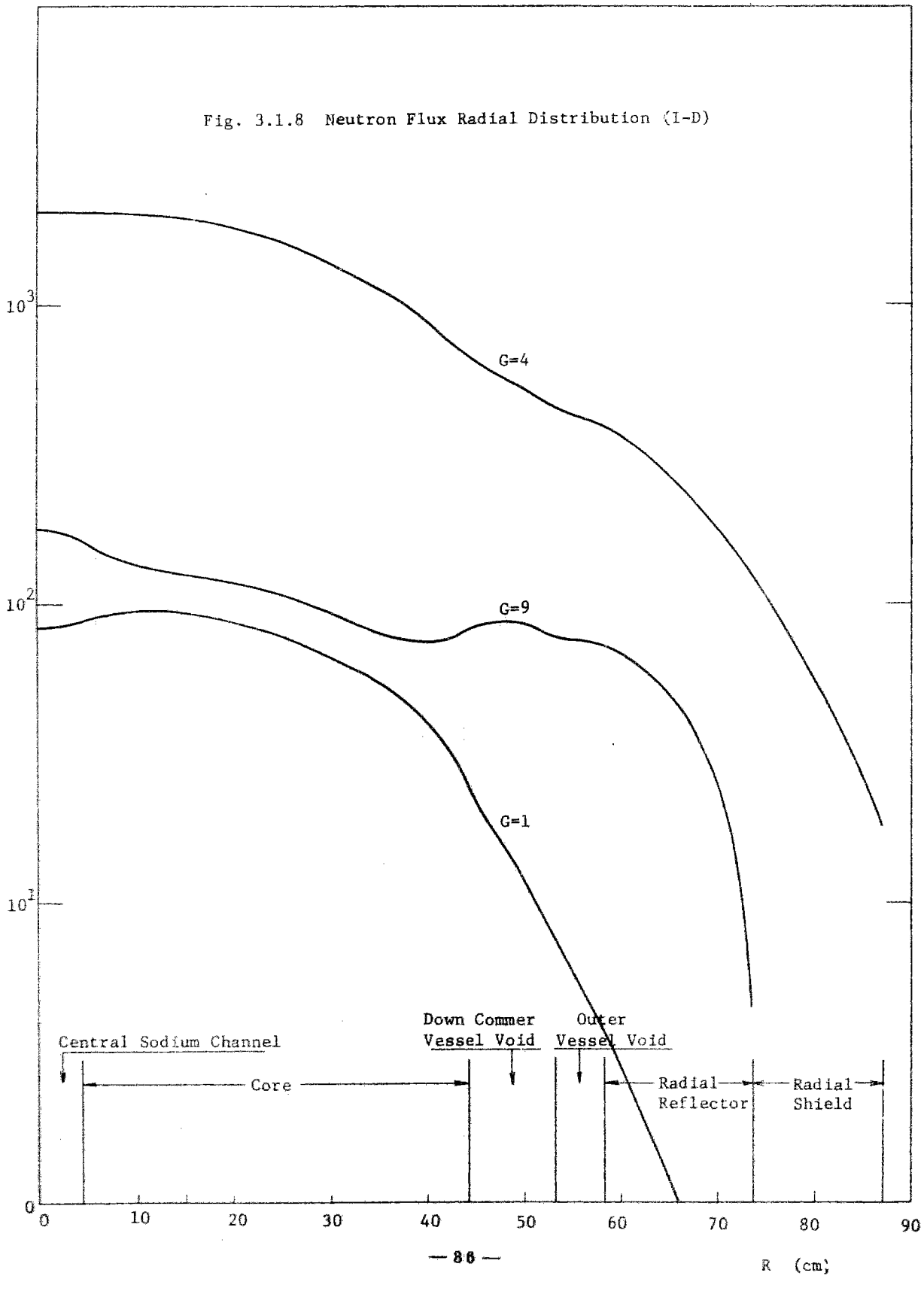

Fig. 3.1.9 Neutron Flux Axial Distribution (I-C)

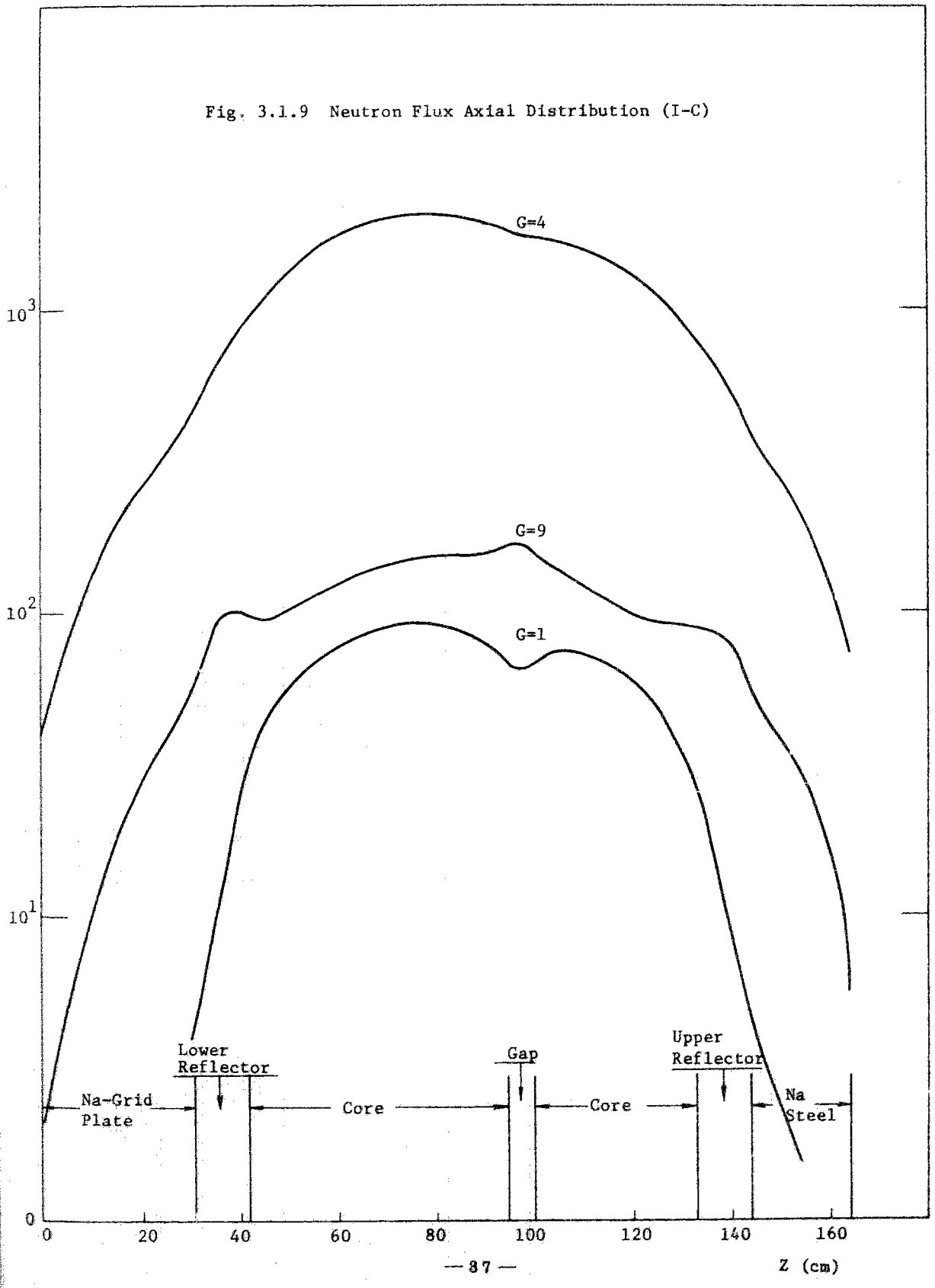

Fig. 3.1.10 Neutron Flux Axial Distribution (I-D)

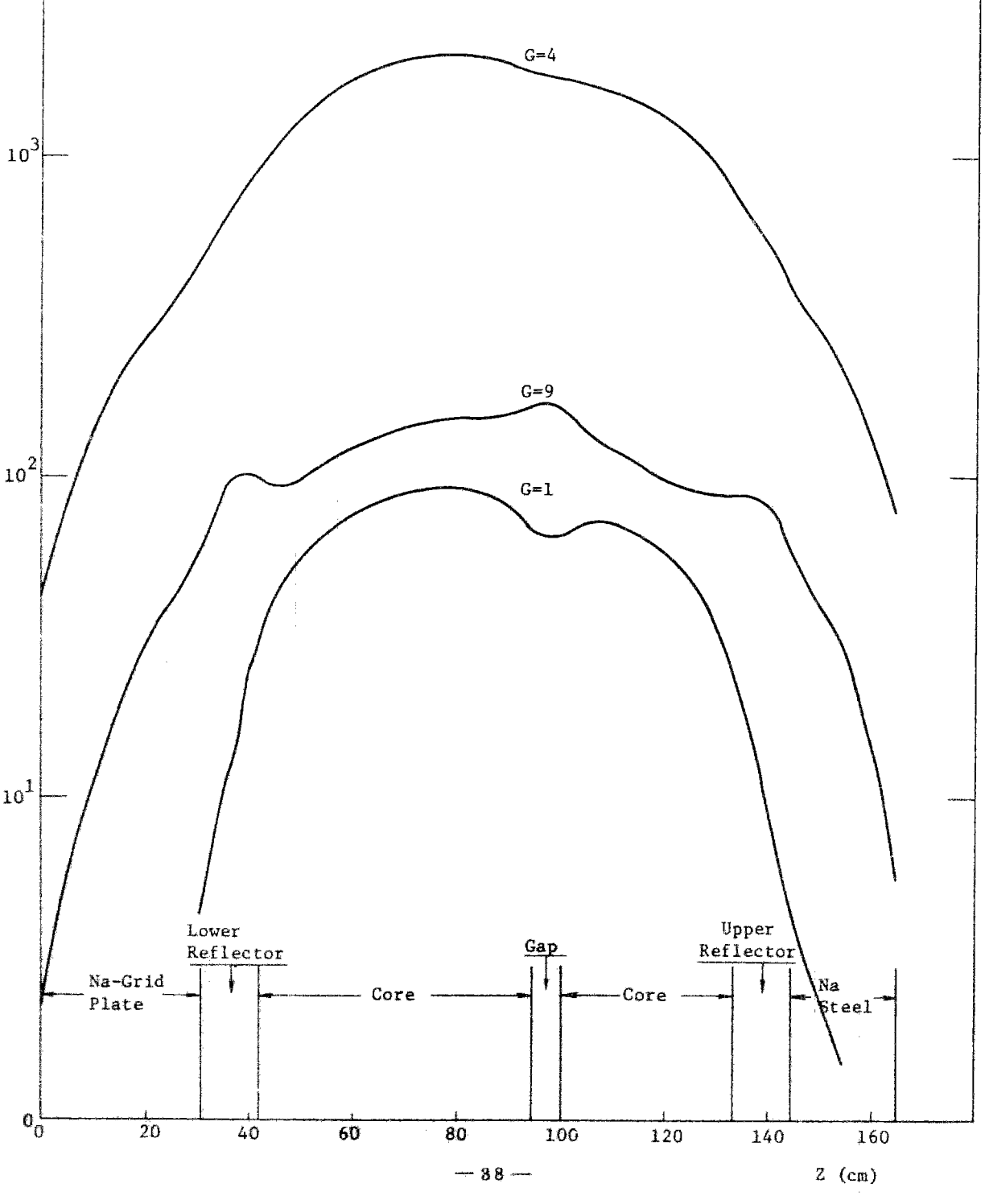

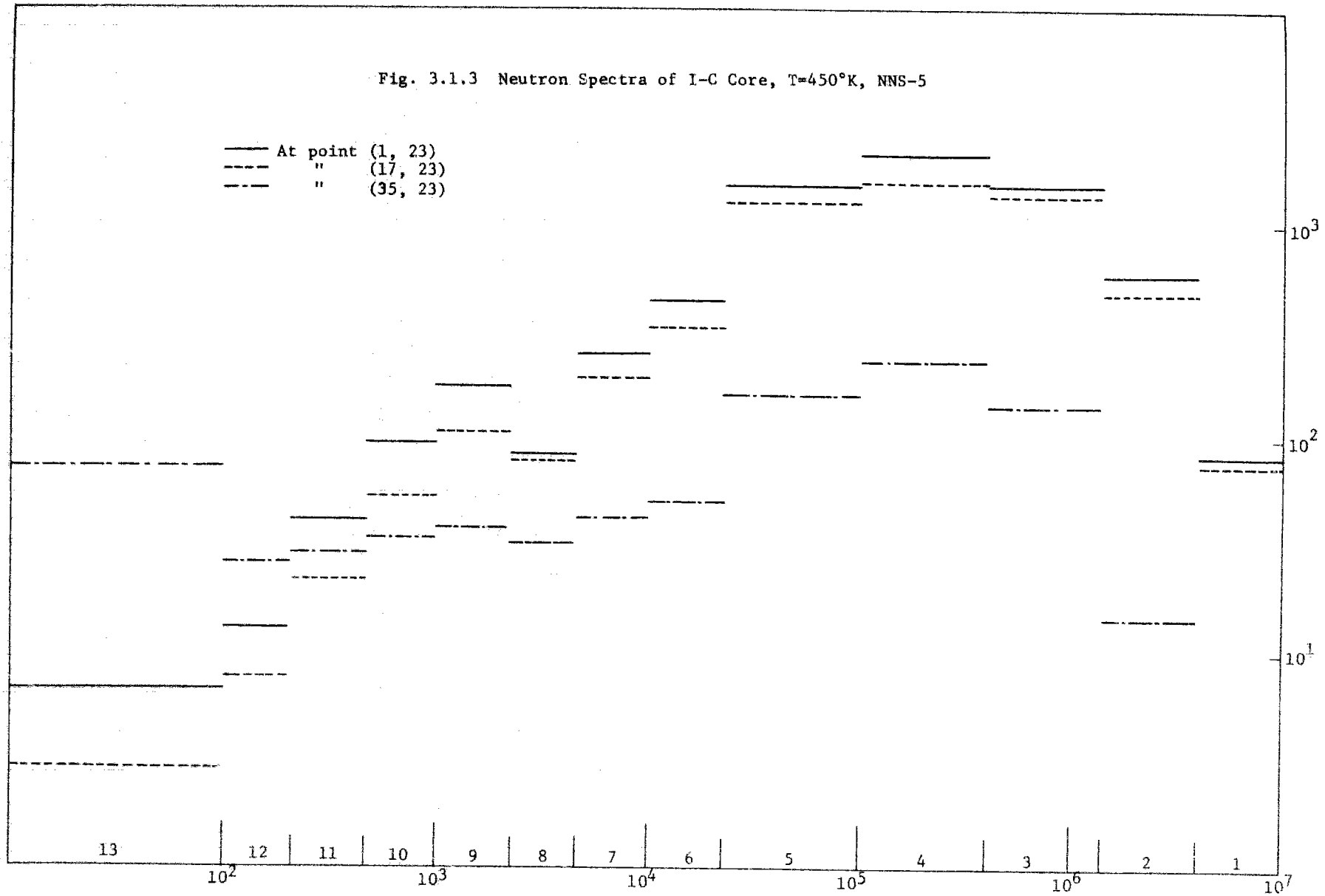

Fig. 3.1.3 Neutron Spectra of I-C Core, T=450°K, NNS-5

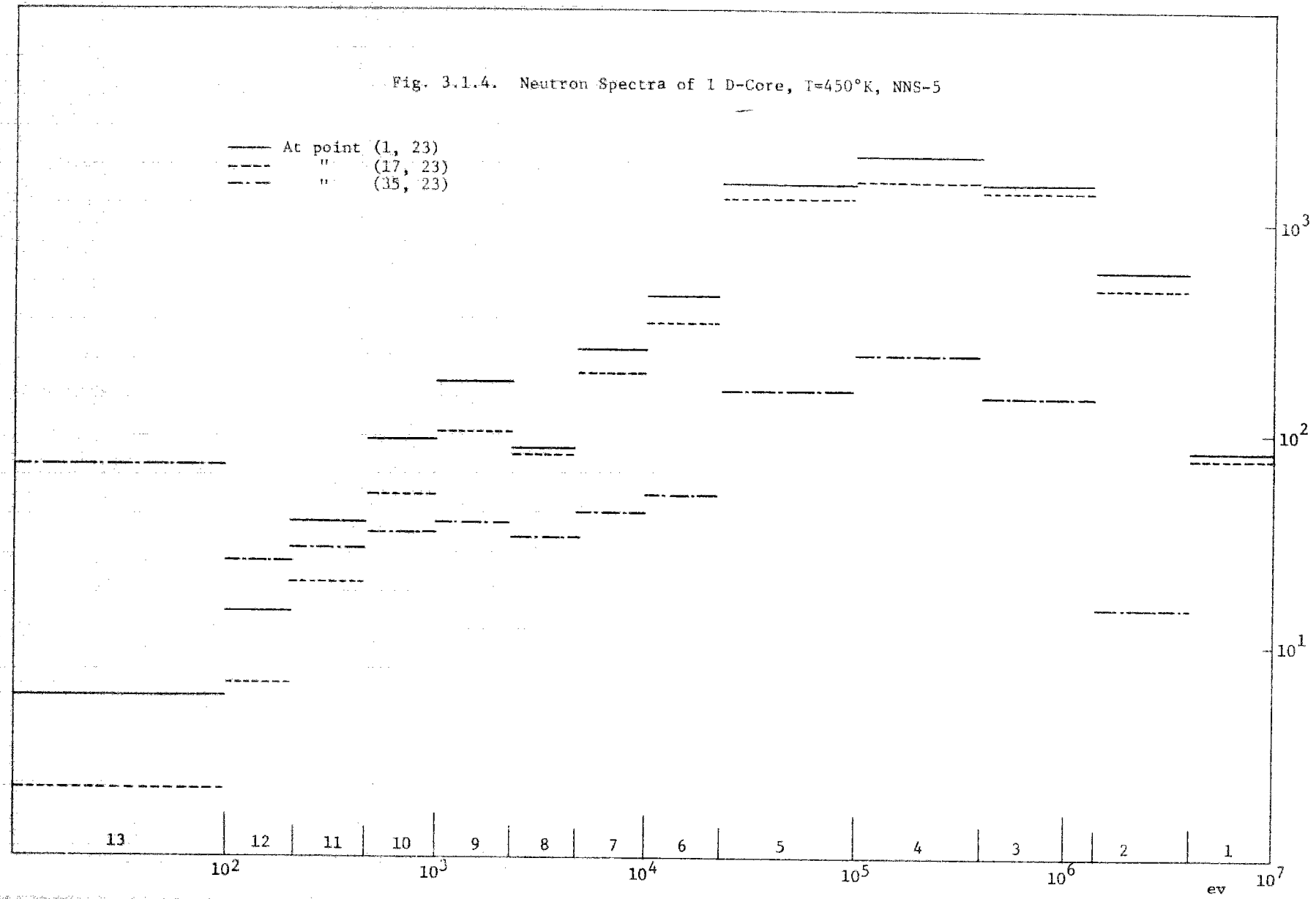

Fig. 3.1.4. Neutron Spectra of 1 D-Core, T=450°K, NNS-5

3.5 Summary

The eigenvalues obtained from the 13-group two-dimensional diffusion calculations and various correction factors are summarized in Table 3.5.1. The two-dimensional eigenvalue calculations were made using only NNS-5 set. The corrected eigenvalue for the minimum critical core I-C at 450°K was so satisfactory as 0.9996. The eigenvalue was somewhat lower for I-D and this was presumably because the amount of B_4C in I-D was evaluated somewhat greater.

When the experimentally obtained values of the excess reactivity are transformed into the form directly comparable with the calculated values, they will have a width according to the source data of β. However, it may be so considered that the corrected eigenvalues would not be so much affected by this where the excess reactivity is not so large.

A comparison of the measured and calcualted values is given in Table 3.5.2. The minimum critical mass is for I-C and its C/E (ratio of calculated to experimental value) is 1.013.

As for the ℓ_p/β_{eff} values, the calculated values were distributed from 1.87×10^{-4} sec to 1.65×10^{-4} sec while the experimental value was 2.0×10^{-4} sec. This width was due to what source data were used for β.

The calculated values are the mean values of ℓ_p/β_{eff} of I-D core disregarding the presence of B_4C and that of I-D core with the presence of B_4C (probably twice as much as the actual quantity of B_4C).

There were considerable discrepancies between the measured and calculated reactivity worth of fuel rods and B_4C rods near the core center.

Tab. 3.5.1 SEFOR Eigenvalues and Various Corrections

(NNS-5)

	I - C	I - D
As calculated	0.98197	0.98293 *
		(1.02398) **
	-0.00003 (K)	-0.00556 (K) ***
Kexcess	-0.00003 (T)	-0.00594 (T)
	-0.00003 (KE)	-0.00630 (KE)
Hetero. correction	0.00689	0.00694
Transp. correction	0.01076	0.01083
Corrected K_{eff}	0.99959	0.99514 (K)
		(1.03619)
		0.99476 (T)
		(1.03581)
		0.99440 (KE)
		(1.03545)

* Eigenvalue calculated using number densities with (**) for regions 2 and 11 (See Tab. 2.3.2.)

** Eigenvalue calculated using number densities with (*) for regions 2 and 11 (See Tab. 2.3.2.)

*** (K), (T), and (KE) denote the source of β-data of Keepin, Tomlinson and Krick & Evans, respectively.

Tab. 3.5.2 Comparison between Measured And Calculated Results

Experiment	Measured	Calculated
Minimum Critical Core Size (Mass of Pu-239 + Pu-241)	284.3 Kg	287.9 Kg
ℓ_p/β_{eff} (Average of two values from the core with and without B_4C)	2.0×10^{-4}sec	1.87×10^{-4}sec (K) 1.75×10^{-4}sec (T) 1.65×10^{-4}sec (KE)
Fuel Rod Worth near core center	+35 ¢	+42.6 ¢ (K)
B_4C Rod Worth near core center	-71 ¢	-93.7 ¢ (K)
Fission Ratio near core center		
$\sigma_f^{238} / \sigma_f^{235}$	0.0252	0.0254 (0.0245)
$\sigma_f^{239} / \sigma_f^{235}$	0.905	0.905 (0.989)

Note:
- o K, T and KE represents the Keepin's, Tomlinson's and Krick & Evans' β-data, respectively.
- o Parentheses in Fission Ratio represent the ratios in I-D core without B_4C.
- o Minimum Critical Mass was determined on I-C core and others on I-D core.

IV. Analysis of Experiment at Zero Power

4.1 Central Fission Rate Ratio

4.1.1 An outline of experiment

Measurements of the fission rate ratio were made on I-D core. The measurements were made at the position of FB rod (position adjacent to the central channel) using depleted U, enriched U and Pu foils. Table 4.1.1 shows the isotopic compositions of these foils. The measured values, together with the calculated values, are shown in Table 4.1.2.

Table 4.1.1 Foil Isotopic Compositions

Foil Type	Isotope	Percent
Enriched Uranium	U -235	93.15
	U -238	6.85
Depleted Uranium	U -235	0.19
	U -238	99.81
Plutonium	Pu-238	0.036
	Pu-239	92.905
	Pu-240	6.444
	Pu-241	0.582
	Pu-242	0.033

4.1.2 Calculational method and results

Table 4.1.2 shows the values obtained by the 13-group diffusion calculation and the measured values. The calculations were made on the model including B_4C and the model not including B_4C. As for the self-shielding factor of resonance, we used the same one used for core dilution.

Table 4.1.2 Central Reaction Rate Ratio Comparison of Calculation with Measurement

	Measured	Calculated (NNS 5)	
		B_4B Included	B_4C Not Included
$\sigma_f^{28} / \sigma_f^{25}$	0.0252	0.0254(1.01)	0.0245(0.97)
$\sigma_f^{39} / \sigma_f^{25}$	0.905	0.905 (1.00)	0.989 (1.09)

Note: Parenthesis denotes C/E values.

From the above table, the measured values and calculated values obtained on the model containing B_4C in the core seem to be well in agreement with one another. In this model however, the amount of B_4C was estimated to be somewhat larger than the actual amount (the actual amount of B_4C is not known precisely at the present moment) and the actual amount of B_4C was somewhere between the values obtained on the two models. With such a value of B_4C, the measured values and calculated values may be considered sufficiently well in agreement with one another.

4.2 Fission Rate Distribution

4.2.1 An outline of experiment

The fission rate spatial distributions were measured on I-D core.

To carry out the experiments, several foil holder rods provided with the same foils (Table 4.1.1) as those which were used in the measurement of the central fission rate ratio were loaded in several positions in the core. Thus measured values are shown in the forms of the axial and radial traverses at typical positions, together with the calculated values, are shown in Fig. 4.2.1 through 4.2.8.

4.2.2 Calculational method and results

The axial and radial distributions of the fission rate at the typical positions, obtained by the 13-groups RZ diffusion calculation, are shown in Table 4.2.1 through Table 4.2.3.

The calculations were carried out on two different models, i.e. a model not including B_4C and the other including homogenized B_4C but no significant difference was observed. Therefore, only the calculated values obtained on the model not including B_4C are given. As for the resonance self-shielding factor which was used in the calculation of the fission rate, we used the same one as for core dilution.

The measured values and calculated values are compared in Fig. 4.2.1 through 4.2.8. As for the calculated values, only those which were on the mesh points could be obtained and therefore the traverse of the calculated values and that of the measured values do not exactly point-wise correspond with one another. However, the difference was 1 cm at most and the resulting differences in the calculated values may be negligible. The discrepancy between the measured and calculated values became more and more pronounced nearer to the core-reflector boundary. Such discrepancy was rarely found in the core with the uranium blanket[10] but only in the core with the metal reflector. Such discrepancy occurred irrespective of the type of metal used for the reflector and therefore it is inconceivable that it was ascribable to the group constants for nickel. We have seen a similar discrepancy in ZPR-III-54 with the steel reflector, FCA-V-2-R with SUS reflector, ZPR-III-47 and ZPPR-2-shield with the nickel reflector. As for V-2-R core, we made S_4 (diagonal transport) calculations and compared thus obtained values with the measured values but they did not show any better agreement as compared with the results of the diffusion calculations.

In the present SEFOR calculations, we also tried a method of using the self-shielding factor for infinite dilution in the vicinity of the core-reflector boundary but little improvement

was made of the disagreement between the measured and calculated values. From what we have discussed so far, it is most probably the only effective method to correct the calculated values obtained on the actual reactor by use of the C/E values obtained on the mockup assembly.

The axial distributions of C/E values in ZPR-III-47 are shown in Fig. 4.2.9 and the calculated values and experimental values after being corrected by the C/E values are shown in Fig. 4.2.10 through 4.2.12. These values now show a much better agreement with one another.

The above-stated discrepancy was not observed for the axial distribution near the core-reflector boundary. (Fig. 4.2.7 through 4.2.8) This fact is worthy of notice.

Table 4.2.1 Calculated Fission Rate Radial Distributions.
37 cm above the Core Bottom, 13 G, RZ, NNS 5

Distance from the Core Center (cm)	Enriched U	Plutonium	Depleted U
4.23	1.000	1.000	1.000
7.70	0.966	0.979	1.032
11.17	0.935	0.952	1.024
14.65	0.897	0.916	0.994
18.12	0.850	0.869	0.946
21.59	0.795	0.812	0.885
25.07	0.731	0.747	0.813
28.54	0.662	0.675	0.731
32.01	0.591	0.599	0.640
35.49	0.523	0.524	0.540
38.96	0.474	0.461	0.430
44.12	0.488	0.442	0.305

Note: Normalized to unity at 4.23cm from the core center.

Table 4.2.2 Calculated Fission Rate Axial Distributions
4.23 cm from the Core Center
13 G, RZ, NNS 5

Distance from the Core Bottom (cm)	Enriched U	Plutonium	Depleted U
2.44	0.575	0.551	0.445
7.33	0.641	0.635	0.601
12.22	0.728	0.729	0.726
17.37	0.821	0.824	0.833
22.76	0.902	0.906	0.917
28.16	0.959	0.962	0.976
36.25	1.000	1.000	1.000
44.35	0.995	0.986	0.958
49.74	0.981	0.958	0.875
53.74	0.973	0.937	0.804
56.33	0.952	0.918	0.792
60.42	0.893	0.872	0.804
66.01	0.816	0.808	0.792
71.60	0.739	0.737	0.744
77.19	0.658	0.656	0.661
82.77	0.578	0.569	0.552
88.36	0.517	0.492	0.413

Note: Normalized to unity at 36.25 cm from the bottom.

Table 4.2.3 Calculated Fission Rate Axial Distributions
44.12 cm from the Core Center
13 G, RZ, NNS 5

Distance from the Core Bottom (cm)	Enriched U	Plutonium	Depleted U
2.44	0.664	0.644	0.499
7.33	0.706	0.698	0.629
12.22	0.770	0.768	0.739
17.37	0.837	0.841	0.824
22.76	0.904	0.906	0.910
28.16	0.954	0.956	0.964
36.25	1.000	1.000	1.000
44.35	1.018	1.011	0.972
49.74	1.033	1.016	0.912
53.74	1.066	1.039	0.854
56.33	1.050	1.023	0.837
60.42	0.964	0.946	0.838
65.01	0.877	0.868	0.815
71.60	0.802	0.796	0.762
77.19	0.726	0.720	0.681
82.77	0.654	0.643	0.578
88.36	0.607	0.585	0.447

Note: Normalized to unity at 36.25 cm from the bottom.

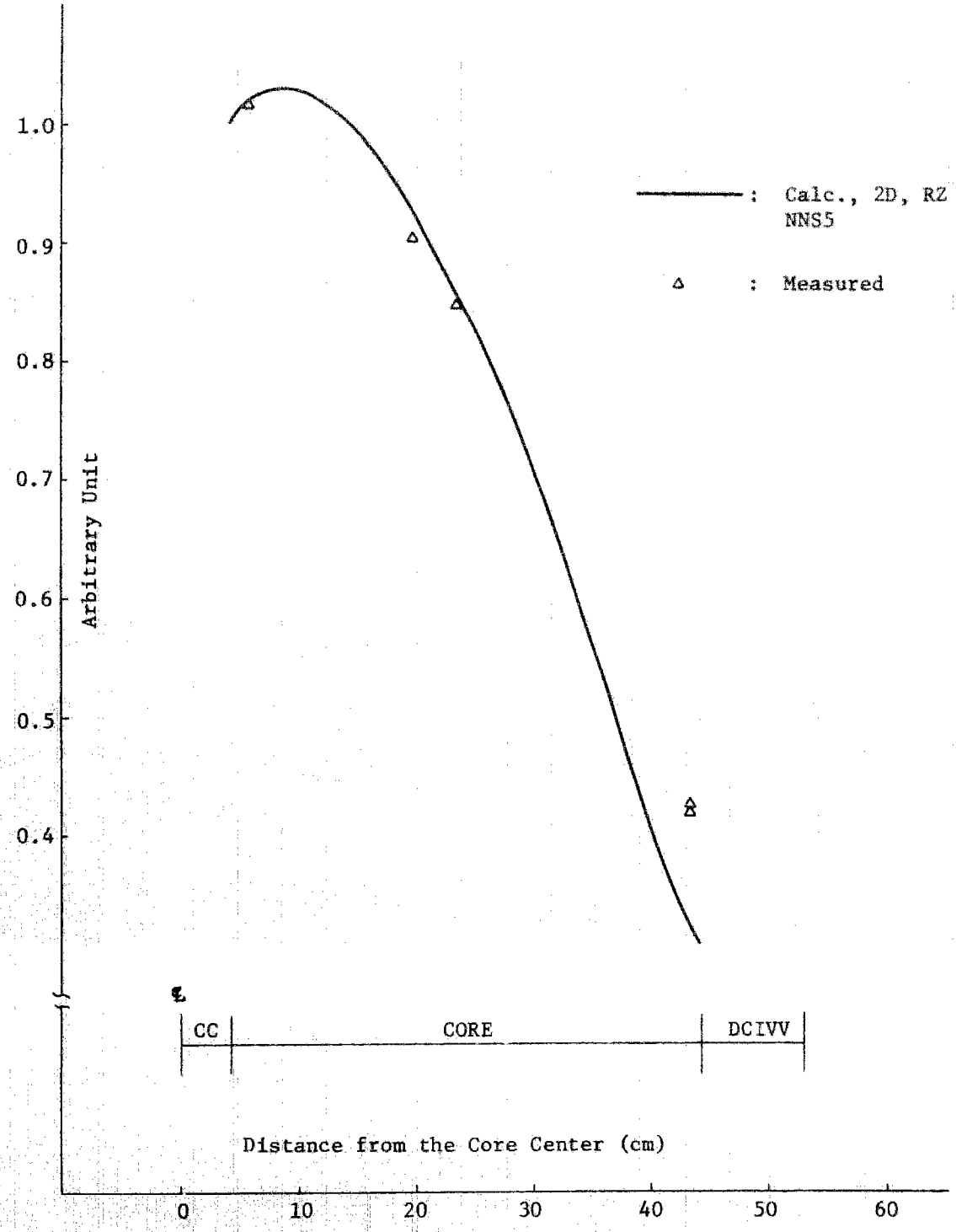

Fig. 4.2.1 Normalized Radial Fission Rate Distribution
Enriched U Foil, 37 cm above the Core Bottom

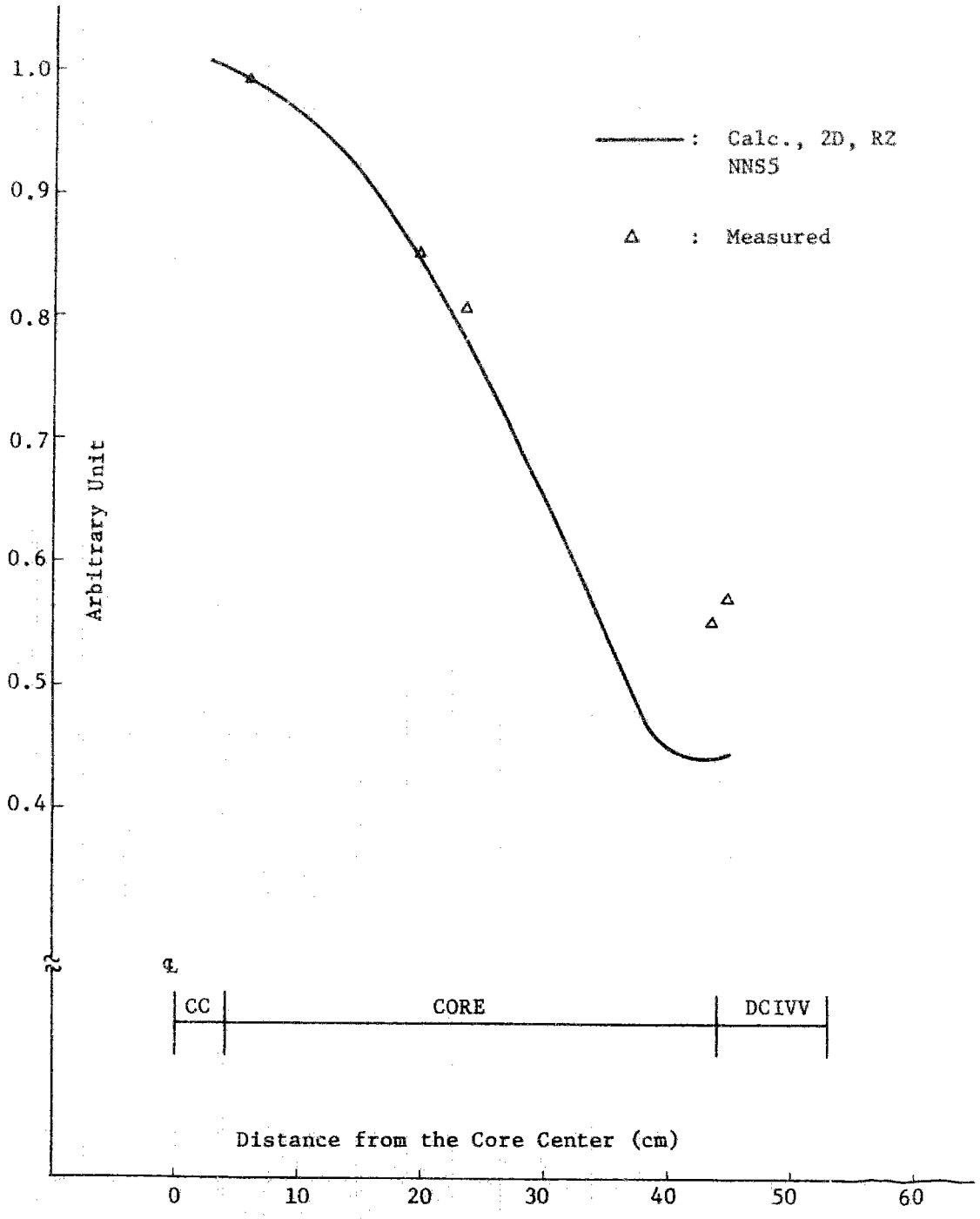

Fig. 4.2.2 Normalized Radial Fission Rate Distribution
Pu Foil, 37 cm above the Core Bottom

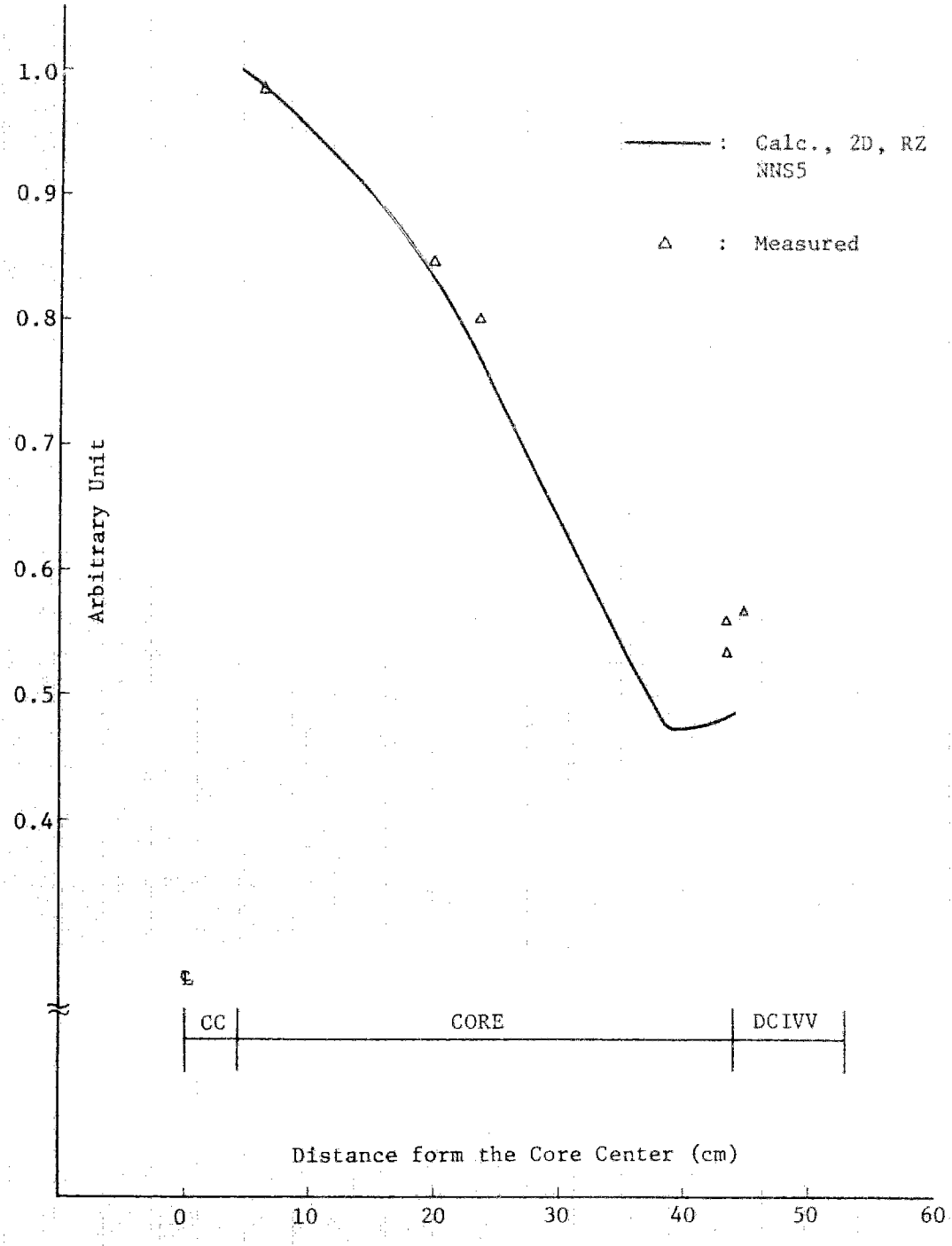

Fig. 4.2.3 Normalized Radial Fission Rate Distribution
Depleted U Foil, 37 cm above the Core Bottom

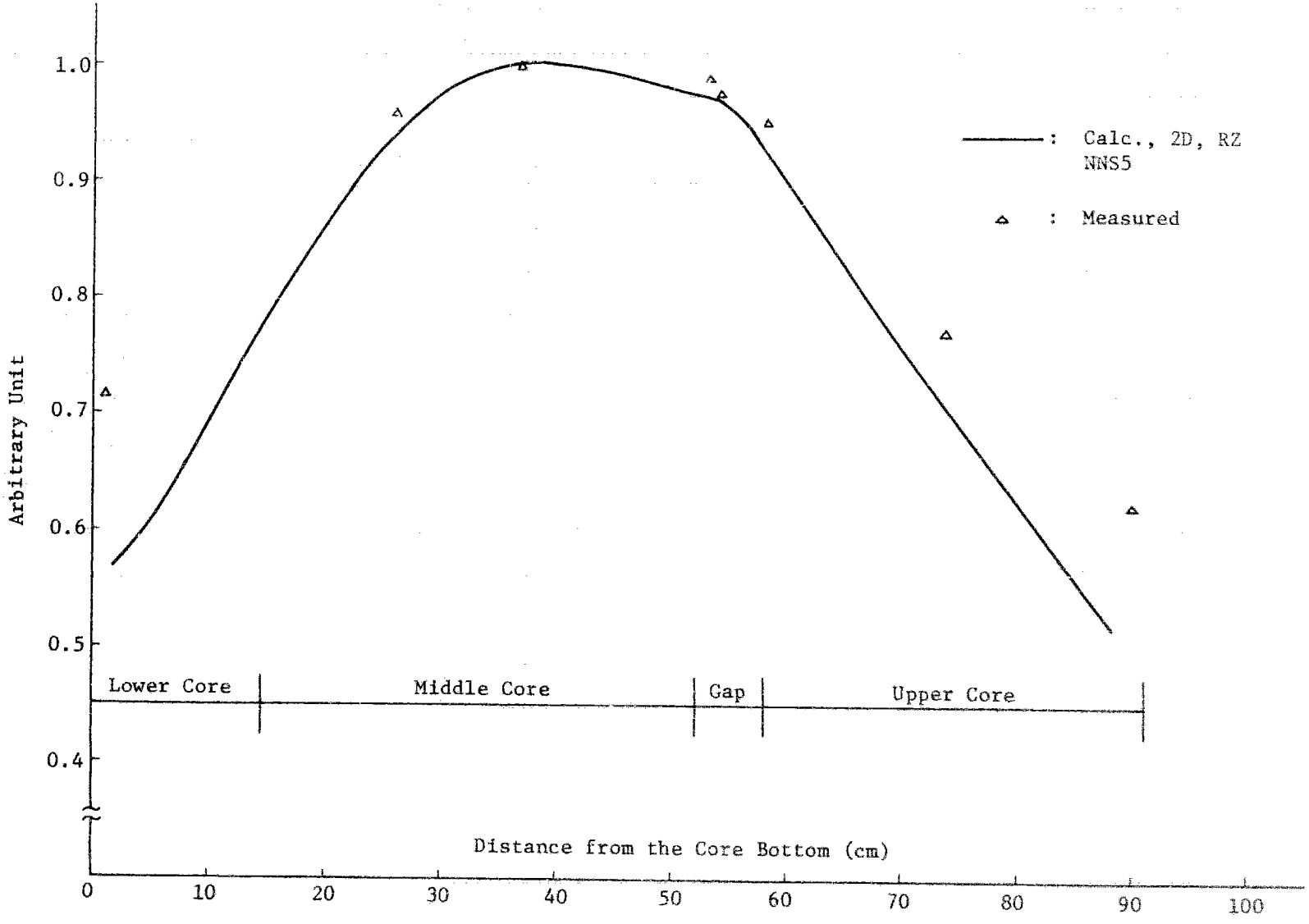

Fig. 4.2.4 Normalized Axial Fission Rate Distribution Enriched U Foil Outside the Central Channel (FB rod)

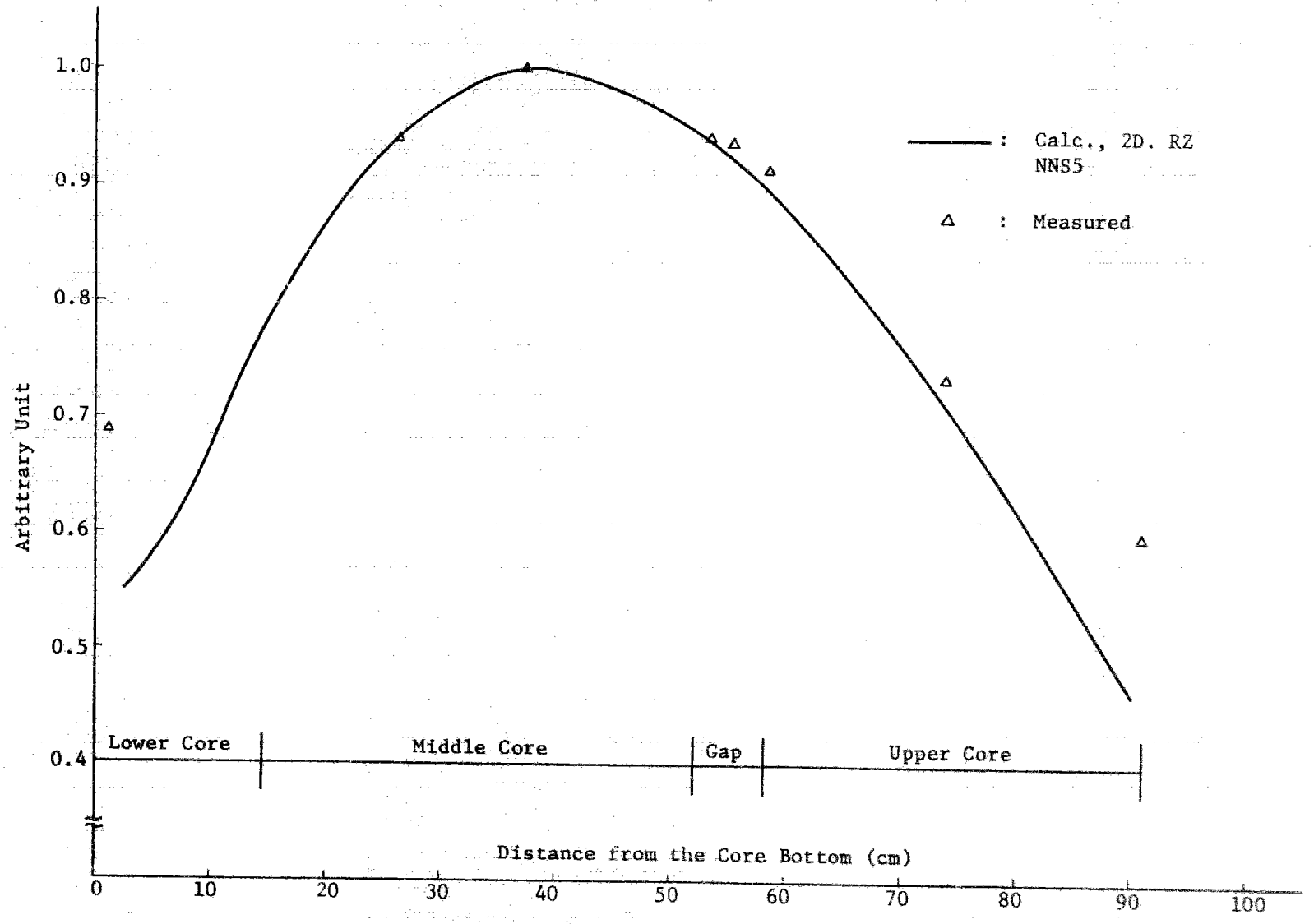

Fig. 4.2.5 Normalized Axial Fission Rate Distribution, Pu Foil Outside the Central Channel (FB rod)

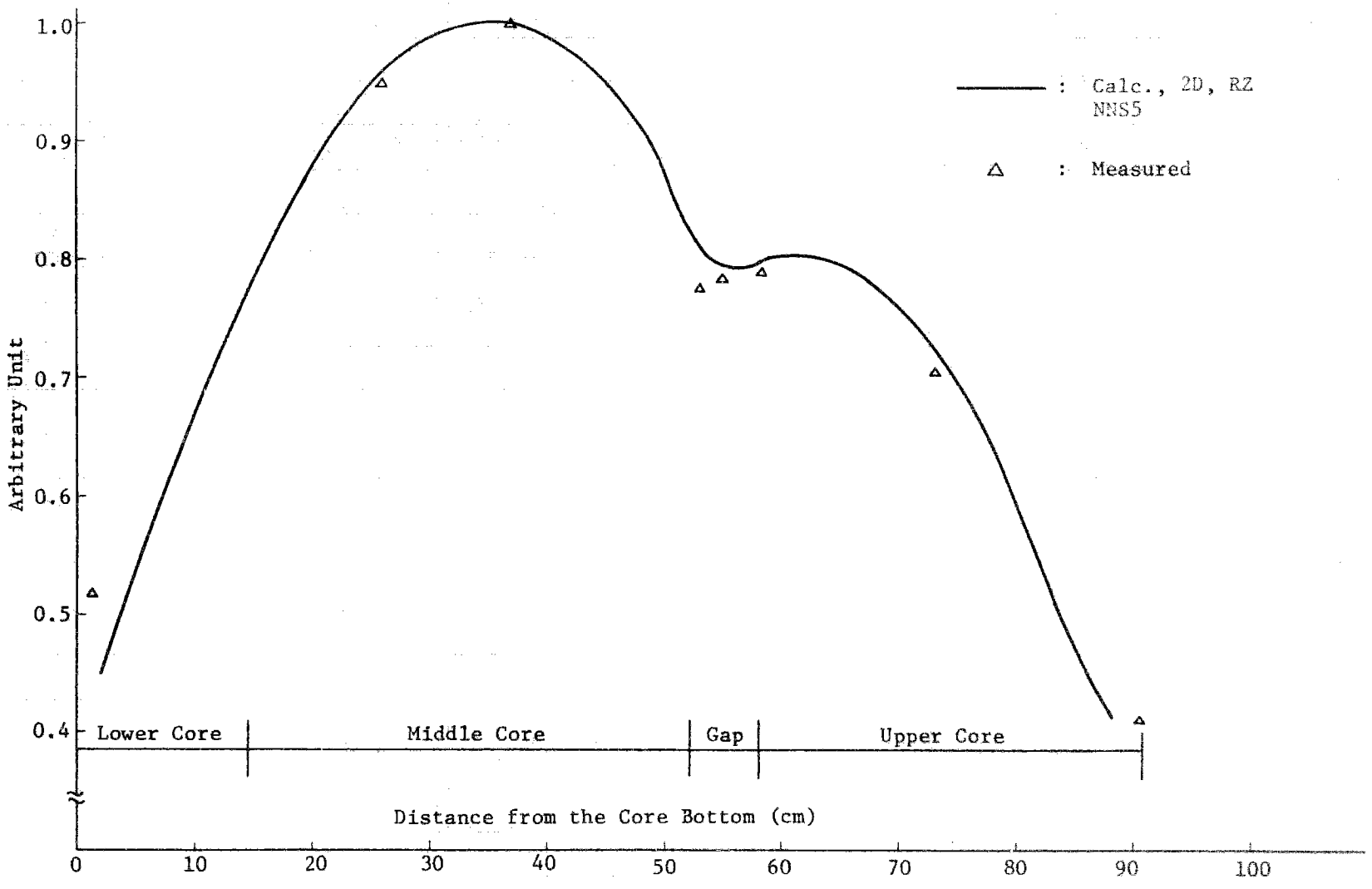

Fig. 4.2.6 Normalized Axial Fission Rate Distribution, Depleted U Foil Outside the Central Channel (FB rod)

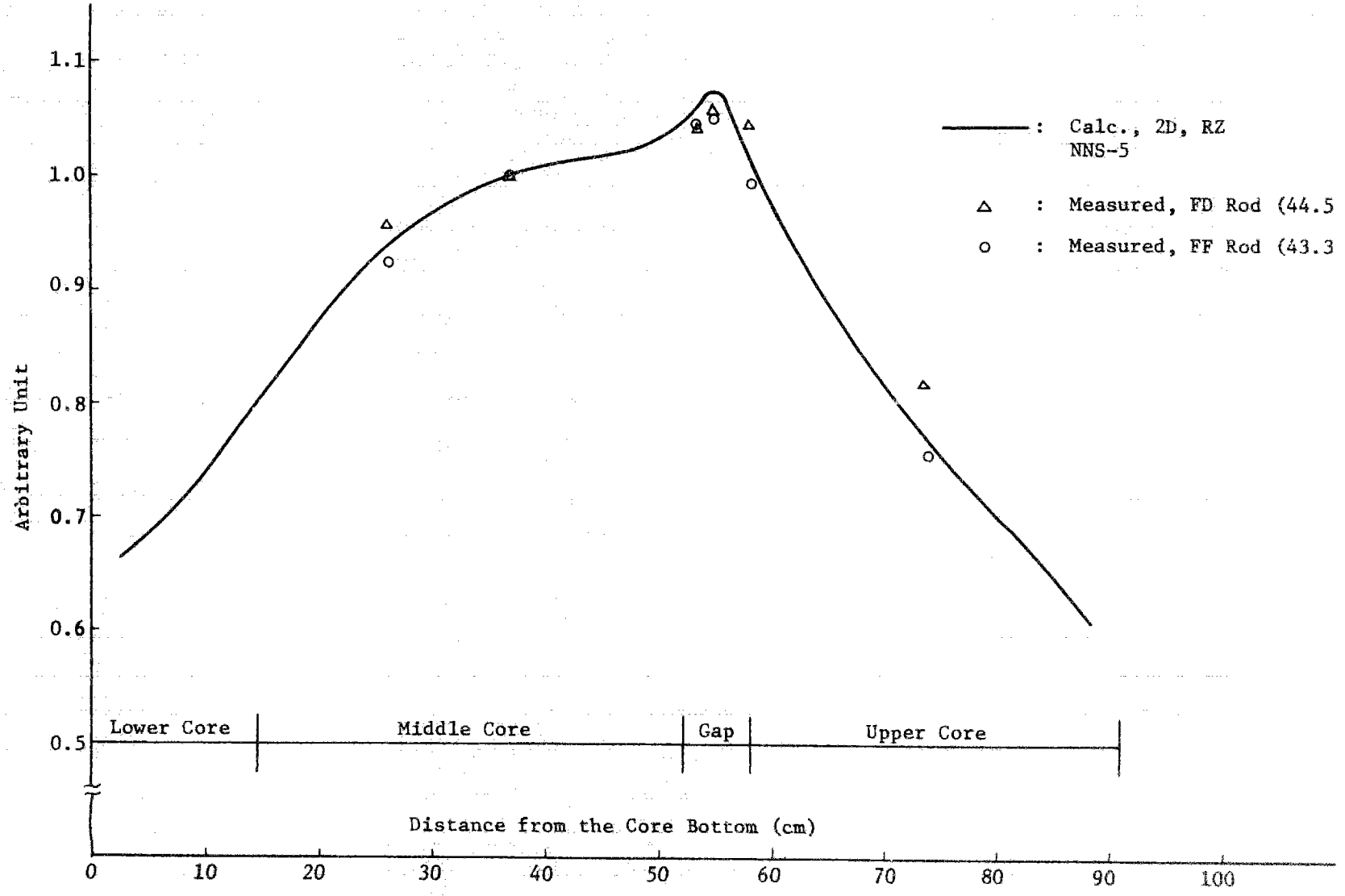

Fig. 4.2.7 Normalized Axial Fission Rate Distribution, Enriched U Foil Core Boundary *) Distance from the Core Centre

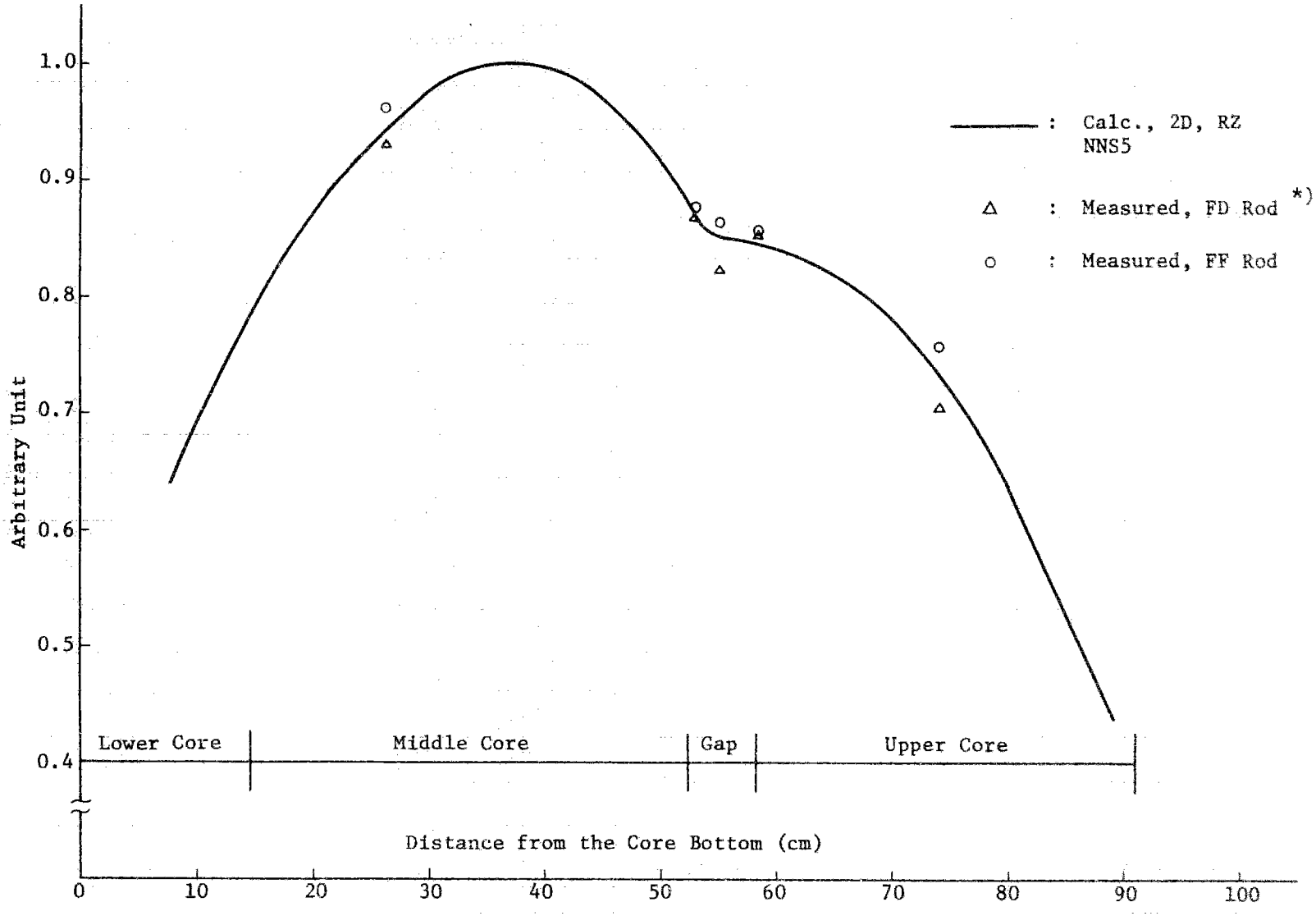

Fig. 4.2.8 Normalized Axial Fission Rate Distribution, Depleted U Foil Core Boundary. *) Normalized to Calculated Value at 53 cm

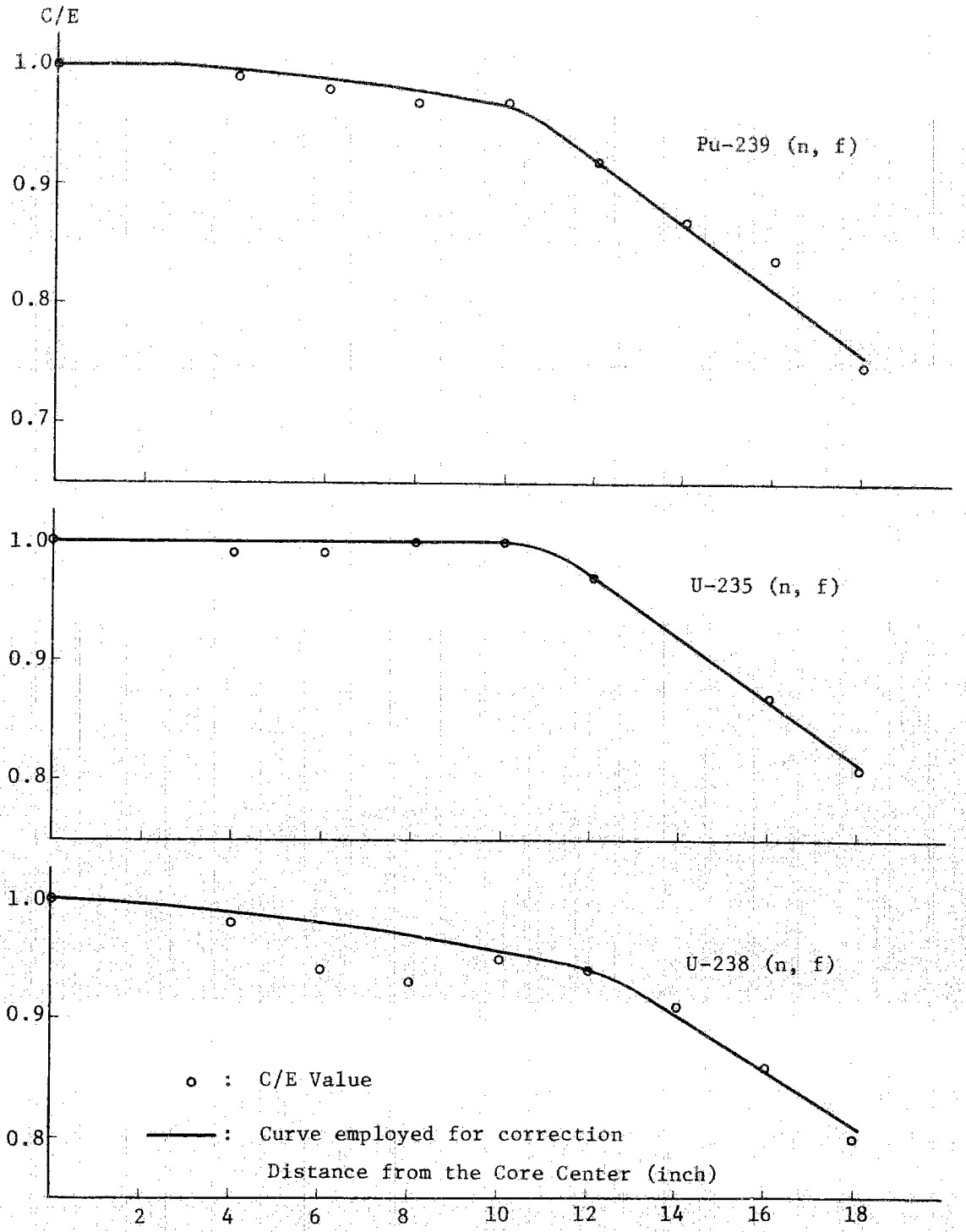

Fig. 4.2.9 Fission Rate C/E Value Axial Distributions in SEFOR Mockup, ZPR-III-47 (NNS5 Calc.)

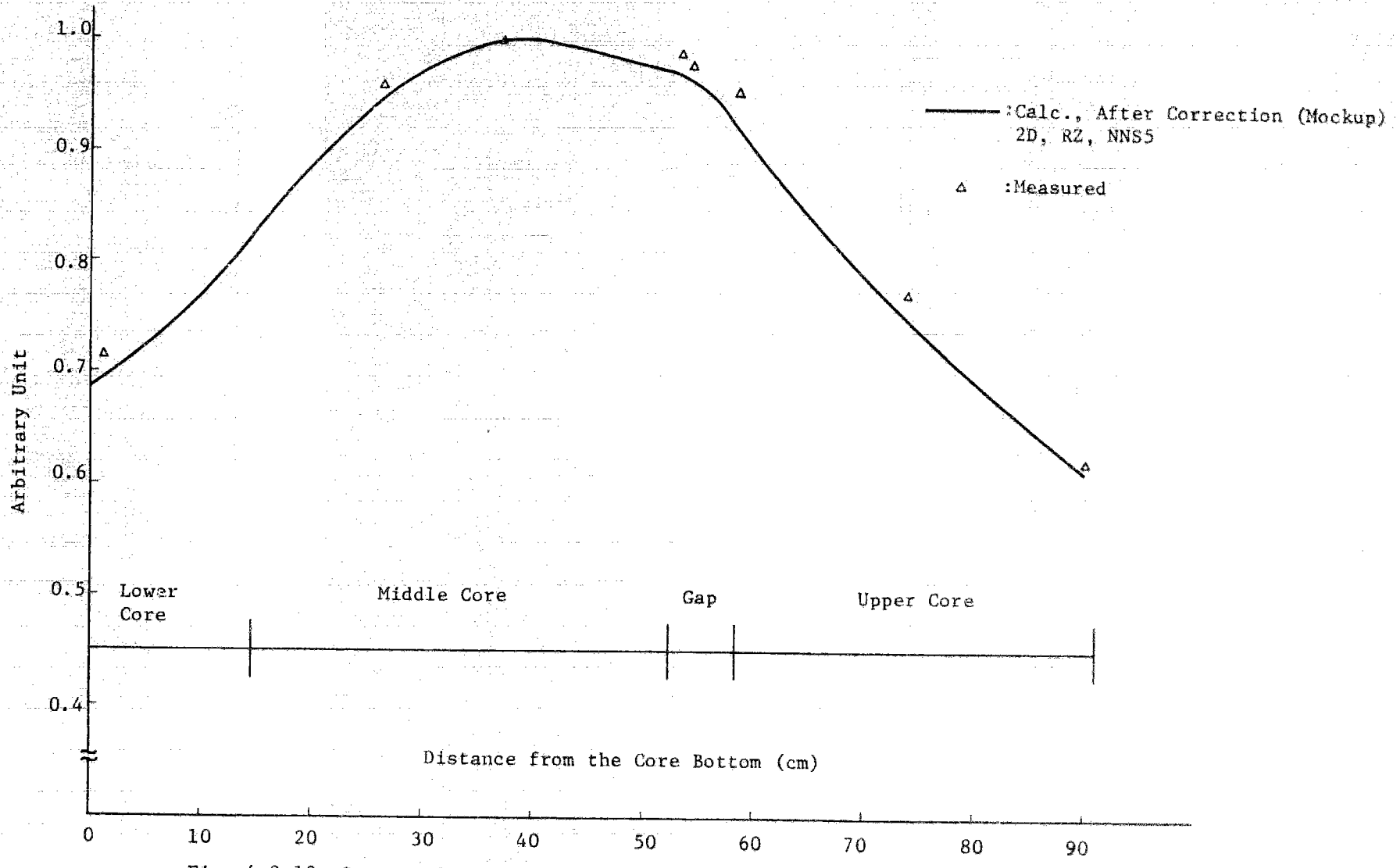

Fig. 4.2.10. Corrected Axial Fission Rate Distribution, Enriched U Foil Comparison of Calculation with Experiment, (FB Rod).

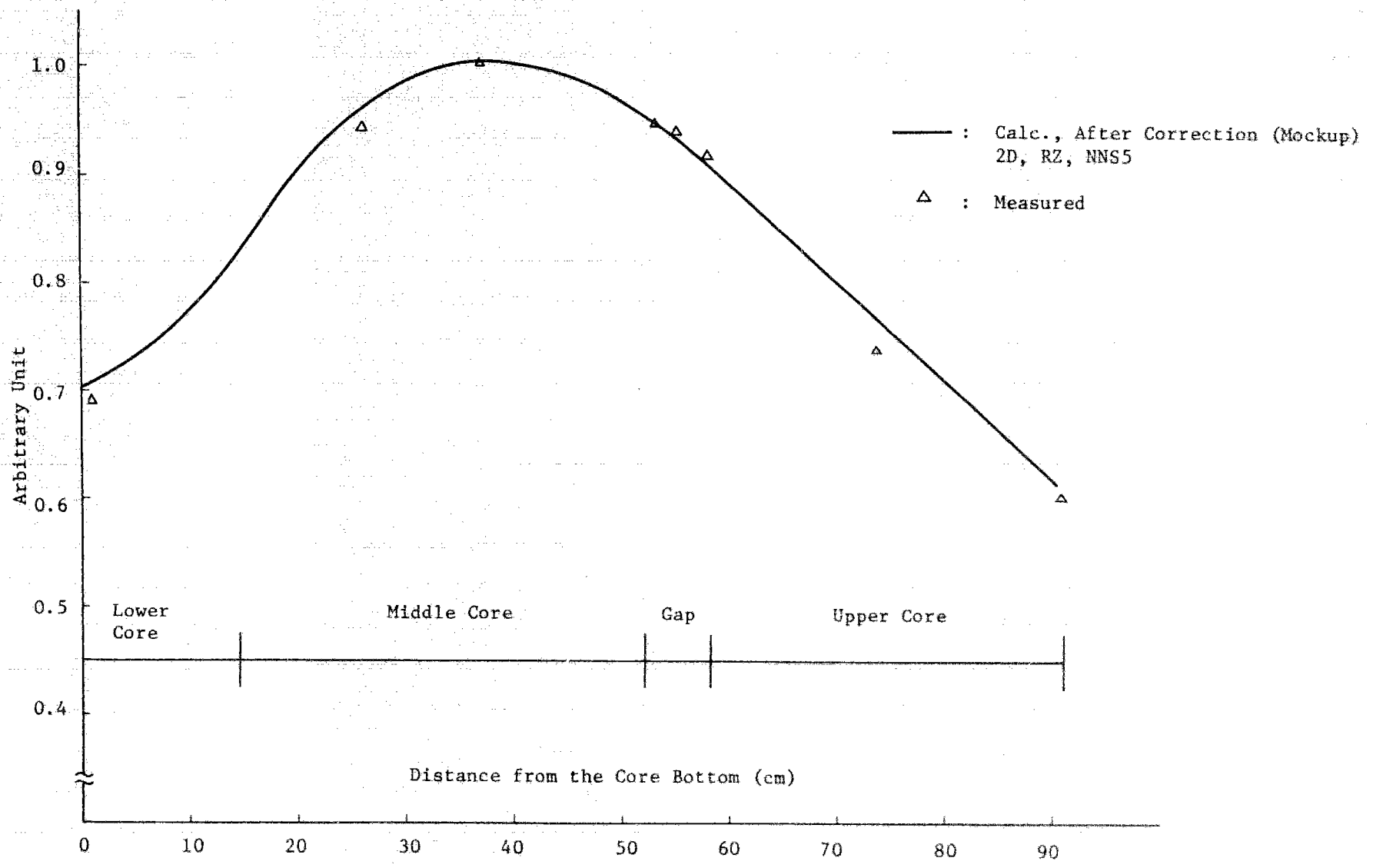

Fig. 4.2.11. Corrected Axial Fission Rate Distribution, Pu Foil Comparision of Calculation with Experiment (FB Rod).

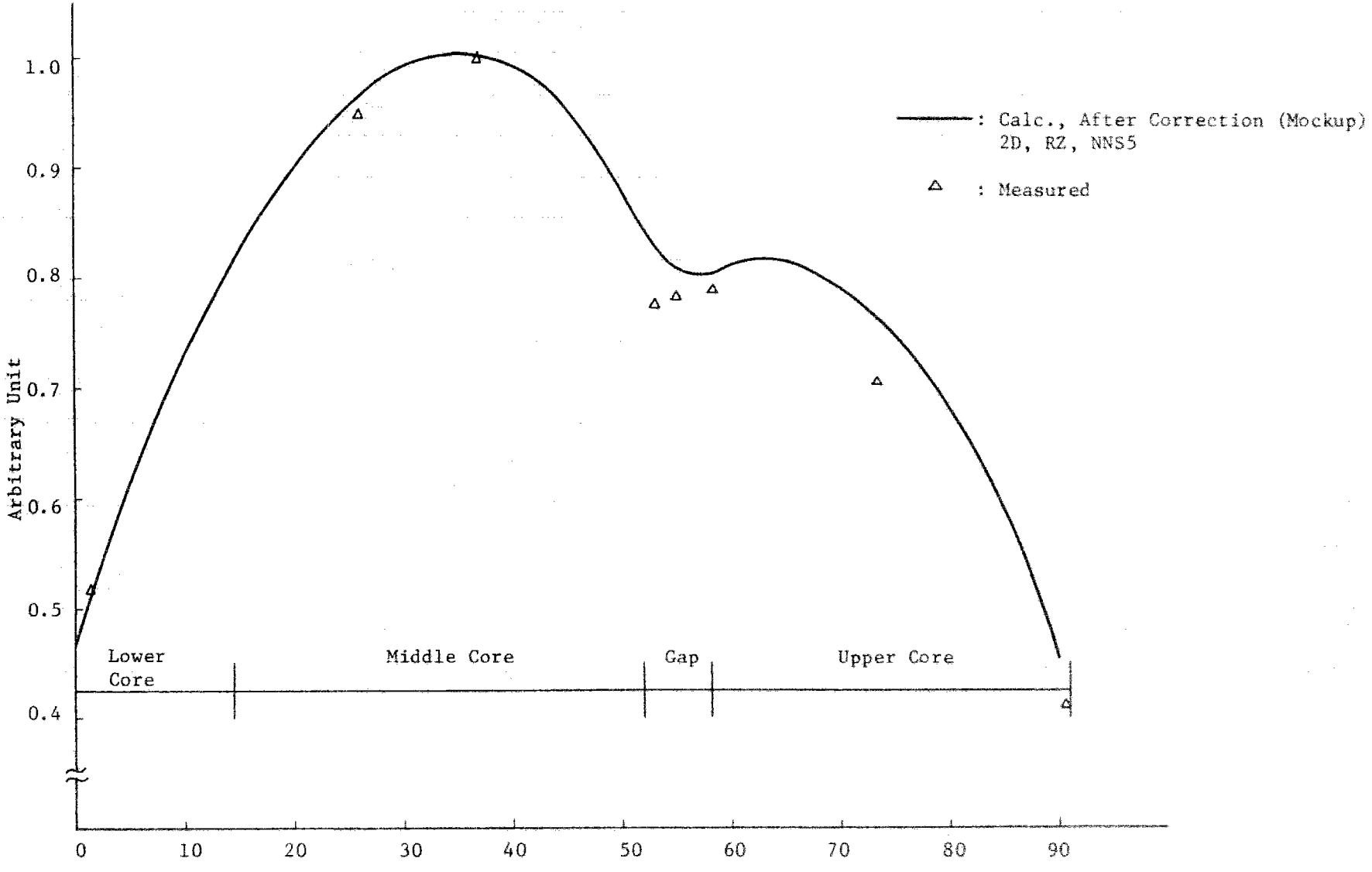

Fig. 4.9.12. Corrected Axial Fission Rate Distribution, Depleted U Foil
Comparison of Calculation with Experiment.

4.3 Material Reactivity Worth Distribution

4.3.1 An outline of experiment

On assembly I-B and assembly I-D were measured the reactivity worths of the fuel, guinea pig, BeO, B_4C, stainless steel and UO_2 rods relative to sodium at several positions in the core. These positions were such that they were not too close to the core poison rod in the core. The compositions of the rods are shown in Table 4.3.1. The element-wise compositions are shown in Table 4.3.2.

Table 4.3.1 Rod Material Volume Fraction in the Core Region

Material	Fuel Rod[1] guinea Pig	BeO Rod[4] Upper	BeO Rod[4] Lower	B_4C Rod	SS Rod	UO_2 Rod
Fuel	0.8384[2]					
UO_2						0.8384
Cladding (SS316)	0.1616	0.1745	0.3229[3]	0.1616	0.1616	0.1616
BeO		0.8255	0.5868			
SS304 or B_4C				0.4982	0.8103	
Void			0.0903		0.0281	
Shaft (SS304)				0.3402		

(1) (Pu239+Pu241)/(U+Pu) = 0.187 for fuel rods
0.250 for g. P. rods

Pu-240/Pu = 0.0824

(2) Exclusive of gap region.

(3) Includes additional SS316 inside the cladding.

(4) In the special tightener rod used for material reactivity worth measurements the BeO and void was replaced With SS304 at a smeared density of 7g/cc.

4.3.2 Calculational method and results

The perturbation calculations were made, using the flux and adjoint flux obtained by the 13-group RZ diffusion calculation. The perturbation region was a sufficiently thin ring-shaped region in a typical position in the radial direction of the core and the self-shielding factors of the samples were those for core dilution. Thus obtained values of the isotopic contributions to the reactivity were reconstructed according to the isotopic composition of each rod to obtain the reactivity worths relative to the sodium. The results are given in Table 4.3.3 and they are graphically shown, together with the measurements, in Fig. 4.3.1 through 4.3.7.

The reactivity worth of Pu fuel was somewhat over predicted in the center of the core but showed an increasingly better agreement nearer to the periphery of the core. The reactivity worth of UO_2 was under predicted in the center of the core and showed a better agreement nearer to the periphery. Similar tendencies were observed in the FCA-V core of the "JOYO" mockup, too.[10] SUS showed an agreement which was better than expected. The agreement seemed to be very bad for BeO and this was due to the fact that the positive reactivity worth of Be and the negative reactivity worth of O offset one another. The calculation accuracy was supposed to be much better for Be and O, independently. On ZPR-III-47, the SEFOR mockup, not only reactivity of BeO but also that of

Be itself was measured and this will be useful in understanding the above-mentioned situation. (Refer to para. 7.1.4.) A tendency for B_4C to be considerably over predicted was also observed in the mockup core.

Table 4.3.2 Isotopic Compositions of Test Rods (mol/Rod in Core)

	Fuel Rod	Guinea Pig	BeO Rod		B_4C Rod	SUS Rod	UO_2 Rod
			Upper	Lower			
Pu239	2.286	3.056					
Pu240	0.2053	0.2743					
U 235	0.0215	0.0257					0.0296
U 238	9.713	8.873					13.461
Be			21.13	2.88			
B 10					4.512		
B 11					11.161		
C					5.668		
O	24.33	24.33	21.13	2.88			27.117
Na							
Cr	1.728	1.728	1.1415	0.4051	6.265	10.473	1.869
Fe	6.431	6.431	4.248	1.508	22.25	36.44	6.955
Ni	1.260	1.260	0.8326	0.2955	3.412	4.882	1.363

Table 4.3.2 Rod Worth Radial Distributions, Calculated (in cents,† relative to sodium)

Radial Position (cm)	Fuel Rod	Guinea Pig	BeO Rod††	B_4C Rod	SUS Rod	UO_2 Rod
5.13	42.59	62.88	2.738	-93.76	-4.67	-19.07
16.02	37.98	55.45	2.539	-75.51	-3.67	-14.95
26.90	26.49	37.91	2.421	-48.39	-1.19	- 7.90
32.34	20.12	28.27	2.354	-34.69	0.063	- 4.33
43.22	9.66	14.82	2.406	-20.99	1.64	- 0.45

† : Keepin's delayed neutron data were used for conversion from ΔK. (β = 0.003094)

††: Relative to Stainless Steel.

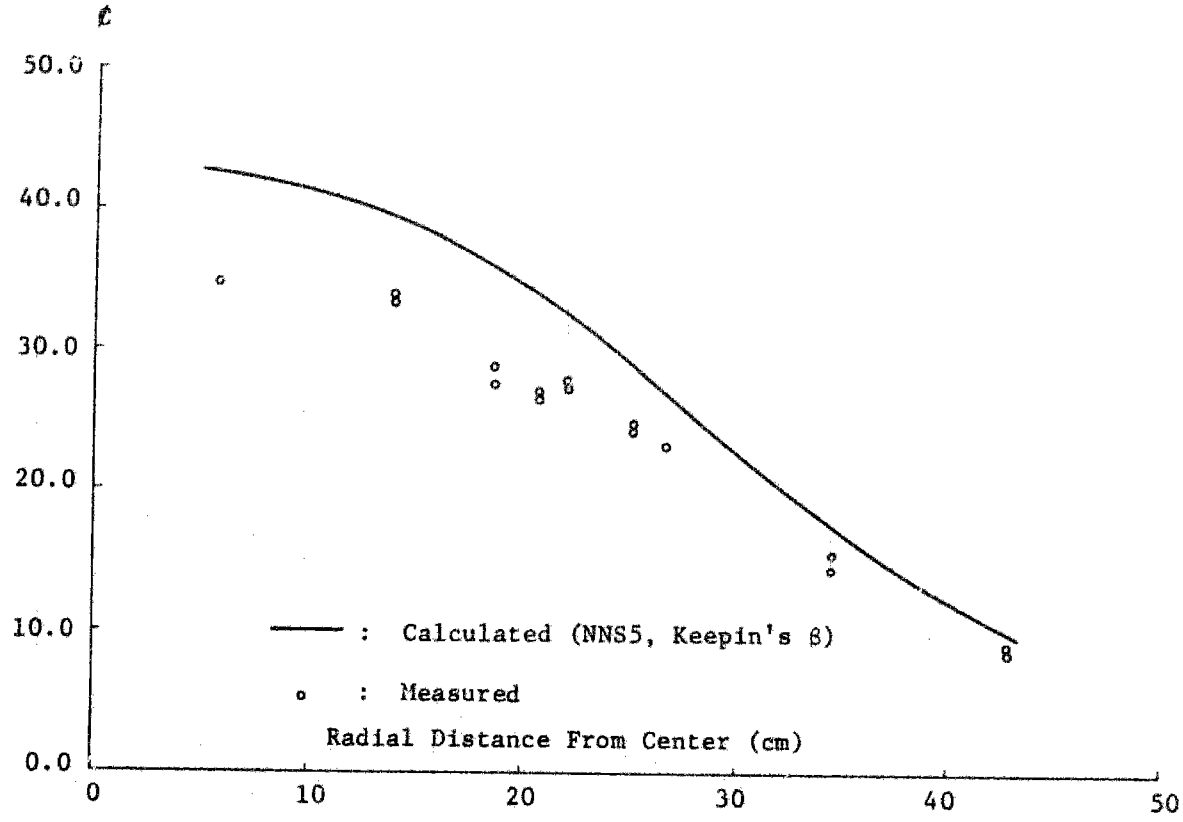

Fig. 4.3.1. Fuel Rod Worth Radial Distribution (Relative to Sodium)

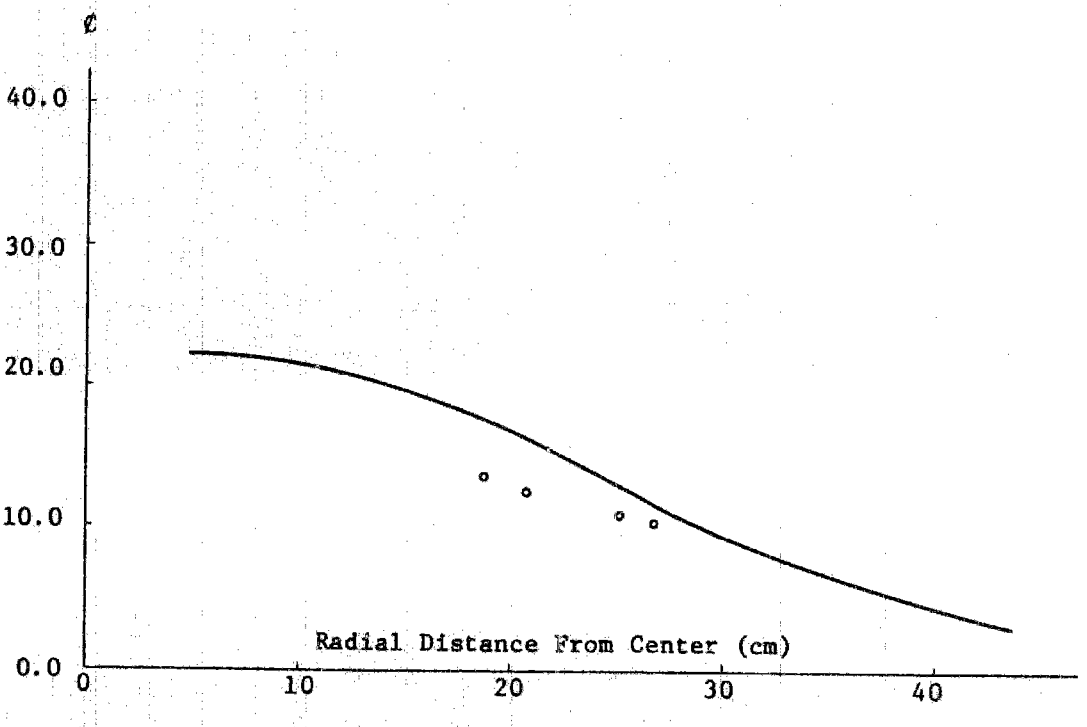

Fig. 4.3.2. Guinea Pig Rod Worth Distribution (Relative to Fuel Rod)

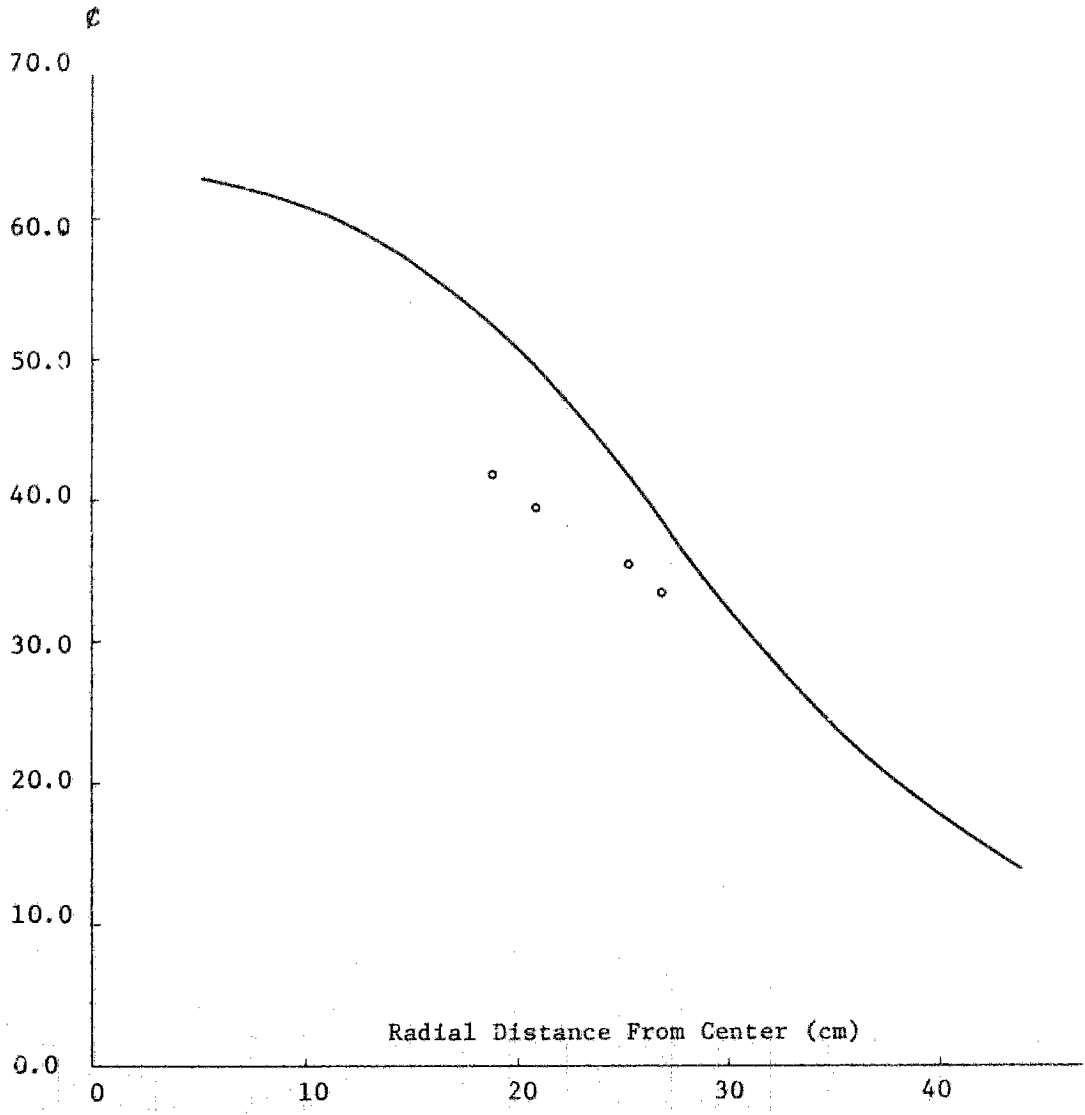

Fig. 4.3.3. Guinea Pig Rod Worth Distribution (Relative to Sodium)

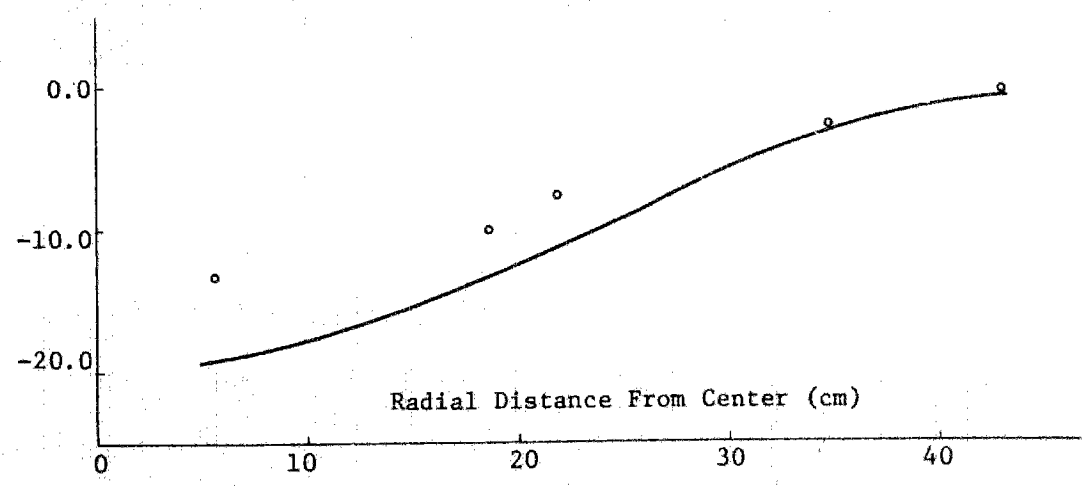

Fig. 4.3.4. UO_2 Rod Worth Distribution (Relative to Sodium)

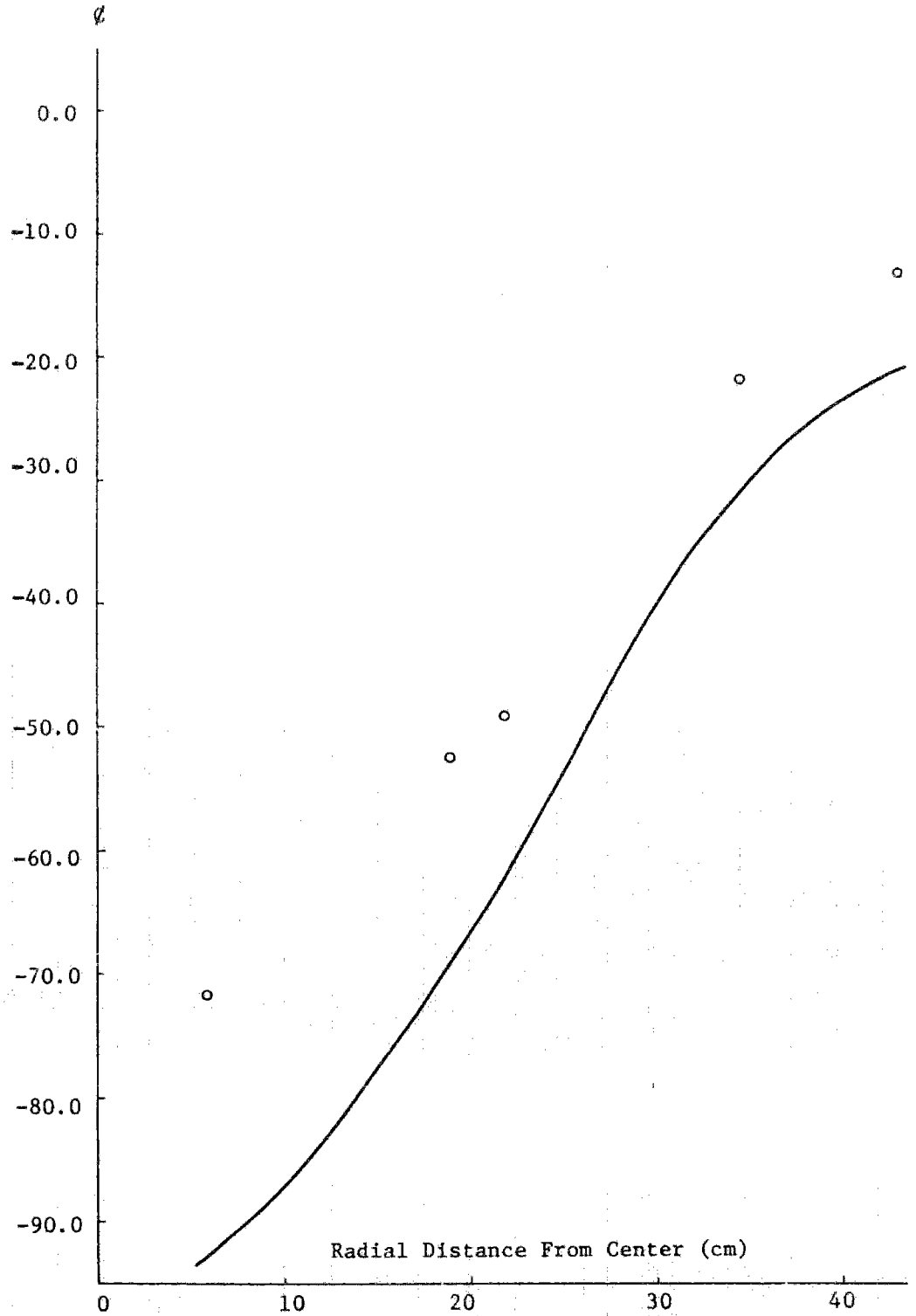

Fig. 4.3.5. B_4C Rod Worth Distribution (Relative to Sodium)

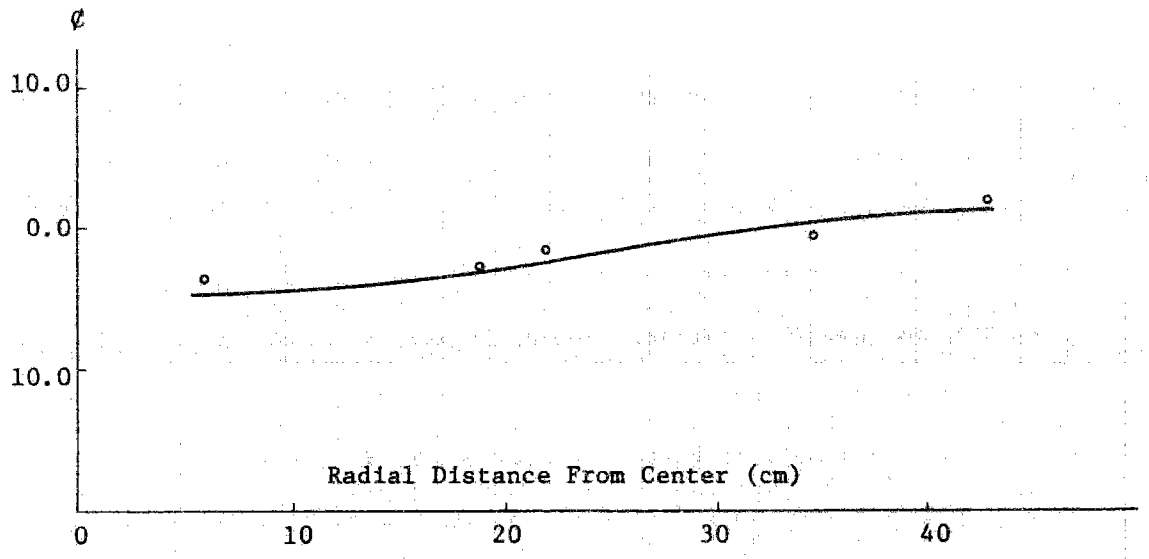

Fig. 4.3.6. Stainless Steel Rod Worth Distribution (Relative to Sodium)

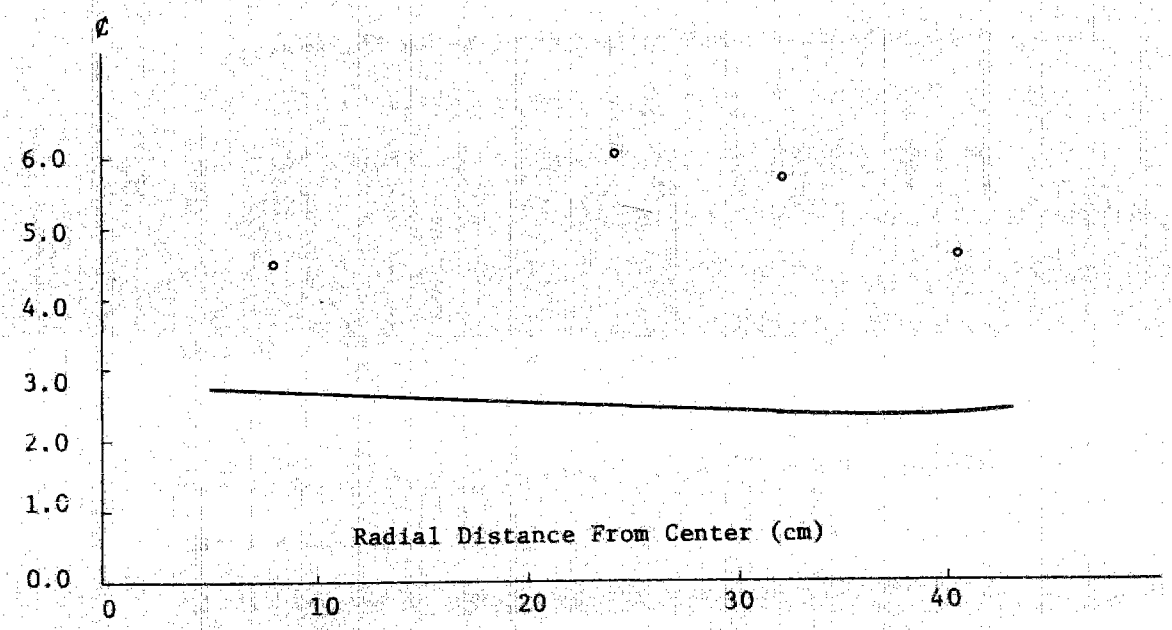

Fig. 4.3.7. BeO Rod Worth Distribution (Relative to SUS)

4.4 Isothermal Expansion Effect

When determining the temperature coefficient by increasing the temperature of sodium in the core at zero power, it is considered that the temperature distribution in the core is flat. Under such conditions the reactivity change caused by the thermal expansion of the core components including the fuel and the accompanying density variations was calculated as follows.

i) Expansion of fuel

Axial expansion:--Since the fuel of SEFOR consists of two segments when considering the axial expansion of the fuel, the changes in the total length of the fuel including the gap between the two segments of fuel and those in the width of the gap itself also must be taken into account. If H is the total length of fuel, G the width of the gap and ρ_F the fuel density, we can write as follows.

$$\frac{1}{\Delta T} \cdot \frac{\Delta K}{K} = \frac{\partial K/K}{\partial H/H} \cdot \frac{1}{H} \cdot \frac{dH}{dT} + \frac{\partial K/K}{\partial \rho_F/\rho_F} \cdot \frac{1}{\rho_F} \cdot \frac{d\rho_F}{dT} + \frac{\partial K/K}{\partial G/G} \cdot \frac{1}{G} \cdot \frac{dG}{dT}$$

$$= \alpha_F \left\{ \frac{\partial K/K}{\partial H/H} - \frac{\partial K/K}{\partial \rho_F/\rho_F} \right\} + \frac{1}{G} \cdot \frac{dG}{dT} \cdot \frac{\partial K/K}{\partial G/G} \qquad (4.4.1)$$

where α_F $\left(= \frac{1}{H} \cdot \frac{dH}{dT}\right)$ is the expansion coefficient of fuel. For the calculation of $(1/G) \cdot (dG/dT)$, we used a model in which the fuel above the gap expanded downward while moving upward as the cladding expanded.

Radial expansion:--The radial expansion of the volume of fuel was accompanied by a decrease in the density to offset one another so that their reactivity effect became zero in the homogeneous calculation.

ii) Expansion of sodium

As a result of thermal expansion, sodium increases in volume and flows out of the system. So, it would be sufficient to consider the reactivity effect of the density variations accompanying the temperature rise.

$$\frac{1}{\Delta T} \cdot \frac{\Delta K}{K} = \frac{\partial K/K}{\partial \rho_{Na}/\rho_{Na}} \cdot \left(\frac{1}{\rho_{Na}} \cdot \frac{d\rho_{Na}}{dT}\right) \qquad (4.4.2)$$

iii) Expansion of cladding

Axial expansion:--When the cladding expands in the axial direction, the resulting elongation and density decrease contribute to the changes of reactivity. However, the elongation was disregarded because it is a phenomenon which occurs where the importance is low and has little effect on the reactivity.

$$\frac{1}{\Delta T} \cdot \frac{\Delta K}{K} = \frac{V_C}{V_C+V_W+V_{TS}+V_{SR}} \cdot \left(\frac{1}{\rho_{sus}} \cdot \frac{d\rho_{sus}}{dT}\right) \cdot \frac{\partial K/K}{\partial \rho_{sus}/\rho_{sus}} \qquad (4.4.3)$$

where V represents volume and the subscripts C, W, TS and SR represent the cladding, wrapper tube, tightener sleeve and side rod, respectively.

Radial expansion:--The radial expansion of volume of cladding is offset by the decrease in density so as to have no effect on the reactivity. However, the effect of the removal of sodium by the volume expansion of SUS must be taken into consideration.

$$\frac{1}{\Delta T} \cdot \frac{\Delta K}{K} = - 2\alpha_{sus} \cdot \frac{V_C}{V_{Na}} \cdot \frac{\partial_{K/K}}{\partial \rho_{Na/\rho_{Na}}} \qquad (4.4.4)$$

iv) Expansion of wrapper tube, tightener sleeve and side rod

Axial expansion:--Only the effect of the decrease of SUS density is taken into consideration.

$$\frac{1}{\Delta T} \cdot \frac{\Delta K}{K} = - \alpha_{sus} \frac{V_W+V_{TS}+V_{SR}}{V_C+V_W+V_{TS}+V_{SR}} \cdot \frac{\partial_{K/K}}{\partial \rho_{sus/\rho_{sus}}} \qquad (4.4.5)$$

Radial expansion:--Consideration is given only to the effects of the increase in the volume of sodium inside of the wrapper tube and the decrease in the volume of sodium between the wrapper tubes due to their expansion.

$$\frac{1}{\Delta T} \cdot \frac{\Delta K}{K} = - 2\alpha_{sus} \cdot \frac{V_W+V_{TS}+V_{SR}}{V_{Na}} \cdot \frac{\partial_{K/K}}{\partial \rho_{Na/\rho_{Na}}} \qquad (4.4.6)$$

v) Expansion of grid plate

When the lower grid plate supporting the fuel assembly is expanded, the spaces among the fuel elements are widened and sodium flows in. And the volume ratio of the fuel in the system decreases due to the differences in the expansion coefficients of tne fuel and SUS. The above factors must be taken into consideration with regard to the reactivity change accompanying the expansion of the grid plate.

$$\frac{1}{\Delta T} \cdot \frac{\Delta K}{K} = -2\alpha_{sus} \left(\frac{\partial K/K}{\partial \rho_F/\rho_F} + \frac{\partial K/K}{\partial \rho_{sus}/\rho_{sus}} \right)$$

$$+ 2\alpha_{sus} \left(\frac{V_F + V_{sus}}{V_{Na}} \right) \frac{\partial K/K}{\partial \rho_{Na}/\rho_{Na}} + \alpha_{sus} \frac{\partial K/K}{\partial R/R} \qquad (4.4.7)$$

From all the above equations, we obtain the following equation.

$$\frac{1}{\Delta T} \cdot \frac{\Delta K}{K} = \alpha_F \left\{ \frac{\partial K/K}{\partial H/H} - \frac{\partial K/K}{\partial \rho_F/\rho_F} \right\} + \left(\frac{1}{G} \cdot \frac{dG}{dT} \right) \frac{\partial K/K}{\partial G/G}$$

$$+ \left(\frac{1}{\rho_{Na}} \cdot \frac{d\rho_{Na}}{dT} \right) \cdot \frac{\partial K/K}{\partial \rho_{Na}/\rho_{Na}}$$

$$+ (-\alpha_{sus}) \cdot \frac{\partial K/K}{\partial \rho_{sus}/\rho_{sus}}$$

$$+ (-2\alpha_{sus}) \cdot \frac{V_{sus}}{V_{Na}} \cdot \frac{\partial K/K}{\partial \rho_{Na}/\rho_{Na}}$$

$$+ (-2\alpha_{sus}) \left\{ \frac{\partial K/K}{\partial \rho_F/\rho_F} + \frac{\partial K/K}{\partial \rho_{sus}/\rho_{sus}} - \frac{V_F+V_{sus}}{V_{Na}} \right.$$

$$\left. \cdot \frac{\partial K/K}{\partial \rho_{Na}/\rho_{Na}} - \frac{1}{2} \cdot \frac{\partial K/K}{\partial R/R} \right\} \qquad (4.4.8)$$

The fourth term of the above equation was obtained from the equations (4.4.3) and (4.4.5) and the fifth term from the equations (4.4.4) and (4.4.6).

In making calculations by the equation (4.4.8), $(\partial K/K) / (\partial H/H)$, $(\partial K/K) / (\partial G/G)$, $(\partial K/K) / (\partial R/R)$ were obtained by use of the two-dimensional RZ 13-group calculation directly from the changes of the eigenvalues when H, G and R were changed several per cent. The results are shown in Table 4.4.1 $(\partial K/K) / (\partial \rho K/\rho K)$ and (K: Fuel, Na, SUS) were obtained by the two-dimensional perturbation calculation as shown also in Table 4.4.1.

Table 4.4.1

$(\partial K/K) \ / \ (\partial H/H)$	0.195
$(\partial K/K) \ / \ (\partial G/G)$	-0.035
$(\partial K/K) \ / \ (\partial R/R)$	0.369
$(\partial K/K) \ / \ (\partial \rho_F/\rho_F)$	0.473
$(\partial K/K) \ / \ (\partial \rho_{Na}/\rho_{Na})$	0.0122
$(\partial K/K) \ / \ (\partial \rho_{sus}/\rho_{sus})$	0.0053

The following equations were used for the linear expansion coefficients of fuel and SUS, respectively.

$$\alpha_F(T) = \frac{7.569\times10^{-6} + 5.784\times10^{-9} \cdot T}{1+7.569\times10^{-6} \cdot T+2.892\times10^{-9} \cdot T^2} \ /°C$$

$$\alpha_{sus}(T) = \frac{1.651\times10^{-5} + 7.530\times10^{-9} \cdot T}{1+1.651\times10^{-5} \cdot T+3.765\times10^{-9} \cdot T^2} \ /°C$$

The following equation (Thomson-Garelis) was used for the sodium density.

$$\rho_{Na}(T) = 0.9490-2.23\times10^{-4} \cdot T-1.75\times10^{-8} \cdot T^2$$

$$(MP \leq T \leq 640°C)$$

The quantities of α_F, α_{sus}, $(1/\rho_{Na}) \cdot (d\rho_{Na}/dT)$ obtained from these equations and those of $(1/G) \cdot (dG/dT)$ obtained directly at different temperatures are shown in Table 4.4.2.

Tab. 4.4.2 Temperature Dependent Linear Expansion Coefficients and Density Derivatives

T°C	176.66	232.22	287.75	343.33	371.11	404.44
α_F	8.5786(-6)	8.8951(-6)	9.2111(-6)	9.5268(-6)	9.6844(-6)	9.8734(-6)
α_{sus}	1.7786(-5)	1.8185(-5)	1.8583(-5)	1.8979(-5)	1.9177(-5)	1.9414(-5)
$d\rho_{Na}/(\rho_{Na}dT)$	-2.5196(-4)	-2.5761(-4)	-2.6341(-4)	-2.6938(-4)	-2.7243(-4)	-2.7614(-4)
dG/(GdT)	0.925 (-4)	0.926 (-4)	0.927 (-4)	0.939 (-4)	0.943 (-4)	0.956 (-4)

The volume ratios (area ratios) of the core components which were used in the calculations were as shown in Table 4.4.3.

Tab. 4.4.3 Volume Fractions of Materials Unit Cell

Material	Volume Fraction
Cladding	0.0987
Side Rod	0.0346
Tightener Sleeve	0.0142
Wrapper Tube	0.0755
Sodium	0.2819
Fuel	0.4951

These values were used to obtain the reactivity effect (non-Dopper effect) due to the thermal expansion and the results are shown in Table 4.4.4.

Tab. 4.4.4 Temperature Dependent Non-Dopper Effect (¢/°F)

Item \ T°F	350	450	550	650	700	760
Axial elongation of fuel	-0.092	-0.096	-0.098	-0.102	-0.103	-0.105
Density decrease in Na	-0.050	-0.053	-0.055	-0.056	-0.057	-0.058
Axial elongation of SUS	-0.002	-0.002	-0.002	-0.002	-0.002	-0.002
Radial elongation of SUS	-0.006	-0.006	-0.006	-0.006	-0.006	-0.006
Radial elongation of grid plate	-0.153	-0.160	-0.165	-0.171	-0.173	-0.176
Total	-0.303	-0.317	-0.326	-0.337	-0.341	-0.347

Note: β_{eff} = 0.00309 (Keepin)

As seen from the table, of the non-Dopper effect, the effect of the radial expansion of the lower grid plate supporting the fuel was greatest, accounting for about 50% of the total non-Doppler effects, followed next by the axial expansion of fuel accounting for about 30% of the total. The effect of the density decrease of sodium was about 15% of the total. It may be considered that

the non-Doppler effect is determined mostly by the above three factors.

4.5 Temperature Coefficients

4.5.1 An outline of experiment

Measurements were made of the temperature coefficients on the assemblies I-D, E, I and J. In this experiment, the reactor power was reduced to a very low level, the sodium temperature was raised and the reactivity changes were measured after the thermal equilibrium was reached. The measured values, together with the calculated values, are shown in Table 4.5.1.

4.5.2 Calculational method and results

The Doppler reactivity was obtained by the perturbation calculation, using the flux and adjoint flux obtained by use of the 13-group RZ diffusion calculation. The calculated values of reactivity of the whole reactor core strongly depended on the quantity of B_4C contained in the core. However, since there are many unknown things about the quantity of B_4C in the poison rod at the present time, we carried out calculations in two extreme cases. One of the models contained no B_4C at all and in the other model the inside of the cladding of poison rod was entirely occupied by B_4C. Fig. 4.5.1 and 4.5.2 show the calculated values of the Doppler reactivity changes obtained by these two models plotted in relation to the logarithms of temperature. A good linearity was obtained

by the perturbation calculation at all temperatures and also by direct calculations at relatively low temperatures (lower than about 1000°K). The Doppler coefficient calculated from the interpolated line shown in the graph are given in Table 4.5.1. In this table, the figures in the column under the heading of "Preferred" represent the quantities of B_4C (in Poison Rod, B_4C 0.4982 v/o) which are considered most likely at the present time, which were obtained from the values in the two extreme case by use of the linear interpolation method. These values were used in the calculation of the Power-Doppler reactivity which we will discuss in the following chapter.

Table 4.5.1 Calculated Doppler Coefficient in SEFOR-I-D

	B_4C Excluded	B_4C Included	Preferred
B_4C Volume Fraction in Poison Rod	0.0	0.8384	0.4982
$T \frac{dK}{dT}$ †	-0.0091	-0.0075	-0.0082

†) in °K unit

The temperature coefficients were obtained from the calculated Doppler reactivity and the calculated reactivity effect due to thermal expansion of the core and are shown together with the experimental values in Table 4.5.2. $T \frac{dK}{dT} = -C.0082$ was used in the calculations of the Doppler components.

Table 4.5.2 Temperature Coefficient in SEFOR-I-E (in ¢/°F†)

Temperature Interval	Doppler Component Calculated	Expansion Calculated	Temperature Coef.	
			Calc'd	Meas'd
350 - 450°F	-0.31	-0.31	-0.62	-0.67
450 - 550°F	-0.28	-0.32	-0.60	-0.64
550 - 650°F	-0.25	-0.33	-0.58	-0.60
650 - 760°F	-0.23	-0.34	-0.57	-0.57

†) Keepin's delayed neutron data were used for conversion from ΔK.

Fig. 4.5.3 shows the calculated reactivity decrease accompanying a uniform rise of the core temperature, which was obtained by temperature coefficient shown in Table 4.5.2, and the corresponding experimental values. The experiment was carried out on the assembly I-E loaded with 14 B_4C rods (the same number as assembly I-D). In Table 4.5.3 are shown the component-wise contributions to the Doppler reactivity change for reference.

Table 4.5.3 Component-wise Contributions to the Doppler Reactivity Change

$\frac{\Delta K}{K}$ total (300 → 2100°F)	Fission	Absorption	Leakage
-0.01478	+0.01044	-0.02535	+0.00013

4.5.3 Review

As seen from Fig. 4.5.2, the direct calculation and perturbation calculations may be assumed to produce the same results at temperatures lower than 1000°K. When the temperature rose higher than 1000°K, the reactivity decreased linearly in the perturbation calculation while the reactivity change showed a tendency to be gradually saturated in the direct calculation. The difference in the calculated values obtained by the two different methods was 2.5% at 1000°K while it was 7.5% at 2100°K. This was presumably due to the fact that the Doppler reactivity began to deviate gradually from the effective range of the reactivity changes in the perturbation calculation. A value ranging from 1.0 to 1.5% which become a problem here represents a considerably large reactivity change. This deviation of the Doppler reactivity from linearity will become a problem when the accuracy of calculation of the Power-Doppler reactivity which will be discussed in the following chapter. However, the perturbation

calculation sufficient within the range of temperatures which are of significance in the calculation of the temperature coefficients in this chapter (450°K - 680°K).

If the experimental values of the temperature coefficient at all the temperatures are averaged in order to have a general understanding of the agreement between the calculated and experimental values of the Doppler reactivity, the mean experimental value of the temperature coefficient becomes 0.619¢/°F. By subtracting the mean value of the reactivity coefficient due to expansion (obtainable only by calculation) from the above value, we obtain the Doppler component of 0.294¢/°F. Since the calculated value of the Doppler component is 0.267¢/°F, the value of C/E becomes 0.91, which may be considered to show a satisfactorily good agreement between the calculated and experimental values.

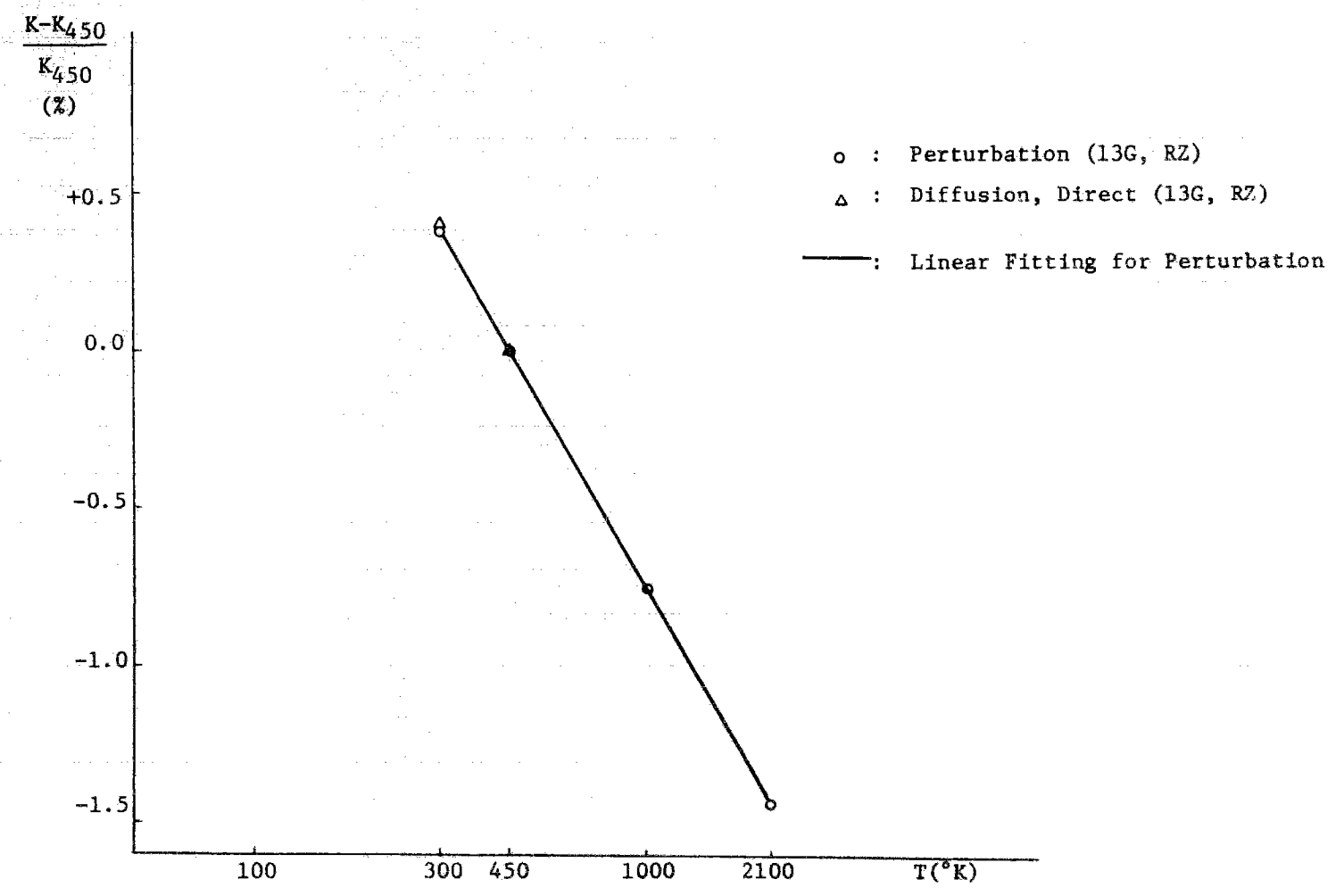

Fig. 4.5.1 Calculated Doppler Effect in SEFOR-I-D
B_4C Excluded in Calculation, NNS-5

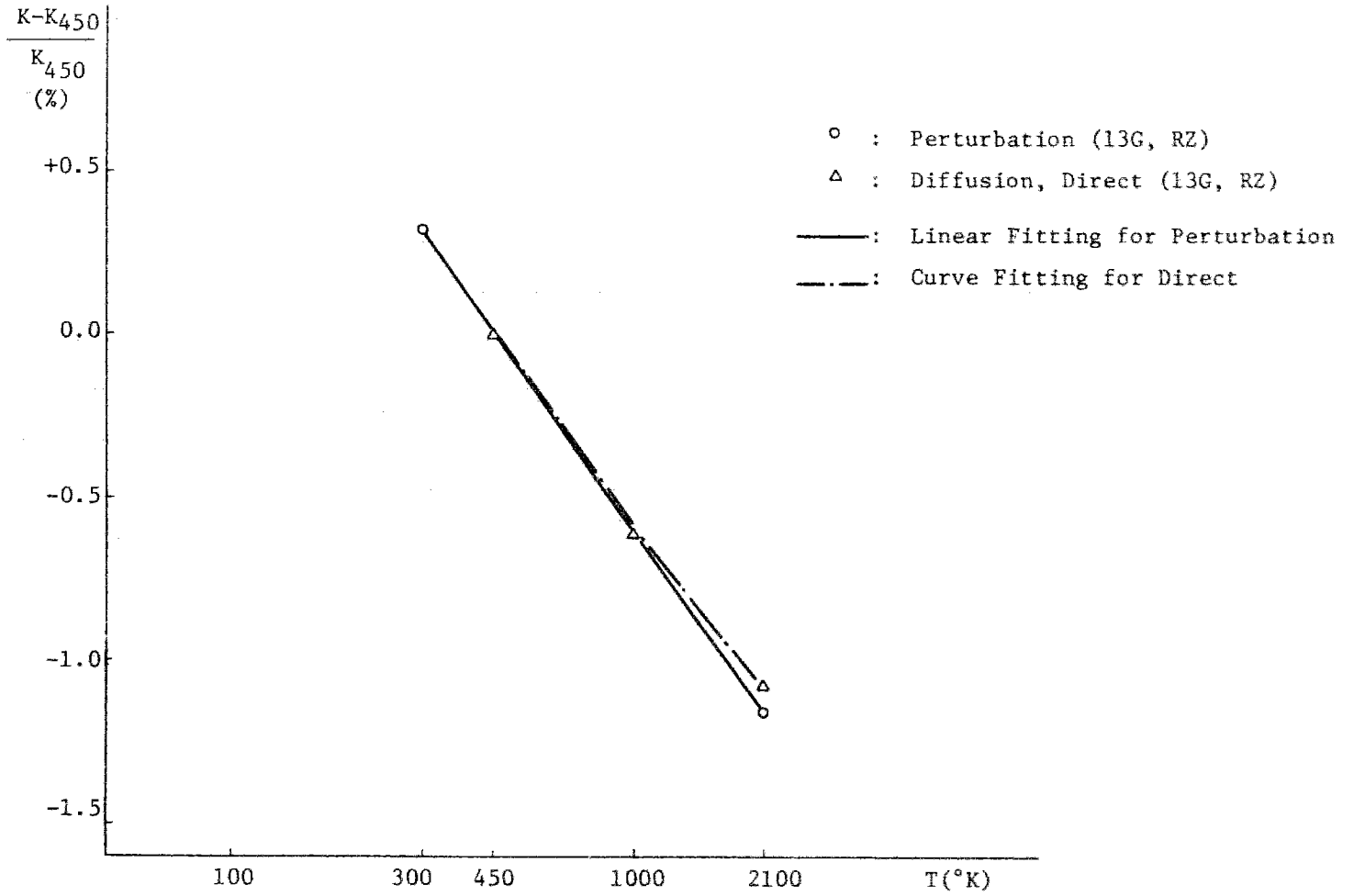

Fig. 4.5.2. Calculated Doppler Effect in SEFOR-I-D
B_4C Included in Calculation (0.8384 v/o in Poison Rod), NNS-5

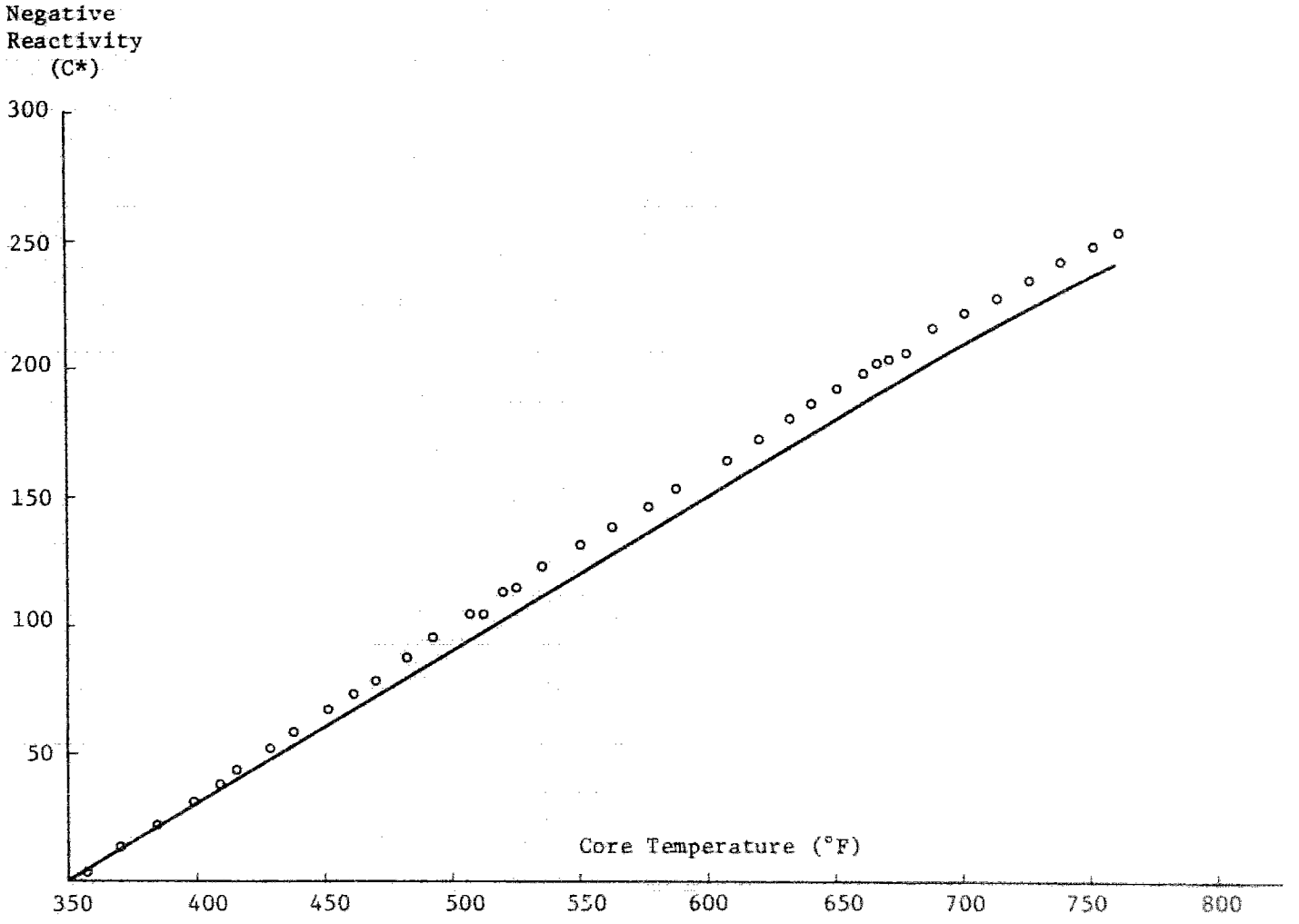

Fig. 4.5.3. Temperature Reactivity Feedback (Assembly I-E)
Doppler component was calculated using $T \frac{\alpha K}{\alpha T} = -0.0082$

*) Keepin's delayed neutron data were used for conversion.

V. Analysis of Experimental Value at On-Power Operations

5.1 Power-Doppler Reactivity

5.1.1 An outline of experiment

Measurements were made of the power-Doppler reactivity on the assemblies I-I*) and I-J**) In this experiment, the temperature of the cooling sodium was maintained constant (760°F) and the reactor power was varied (o to 5MW for I-I and 0 to 17.2MW for I-J) to measure the reactivity change from the calibration curve of the nickel reflector. The measured values are shown in Table 5.1.1.

5.1.2 Calculational method

The spatial dependence of the local Doppler coefficient Γ is supposed to be approximately in agreement with that of the product of flux and adjoint flux. Hence, we can write

$$\Gamma(r) = \frac{dk}{dT}(r) = -\frac{A(r)}{T^m} \qquad (m: \text{constant})$$

$$A(r) = \text{Const.}\ \phi(r)\ \phi^*(r)$$

Footnote:

*): 12 B_4C rods loaded.

**): 11 B_4C rods loaded.

The reactivity change δK_D due to the Doppler effect in the entire core is the integration of the local Doppler reactivity change over the whole core and therefore

$$\delta k_D = \frac{-\frac{A}{1-m}\int_{CORE}\phi(r)\ \phi^*(r)[T(r)^{1-m} - T_0(r)^{1-m}]dV}{\int_{CORE}\phi(r)\ \phi^*(r)dV} \quad (m \neq 1.0) \qquad (1)$$

$$\delta k_D = \frac{-A\int_{CORE}\phi(r)\ \phi^*(r)[\ell_n T(r) - \ell_n T_0(r)]dV}{\int_{CORE}\phi(r)\ \phi^*(r)dV} \quad (m = 1.0) \qquad (1)'$$

Assuming $\phi^*(r) \propto \phi(r)$, the equations (1) and (1)' can be rewritten as follows, using the spatial distribution of power P (r)

$$\delta k_D = \frac{-\frac{A}{1-m}\int_{CORE}[P(r)]^2[T(r)^{1-m} - T_0(r)^{1-m}]dV}{\int_{CORE}[P(r)]^2dV} \quad (m \neq 1.0) \qquad (2)$$

$$\delta k_D = \frac{-A\int_{CORE}[P(r)]^2[\ell_n T(r) - \ell_n T_0(r)]dV}{\int_{CORE}[P(r)]^2dV} \quad (m = 1.0) \qquad (2)'$$

where T(r) and To(r) represent the spatial distributions of fuel temperatures at on-power and zero-power operations, respectively. In integrating the equation (2), we used the following three methods.

1) Method I

From the radial temperature distribution $T_i(\rho)$ (ρ is the radial co-ordinate in pellet) in the fuel pellet located in the spatial region i, we calculated the following quantity.

$$\langle T_i^{1-m} \rangle = \frac{\int_{\rho=0}^{R} 2\pi\rho T_i(\rho)^{1-m} d\rho}{\int_{\rho=0}^{R} 2\pi\rho d\rho} \tag{3}$$

or

$$\langle \ell_n T_i \rangle = \frac{\int_{\rho=0}^{R} 2\pi\rho \ell_n T_i(\rho) d\rho}{\int_{\rho=0}^{R} 2\pi\rho d\rho} \tag{4}$$

Using this quantity, the integral of (2) or (2)' was replaced by the sum over i. Where R is the radius of pellet.

2) Method II

The average temperature of fuel pellet in the spatial region i was calculated as follows

$$\langle T_i \rangle = \frac{\int_{\rho=0}^{R} 2\pi\rho T_i(\rho) d\rho}{\int_{\rho=0}^{R} 2\pi\rho d\rho}. \tag{5}$$

Using this, the integral of (2) or (2)' was replaced by the sum over i.

3) Method III

Using the same $\langle T_i \rangle$ as in Method II, the average fuel temperature of the entire core was calculated as follows.

$$\bar{T} = \frac{\sum_i \langle T_i \rangle V_i}{\sum_i V_i} \tag{6}$$

where V_i is the volume of fuel in the region i.

Using this, we obtained the Doppler reactivity changes as follows.

$$\delta k_D = -\frac{A}{1-m}(\bar{T}^{1-m} - T_o^{1-m}) \qquad (m \neq 1.0) \qquad (7)$$

$$\delta k_D = -A(\ell_n \bar{T} - \ell_n T_0) \qquad (m = 1.0) \qquad (7)'$$

In this method, however, the space dependence of the local Doppler coefficient is not considered.

For all the three methods above, the core was divided into 665 R Z regions (19 regions in R dir ction, 35 regions in Z direction). Each of these regions corresponds to the above-stated region i. $T_i(\rho)$ was obtained by solving the thermal diffusion equation from the thermal power in the region i and the boundary condition that the temperature of the coolant was constant (760°F). Since was used the Doppler coefficient which was discussed in the preceding chapter, m was 1.0 in all cases.

5.1.3 Calculation results and review

The calculated values of the power-Doppler reactivity obtained by the three methods discussed in the preceding section are given in Table 5.1.2. These values are equal to the power-Doppler reactivity δk_D divided by the isothermal Doppler coefficient (whole core) A. If these values are multiplied by the Doppler coefficient, we obtain the

reactivity change in the unit of ΔK. Table 5.1.3 shows the fuel temperatures at some typical points in the core at on-power operation.

Table 5.1.2 Power-Doppler Reactivity Effect Calculated

Power (M_W)	Power-Doppler Reactivity $\delta k_D/A$		
	Method I	Method II	Method III
0.0	0.0	0.0	0.0
0.4	0.0371	0.0371	0.0275
0.8	0.0719	0.0720	0.0536
1.0	0.0884	0.0886	0.0662
2.5	0.198	0.198	0.152
5.0	0.336	0.340	0.268
7.0	0.424	0.431	0.344
10.0	0.532	0.546	0.442
15.5	0.691	0.718	0.592
17.2	0.733	0.765	0.632

Table 5.1.2 Fuel Temperature Distributions at On-Power Operation (Assembly-I-D)+

Power (M_W)	Center Z≈45cm++ R≈5		Middle Z≈45 R≈25		Boundary Z≈45 R≈40	
	Rod Center	Rod Average	Rod Center	Rod Average	Rod Center	Rod Average
0.0	760	760	760	760	760	760
1.0	1000	930	940	890	870	840
5.0	1930	1490	1650	1340	1300	1140
10.0	3140	2060	2560	1790	1840	1440
17.2	4500	2830	3810	2410	2650	1830

+) in degree Fahrenhuit ++) measured from core bottom

The power-Doppler reactivity of SEFOR was calculated from the isothermal Doppler coefficient $T\cdot\frac{\Delta k}{\Delta T} = 0.0082$ obtained from the result of the two-dimensional 13-group calculation (refer to Section 4.5) and the most accurate method I in Table 5.1.2. These calculated values, together with the experimental values, are graphically shown in Fig. 5.1.1.

The calculated values obtained by use of Keepin's delayed neutron data are approximately 12% higher than experimental values and those which are obtained by use of the data of Tomlinson and Krick & Evans are about 4% and 1% higher, respectively.

In preceding chapter 4.5.3, we stated that the C/E value of the Doppler reactivity, based on the experimental values of the temperature coefficient was 0.91. This appears to contradict

the above results (the calculated values are slightly higher). Several causes for this are conceivable and one of the main causes presumably is the deviation of the Doppler reactivity from linearity. As a matter of fact at 5MW operation the average temperature of fuel rod in the core center exceeded 1000°K and it reached 1800°K at 17MW operation. At higher temperatures, the Doppler reactivity increasingly lose its linearity and would be gradually saturated and consequently the reactivity change would be reduced accordingly. Therefore, the reactivity change is overestimated in the calculation carried out, assuming $T \cdot \frac{\Delta k}{\Delta T}$ to be constant over entire temperature range. For the deviation of the Doppler reactivity from linearity, refer to Section 4.5.3.

There were some differences in the results of Method I and Method II at high power operation but they generally agreed well with one another. On the other hand, Method III produced greatly lower values even at the low power operation than the other two methods with a high degree of accuracy. This fact suggests that it is indespenable to correctly consider the space dependence of the local Doppler reactivity when calculating the Doppler reactivity of the entire core. In a simply survey the approximation by replacing $\phi(r)\ \phi^*(r)$ by the square of power distribution seems to be satisfactorily accurate.

Table 5.1.1 Doppler Component of Measured Power-Reactivity Effects

Date (1970)	Thermal Power (MW)	Doppler Effect* (¢)
7/2	0.0	0.0
7/2	0.4	- 7.6
7/2	0.8	- 13.2
7/2	1.0	- 17.4
7/2	1.0	- 18.1
7/3	2.0	- 33.2
7/9-7/24	5.1	- 75.6
8/6-8/16	0.0	0.0
8/6	2.2	- 30.2
8/7	5.2	- 73.3
8/14	4.9	- 71.9
8/14	6.0	- 84.5
8/14	7.0	- 95.0
8/14	8.0	-105.3
8/14	9.1	-117.1
8/14-8/17	10.0	-126.1
8/23-8/30	0.0	0.0
8/23	5.1	- 71.5
8/29	10.1	-122.5
8/29	11.2	-130.3
8/29	12.5	-140.1
8/29	13.2	-146.1
8/29	14.0	-152.4
8/29	15.5	-163.2
8/29	14.8	-159.8
8/30	14.8	-158.9
8/30	15.1	-159.4
9/4	9.9	-118.0
9/5	10.1	-120.3
9/5	15.0	-159.6
9/5	15.0	-160.0
9/5	17.2	-175.7
9/5	17.2	-175.9

* Obtained from the last column of Table 6 by accounting for the calculated fuel-fuel clad axial expansion reactivity effect of -0.5¢/MW. A preliminary estimate of the standard deviation in the Doppler reactivity values is ±2.0¢ or 5% whichever is larger. The preliminary estimate of the standard deviation in power is ±0.3MW or 5% whichever is larger, for power level > 2MW.

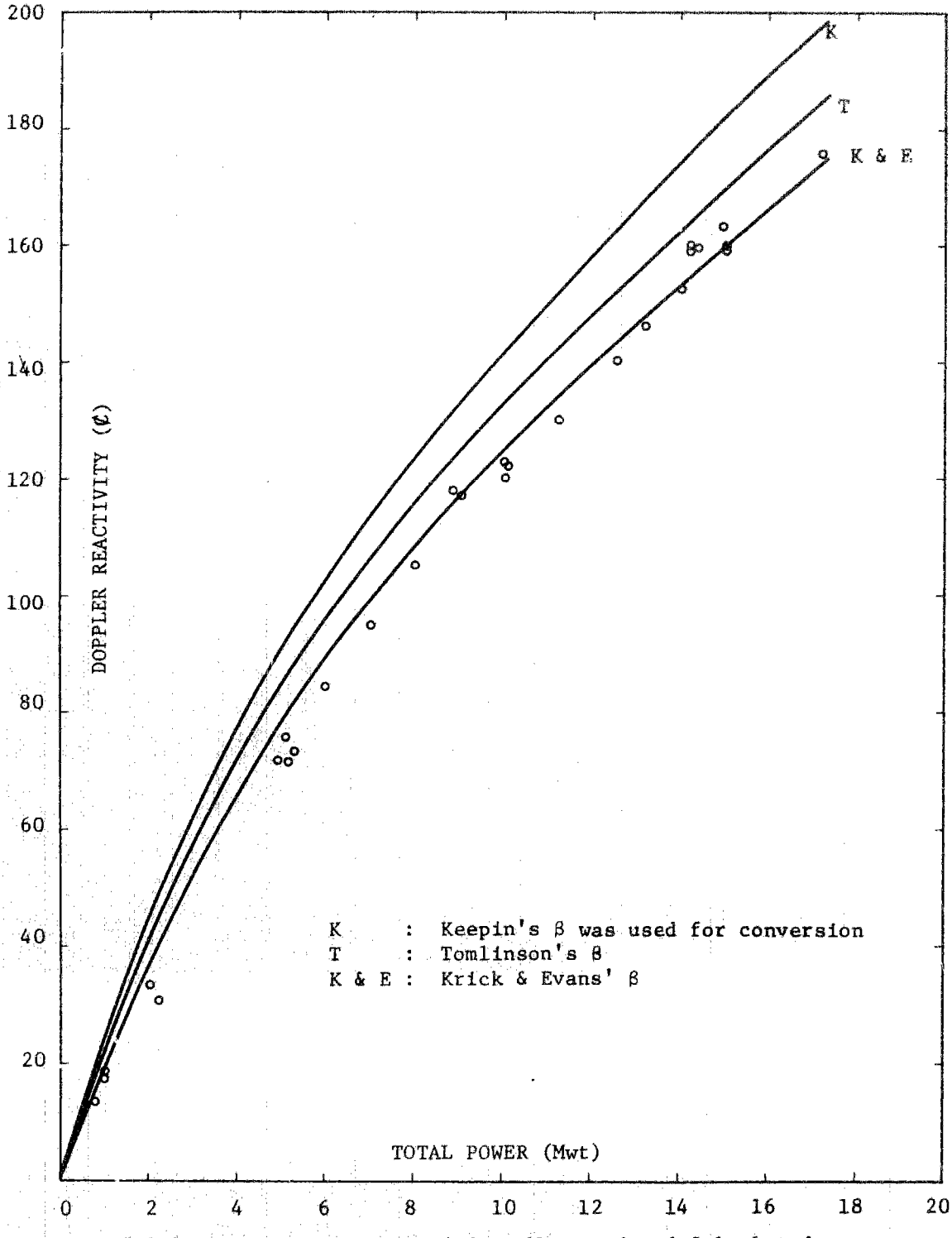

Fig. 5.1.1. Doppler Power Reactivity, Measured and Calculated, B_4C (0.4982 Volume Fraction in Poison Rod)
$T\frac{\Delta K}{\Delta T}$ = 0.0082 (2Dim, RZ Perturbation, NNS-5)

VI. Evaluation of Doppler Reactivity Analysis

6.1 Problems about the group constants

o In this analysis we used mainly NNS-5 nuclear constants set. As was discussed Chapter III, the C/E of the minimum critical mass was 1.013, showing a very good agreement. No problem arose because the excess reactivity of the minimum critical core was small but if the excess reactivity is large the corrected eigenvalues will have a certain width depending on which of β source data to be used as seen in the case of I-D core. This fact must be taken into consideration when checking the group constants in respect to the critical mass. From β source data, the C/E of ℓ_p/β_{eff} are distributed within the range from 0.935 to 0.825. Keepin's data brought C/E closest to 1. As for the reactivity worth of the fuel rod near the core center, C/E was so large as 1.22, showing a poor agreement between the calculated and experimental values. It is considered necessary to make a study about the calculation method to be used before considering the above problem, directly relating it with the problem of the group constants set. The C/E of the spectrum index was nearly 1.00, showing a very good agreement.

o Next, we carried out the 25-group one-dimensional cylindrical calculations in order to see the differences in the eigenvalue change at different temperatures depending on the nuclear constants set employed. Thus obtained results are shown in Table 6.1. A graph in which the logarithms of temperature are

located on the horizontal axis and K_{eff} values on the vertical axis is shown in Fig. 6.1. In this graph, however, in order to make the difference of the gradient easier to see, the values of K_{eff} at 300°K are normalized to the NNS-5 value at 300°K. JAERI·FAST set gives almost no difference in K_{eff} at 300°K and 450°K and K_{eff} dropped almost linearly with $\ell_n T$ higher than 450°K. The reason is not clear at the present moment. The values of $(K_{T_1} - K_{T_2})/\ell_n(T_1/T_2)$ at temperatures ranging from 300°K to 2100°K are shown in Table 6.2. At temperatures ranging from 300°K to 450°K, NNS-5 gave the Doppler coefficient about 25% higher than that which was given by ABBN and it also gave a value about 8.5% and 18% higher than ABBN and JAERI·FAST-2, respectively, at temperatures ranging from 450°K to 900°K. These relationships were reversed at temperatures higher than 900°K but the values showed a generally stabilized gradient except for the values obtained by NNS-5 at temperatures ranging from 1500°K to 2100°K. The temperatures used in this study ranged from 450°K to somewhere around 680°K on the average for the whole system in the experiments at zero power operation and they ranged from 680°K to about 1300°K at power operation, coming into the temperature range of 450°K to 1500°K. Such being the case, if the comparison is made roughly between the average values obtained by the different sets of nuclear constants at 450°K to 1500°K, NNS-5 ABBN and JAERI·FAST-2 will give such values as -0.0066, -0.0063 and -0.0060, respectively, so that the disparities between the highest and lowest values are ±5% at most.

At 450°K to 900°K, however, it is possible to produce a disparity of somewhere around ±11 as shown in Table 6.2.

o In order to compare the measured values and calculated values of Doppler coefficients, it is necessary to evaluate the reactivity effect due to the thermal expansion of the entire core. However, the reactivity effect due to thermal expansion is difficult to evaluate accurately and the values generally have a considerable width due to the temperature dependent experimental formulae for the linear expansion coefficient and the expansion elements to be considered. This width is estimated to be about 20% from the results of various trial calculations. At zero operation, the Doppler reactivity and the reactivity effect due to thermal expansion are of the magnitude of the same order and therefore the uncertainty of C/E arising from the reactivity effect due to thermal expansion is estimated to be about 10%. At high power operation, since the thermal expansion effect is only 5% of the total at most (approx. -0.5 ¢/MW), the uncertainty arising from thermal expansion is negligible. Hence, if the nuclear constants set is to be checked from the standpoint of the Doppler coefficient, it is conceivable to do so in the form of the power coefficient. However, this method is not necessarily appropriate because various assumptions are used in the process of calculating the power coefficient. (5.1) Such being the case, in this study we compared the isothermal experimental values and calculated values at zero power operation.

Table 6.1 K_{eff} Values Versus Temperature Using Various Cross Section Sets (25G 1 Dim. diffusion)

T°K	T°F	NNS-5	ABBN	JAERI.FAST-2
300	80.6	1.019705	1.072539	1.038846
450	350.6	1.016597	1.070204	1.038829
900	1160.6	(1.01175)	1.065767	(1.03489)
1500	2240.6	1.008619	1.062610	1.031551
2100	3320.6	1.006972	1.060494	1.029370

Note: Values in parentheses are graphically interpolated.
These values were calculated using number densities 2**. (see Tab. 2.3.2) (direct calculation)

Table 6.2 Tdk/dT Values Using Various Cross Section Sets (25G 1 Dim. diffusion)

Temperature Interval (°K)	NNS-5	ABBN	JAERI·FAST-2
300 - 450	-0.0077	-0.0058	-0.00004
450 - 900	-0.0070	-0.0064	-0.0057
900 - 1500	-0.0061	-0.0062	-0.0065
1500 - 2100	-0.0049	-0.0063	-0.0065

Note: These values were calculated using number densities 2**. (see Tab. 2.3.2) (direct calculation)

Fig. 6.1. k_{eff} vs $l_n T°K$ Curves

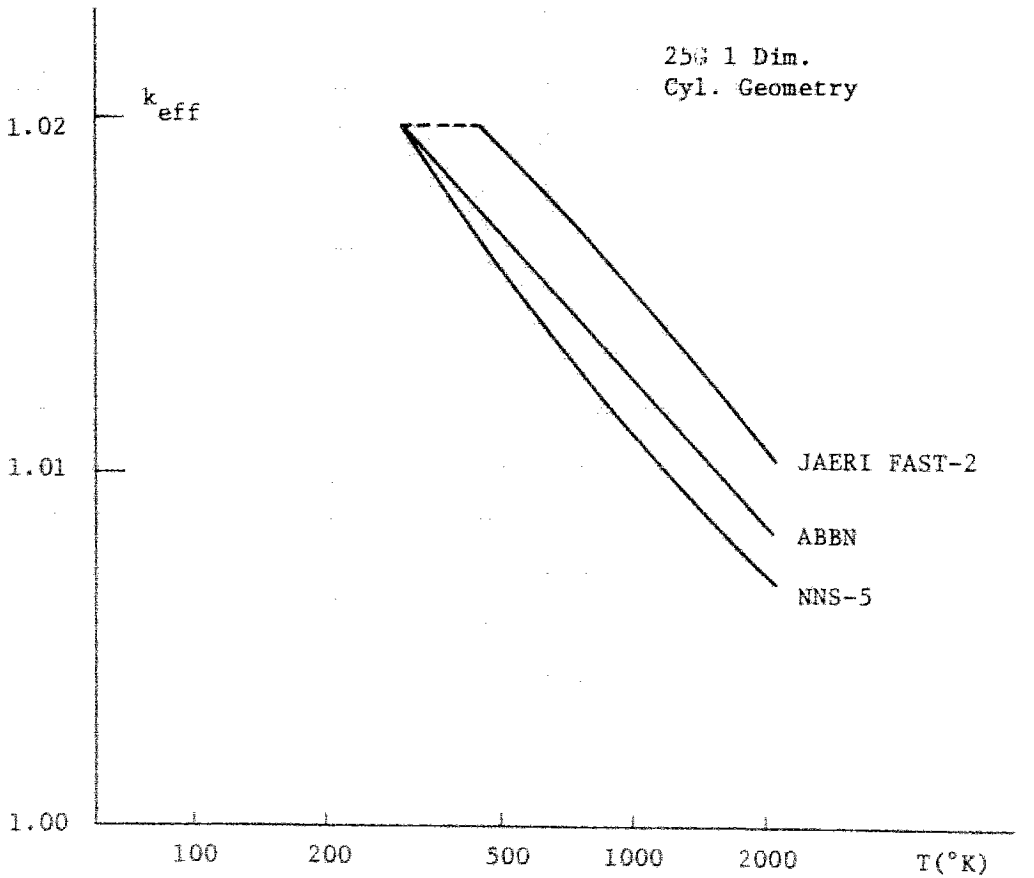

6.2 Problems about Analysis Model

6.2.1 Analysis of experimental values at zero power operation

In the case of zero power experiments, when measuring the temperature coefficient, the temperature of sodium was raised outside the core and two to three hours elapsed before the measuremer s were actually started. Therefore, we constructed the thermal expansion model, assuming the core had completely reached the thermal equilibrium, and obtained good results. Since the reactivity effect due to thermal expansion is the same order in magnitude to the Doppler reactivity effect, if this is not correctly evaluated, large errors will be introduced into the Doppler reactivity to be derived from the measured values of the temperature coefficient.

The results of the preliminary analysis revealed that the effect of heterogeneity on the Doppler reactivity was almost negligible. So, we did not try to make a detailed study on this problem.

6.2.2 Analysis of experimental values at on-power operation

In this case, we carried out calculations on a model constructed on the assumption that the temperature distribution in the core was proportional to the power distribution. We used a power distribution which was obtained from the 13-group RZ calculation. As shown in Section 4.2, the calculated values of the fission rate distributions of Pu^{239} and U^{235} were so widely deviated from the experimental values near the boundary in the

core that it could not be said that a good approximation was obtained. We think we should have used the calculated values of the power distribution after correcting them by the C/E of the fission rate distribution in the mockup core. However, as is presumable from the equation (2) in Section 5.1, the results will remain little changed even if the above operation is done.

The ratio of the effect of expansion at on-power operation to the total reactivity effect decreased as the power increased and amounted to less than 5% at 20MW. So, this is not much problem. However, if this problem is to be strictly considered, we found that it would be difficult to construct model for the calculation of the axial elongation of the fuel of the two-division type in particular because the temperatures of the fuel, cladding, coolant and structures differed greatly.

VII. Analysis of Doppler Experiments on Critical Assemblies

7.1 ZPR-III Assembly 47 (SEFOR mockup)

7.1.1 Calculation system and method

The details of the experimental system and measurements are given in "Compilation of Fast Critical Experiments, Vol. 5" (compiled by Tokyo Shibaura Electric Co., Ltd., to be published in March 1973). So, in this study we will discuss the simplified calculational system set up for the analysis of the central sample Doppler experiment.

The SEFOR mockup experiments carried out by use of ZPR-III involved experiments on three kinds of cores, i.e. the one-segment core (Assembly 47, Loading 15), the two-segment core (Assembly 47A, Loading 30), and the three-segment core (Assembly 47A, Loading 43). Since the central sample Doppler reactivity had been measured in the one-segment core, the analysis here will be restricted to the R-Z calculational model of one-segment core. The actual drawer loading is considerably non-uniform and complicated but here we employed a simplified model in which the drawer composition was region averaged. The R-Z calculational system and the region averaged atomic number densities are shown in Fig. 7.1.1 and Table 7.1.1, respectively.

In carrying out the calculations, we used the 13-group two-dimensional R-Z diffusion code based on NNS-5 set and the

perturbation calculation code. The group division of the 13-group set was the same as that which was used in the SEFOR calculation which had been used up to the preceding chapter. The division was as follows.

2/4/6/8/10/11/12/13/14/15/16/17/25

The mesh division used in the two-dimensional calculation is also shown in Fig. 7.1.1. The contraction from the 25-group NNS-5 set to 13 groups was done by use of the neutron spectrum obtained by the one-dimensional cylindrical calculation. The one-dimensional cylindrical calculational system was nothing but the radial region on the mid-plane of the two-dimensional system and the same mesh division as in the two-dimensional calculation was used. However, as for the spectra to be used for the contraction in Region 5 (axial reflector) and Region 6 (axial Na-steel) in the R-Z system, we used the spectra which were used in Region 3 (radial Na-steel) and Region 4 (radial reflector) in the one-dimensional calculation. As for the axial buckling, we used the one-group value $B_Z^2 = 2.31 \times 10^{-4} cm^{-2}$ by mistake and obtained as one-dimensional eigenvalue K = 1.051. The two-dimensional eigenvalue was K = 0.9822, the axial buckling in the core by one-group contraction $B_Z^2 \approx 7 \times 10^{-4} cm^{-2}$ and the axial buckling in the axial reflector was $5.5 \times 10^{-4} cm^{-2}$. (This B_Z^2 corresponds about 15 cm of reflector saving).

However, two-dimensional calculations were made by the

13-group set and therefore the effect of the contraction spectra was presumably small. So, we did not carry out re-calculations by correcting the values of buckling used in the one-dimensional calculation.

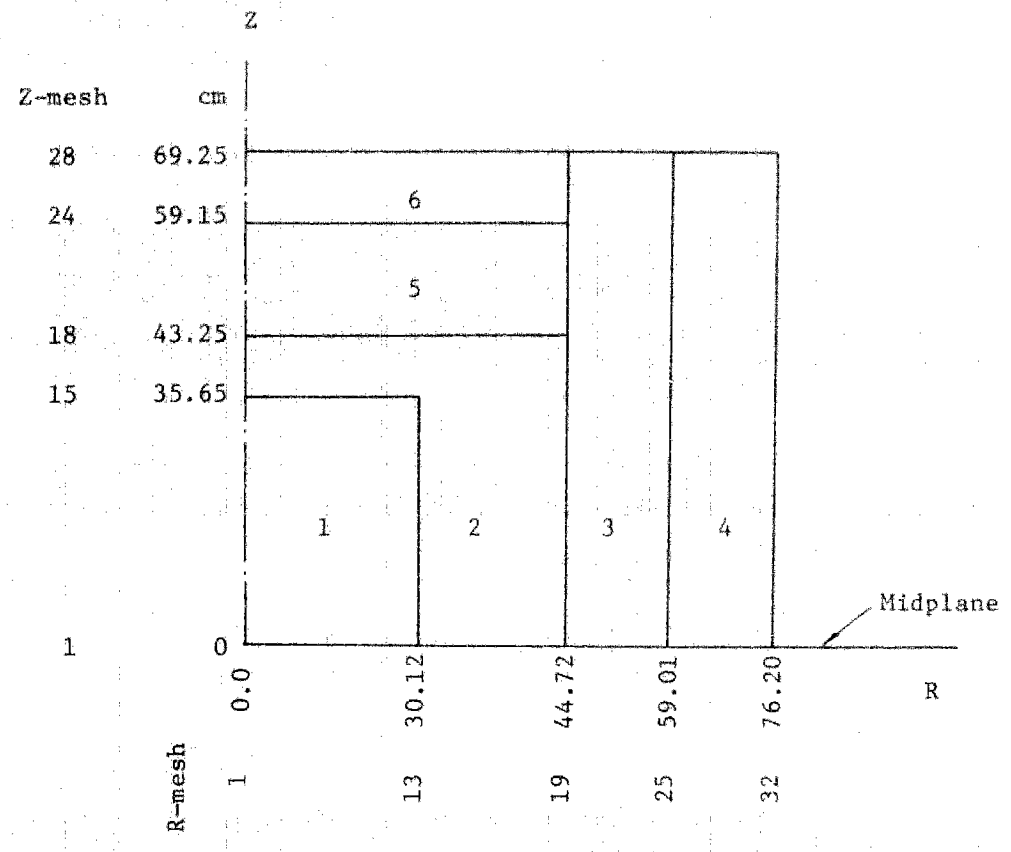

Fig. 7.1.1 R-Z Calculational Model of ZPR-III Assembly 47, Ldg. 15

Compositions : 1. New Pu core, 2. Oil Pu core
3. Radial sodium-steel, 4. Radial Ni reflector
5. Axial Ni reflector, 6. Axial sodium-steel

Mesh Divisions :

R-mesh	ΔR, cm	Outer Radius, cm	Z-mesh	ΔH, cm	Height, cm
1 - 13	2.510	30.12	1 - 15	2.546	35.65
13 - 19	2.433	44.72	15 - 18	2.533	43.25
19 - 25	2.382	59.01	18 - 21	2.517	50.80
25 - 32	2.456	76.20	21 - 24	2.783	59.15
			24 - 28	2.550	69.35

Table 7.1.1 Average Atomic Compositions of ZPR-III Assembly 47, Loading 15 (One-Segment Core). (10^{22} atoms/cc)

	Core (New Pu) 1	Core (Old Pu) 2	Radial Na/SS 3	Radial Reflector 4(Ni)	Radial Reflector 7(SS)	Axial Reflector 5	Axial Na/SS 6
$Pu^{239+241}$	0.1480	0.1513					
Pu-240	0.0132	0.0072					
U-235	0.0015	0.0015					
U-238	0.7742	0.7893					
Be	0.5680	0.5413					
C	0.3359	0.3359				0.1755	0.3761
O	1.5663	1.5287					
Na	0.6628	0.6601	0.6156				
Al	0.6986	0.7723	0.0491	0.6160	0.6116	0.5335	1.0758
Cr	0.2579	0.2816	0.4253	0.1181	1.2385	0.3190	0.7049
Mn	0.0158	0.0172	0.0260	0.0072	0.0758	0.0195	0.0432
Fe	0.9847	1.0748	1.6235	0.4510	4.7278	1.2177	2.6909
Ni	0.1398	0.1526	0.2304	6.5881	0.6710	4.5325	0.3819
Mo	0.0515						

Note: Composition of SOS-304 were assumed as 69.7 W/O Fe, 17.0 W/O Cr, 10.4 W/O Ni and 1.1 W/O Mn.

7.1.2 Effective multiplication factor, kinetic parameter, etc.

Effective Multiplication Factor:

The value obtained by the homogeneous and diffusion calculations with R-Z geometry (NNS-5 set) was K = 0.9825, the measured value was 1.000 but the excess reactivity was 0.030% ΔK. The above calculated value needs the following corrections.

(i) Difference between the calculational system and experimental system

The loaded mass of the core was 314.31 kg in Pu-fissile in the actual system and in the calculational system it was 323.7 or 2.9% larger. So, the effective multiplication factor required a negative correction of about 0.5% ΔK. This difference in the loaded mass was caused because the radius of the horizontal section of the as-built system was taken, not because the transformation into an equivalent-area cylinder for the radius of the outside core of the calculational system.

(ii) Effects of smoothing of the core boundary

These effects cause the necessity of a negative correction of the calculated value but the correction is probably not very large. These effects are not experimentally measured.

(iii) Effects of homogenization in each region

No calculations of these effects were made because the drawer loading was so complicated.

(iv) Heterogeneity effects of the plate in the drawer

No calculations were made. The calculated value obtained by

GE was +0.3% ΔK but this value seems to be slightly too small from the comparison of the value of the heterogeneity effect in SEFOR-I-C calculated by us and the similar value calculated by GE.

(v) Transport theory correction

No calculations were made. It is estimated at about +1% ΔK in view of the results of calculation made on SEFOR-I-C core.

If the above corrections are made, the calculated value of the effective multiplication factor is estimated to be $0.99 \lesssim K \lesssim 1.00$. No further detailed study was made of the effective multiplication factor because the experimental system was so complicated and the objective of this analysis was the analysis of the sample Doppler experiments.

Kinetic Parameter:

The calculated values and measured values are compared in Table 7.1.2.

Table 7.1.2 Comparison of Calculated and Measured ℓ/β Value for ZPR-III Assembly 47

Calculated (Keepin's beta)			Measured
ℓ_p, μsec.	β_{eff}, 10^{-3}	ℓ_p/β_{eff}, 10^{-4}sec.	ℓ_p/β_{eff}, 10^{-4}sec.
0.6367	3.168	2.01	2.05

Note: The beta data of Tomlinson and Krick-Evans give ℓ/β = 1.88 and 1.77 (in 10^{-4} sec.), respectively.

The calculated value of Inhour/(% $\Delta K/K$) is as follows.

Ih/(% $\Delta K/K$ = 989.8 (beta data of Keepin)

= 929.3 (beta data of Tomlinson)

= 886.8 (beta data of Krick and Evans)

7.1.3 Central spectrum, spectrum index and reaction rate distribution

Table 7.1.3 shows the normalized neutron spectrum at the core center, which was obtained by the 13-group R-Z diffusion calculation and it is graphically shown in Fig. 7.1.2. The group-wise contributions of B-10 absorption rate are shown in Table 7.1.4 for reference.

A strong neutron absorption occurred at 200 eV ∿ 400 KeV, indicating the spectrum is actually considerably soft. The absorption below 100 eV and over 400 KeV was about 10% of the total.

Table 7.1.5 shows a comparison of the calculated values and measured values of the spectrum index at the core center. The values obtained by GE are also shown for reference. Since there was a disparity of about 10% between the measurements of F^{28}/F^{25} by use of the counter and the radiochemical measurements thereof and the plate heterogeneity was not taken into consideration in the calculations, it was difficult to make a precise comparison of the calculated values and measured values but it may be safely said that the C/E ratio is satisfactorily within 1.0 + 0.1.

The calculated and measured values of Z axial fission rate distributions of ^{239}Pu, ^{235}U and ^{238}U and ^{10}B absorption rate distribution are shown in Table 7.1.6 and Fig. 7.1.2 through 7.1.5. Similar measurements were also made in the radial direction but the distribution was greatly distorted because of the considerably high degree of nonuniformity in the core that it was not much significant to compare the measured values with the values calculated on a simple and clean model. The measured distribution of ^{10}B absorption rate in Fig. 7.1.5 suggests the possible mistake in the plotting of the counter position in the original reference. So, the plot obtained by shifting the counter position by 2 inches is also given in the same figure. From the overall comparison of the calculated and measured values, it was found that the calculated values underestimated the reaction rate distribution by about 20% from the top end of the core to the inside of the axial reflector. A tendency to make such an underestimation in the non-uranium reflectors including the iron reflector has occurred to a greater or less extent in the analysises so far made in the United States and Germany. A similar tendency was also observed when we analyzed the results of experiments carried out on FCA-V-2-R (JOYO Mark 2 core mockup), ZPR-III-54 and ZPPR-1 assemblies.

Table 7.1.3 Normalized Neutron Spectrum and Adjoint Spectrum at the Core Center of ZPR-III Assembly 47 (13-group R-Z Diffusion Calculation, NNS-5 Set)

Group	E_L	Δu	$\bar{\phi}_i \Delta u$	$\bar{\phi}_i$	$\bar{\phi}^*_i$	$\frac{\phi^*_i \phi_i \Delta u}{\sum \phi^* \phi_i \Delta u}$
1	4.0 MeV	0.96	0.0137	0.0143	1.330	0.01705
2	1.4	1.05	0.0856	0.0815	1.233	0.0985
3	0.4	1.26	0.2159	0.1713	1.078	0.2172
4	0.1	1.38	0.2810	0.2036	1.047	0.2746
5	21.5 KeV	1.54	0.2172	0.1410	1.001	0.2029
6	10.0	0.77	0.0741	0.0962	1.000	0.0692
7	4.65	0.77	0.0452	0.0586	1.041	0.0439
8	2.15	0.77	0.0190	0.0247	1.106	0.0197
9	1.0	0.77	0.0249	0.0324	1.164	0.0271
10	465 eV	0.77	0.0141	0.0183	1.310	0.0173
11	215	0.77	0.00593	0.00770	1.386	0.00767
12	100	0.77	0.00237	0.00308	1.507	0.00334
13	0.215	6.16	0.00101	0.00016	1.818	0.00171
		Sum	1.0000			1.0000

*) Adjoint spectrum was normalized to 1.0 at 6-th Group.

Table 7.1.4 Normalized B-10 Absorption Rate at the Core Center of ZPR-III Assembly 47

Group	E_L	Δu	α_a(B-10), barns	$\alpha_{ai}\bar{\phi}_i\Delta u$	$\alpha_{ai}\bar{\phi}_i$
1	4.0 MeV	0.96	0.3877	0.0053	0.0056
2	1.4	1.05	0.4240	0.0363	0.0346
3	0.4	1.26	0.5501	0.119	0.0943
4	0.1	1.38	1.416	0.398	0.288
5	21.5 KeV	1.54	2.893	0.628	0.408
6	10.0	0.77	4.989	0.369	0.480
7	4.65	0.77	7.293	0.329	0.428
8	2.15	0.77	10.72	0.204	0.265
9	1.0	0.77	15.78	0.393	0.511
10	465 eV	0.77	23.24	0.266	0.346
11	215	0.77	34.19	0.203	0.263
12	100	0.77	50.32	0.119	0.155
13	0.215	6.16	158.9	0.161	0.0261
				Sum($\bar{\alpha}_a$) =	3.231

Table 7.1.5 Central Reaction Rate Ratios in ZPR-III Assembly 47. Comparison of Calculation with Measurement

	Measured		Calculated	
	Counter	Radiochemical	Present	GE*)
$\sigma_f^{28}/\sigma_f^{25}$	0.0264 ± 0.0005	0.0242 ± 0.00021	0.0230	0.0243
$\sigma_f^{28}/\sigma_f^{25}$	1.45 ± 0.02		1.352	
$\sigma_f^{49}/\sigma_f^{25}$	0.916 ± 0.015		0.875	0.87
$\sigma_f^{40}/\sigma_f^{25}$	0.209 ± 0.003		0.192	0.159
$\sigma_c^{28}/\sigma_f^{25}$		0.137 ± 0.010	0.129	0.124
$\sigma_c(Mn)/\sigma_f^{25}$		0.0358 ± 0.008	0.0445	

*) A.B. Reynolds et al., ANL-7320, pp. 569-585 (1966)

Table 7.1.6 Calculated Axial Reaction Rate Traverse in ZPR-III Assembly 47

Z Mesh Point	Z, in (approx.)	$Pu^{239}(n,f)$	$U^{235}(n,f)$	$U^{238}(n,f)$	$B^{10}(n,\alpha)$
1	0	1.000	1.000	1.000	1.000
5	4	0.962	0.963	0.963	0.963
7	6	0.917	0.917	0.916	0.917
9	8	0.854	0.854	0.853	0.855
11	10	0.776	0.777	0.772	0.779
12	11	0.732	0.734	0.725	0.737
13	12	0.686	0.689	0.674	0.695
14	13	0.638	0.644	0.618	0.655
15	14	0.591	0.601	0.556	0.634
16	15	0.547	0.564	0.486	0.617
17	16	0.515	0.543	0.406	0.634
18	17	0.535 (0.608)	0.557	0.309	0.758
19	∿18	0.785	0.662	0.217	1.086
20	19	0.867	0.696	0.153	1.251
21	20	0.865	0.673	0.108	1.274
22	∿21	0.782	0.595	0.0733	1.164
23	∿22	0.637	0.478	0.0498	0.949
24	23	0.476	0.337	0.0330	0.709
25	24	0.379	0.267	0.0248	0.564
26	25	0.279	0.197	0.0184	0.413
27	26	0.178	0.126	0.0133	0.259
28	27	0.0760	0.0551	0.0091	0.103

Table 7.1.6a Comparison of Measured and Calculated Axial Reaction Rate Distributions in ZPR-III Assembly 47

Z, Inches (approximate)	Pu^{239}(n, f)		U^{235}(n, f)		U^{238}(n, f)	
	$E_{xp.}$ *	Calc.	$E_{xp.}$ *	Calc.	$E_{xp.}$ *	Calc.
0	1.00	1.00	1.00	1.00	0.99	1.00
2	0.98		0.99		1.01	
4	0.97	0.962	0.97	0.963	0.98	0.963
6	0.94	0.917	0.92	0.917	0.97	0.916
8	0.88	0.854	0.85	0.854	0.915	0.853
10	0.80	0.776	0.78	0.777	0.81	0.772
12	0.745	0.686	0.71	0.689	0.72	0.674
14	0.68	0.591		0.601	0.61	0.556
15	0.65	0.547	0.65	0.564	0.565	0.486
17 core boundary	0.71	(0.535 0.608	0.69	0.557	0.385	0.309
19	0.90	0.867		0.696		0.153
20	0.92	0.865		0.673	0.15	0.108
21	0.83, 0.86	0.782	0.725	0.595	0.08	0.0733
22	0.75	0.637		0.478		0.0498
23 reflector boundary	0.61	0.476	0.51	0.337		0.0330
25	0.46	0.279	0.35	0.197		0.0184
27 Na-steel boundary	0.30	0.076	0.20	0.0551	0.015	0.0091

*) Read from graphs

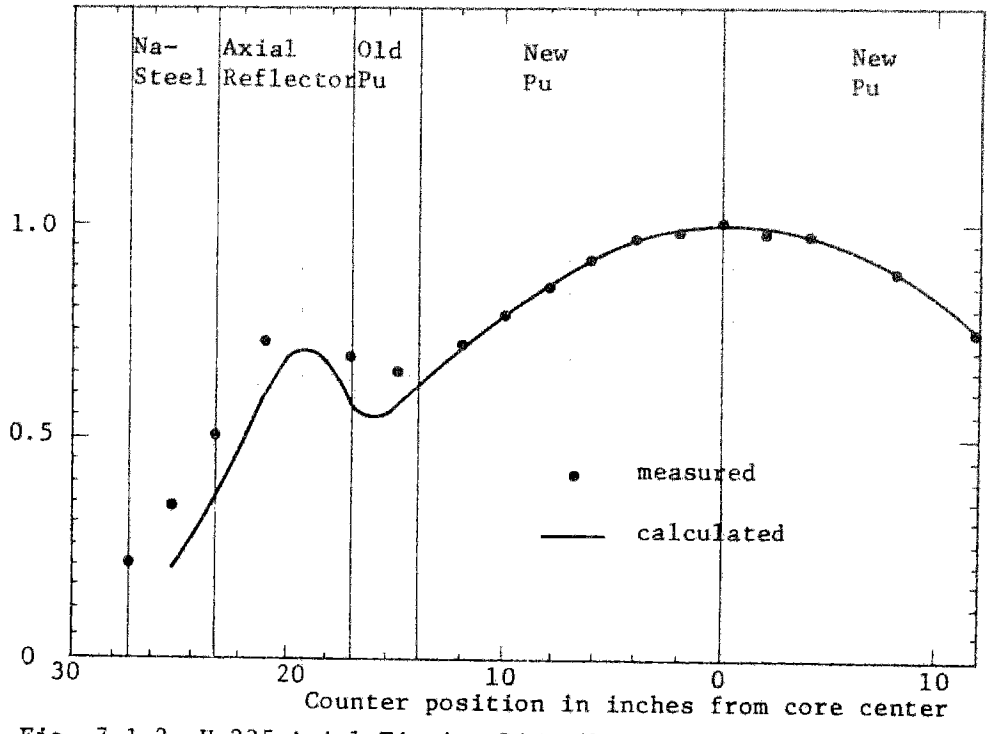

Fig. 7.1.2. U-235 Axial Fission Distribution in ZPR-III Assembly 47 Ldg. 15

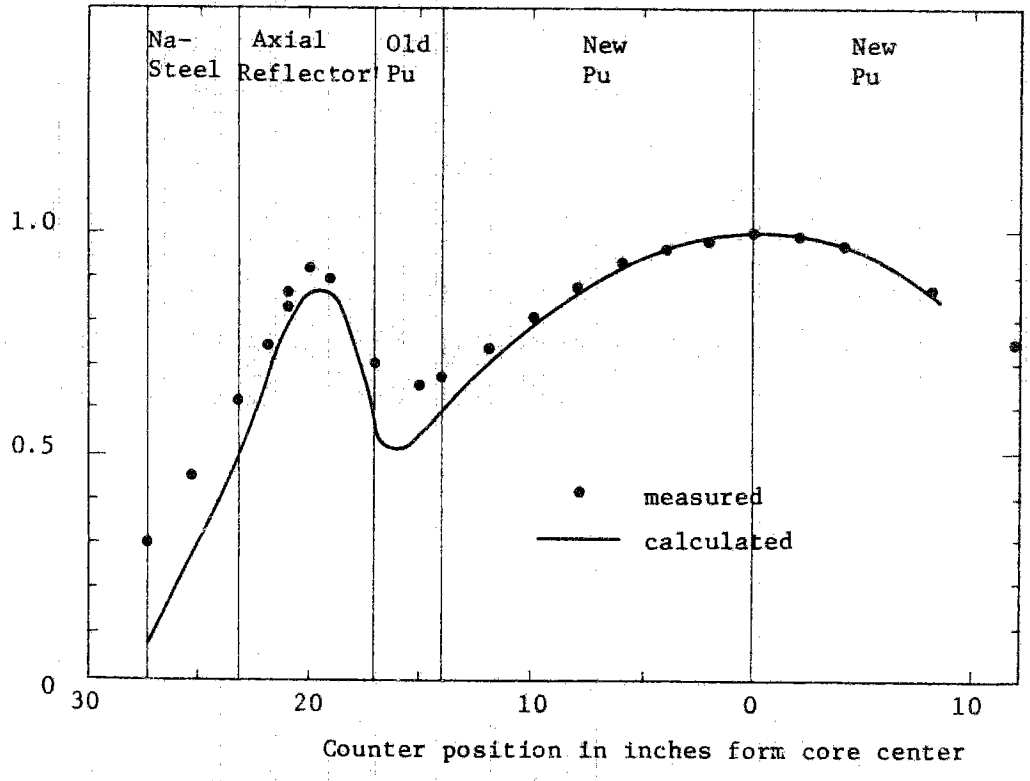

Fig. 7.1.3 Pu-239 Axial Fission Distribution in ZPR-III Assembly 47 Ldg. 15

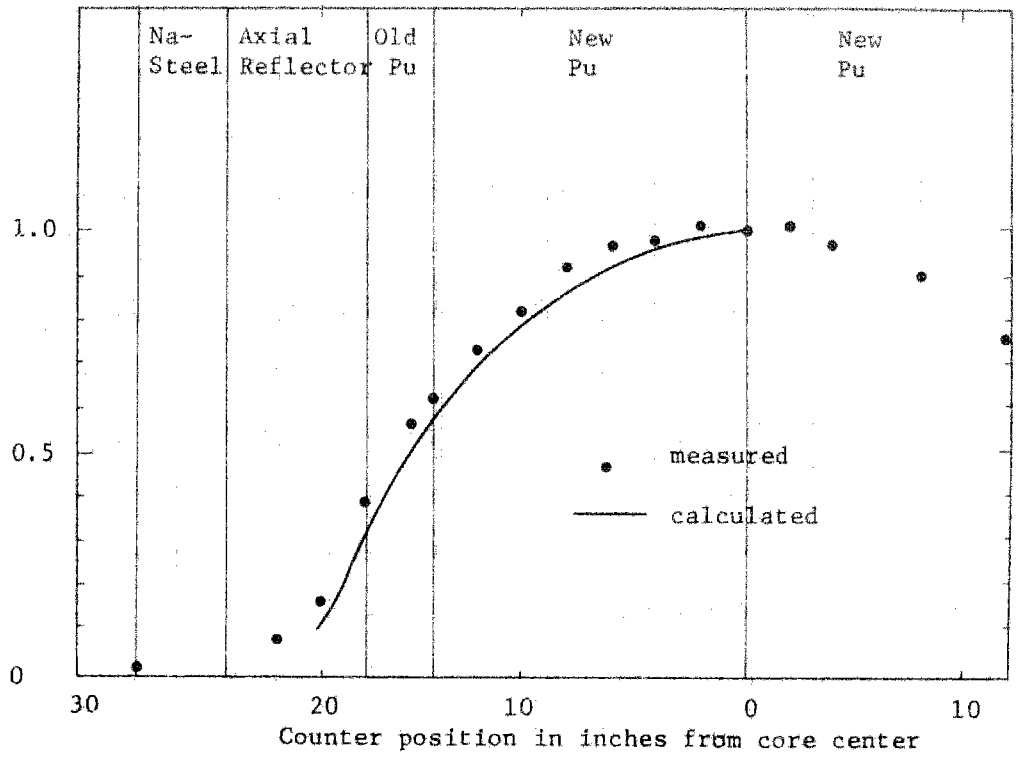

Fig. 7.1.4. U-238 Axial Fission Distribution in ZPR-III Assembly 47 Ldg. 15

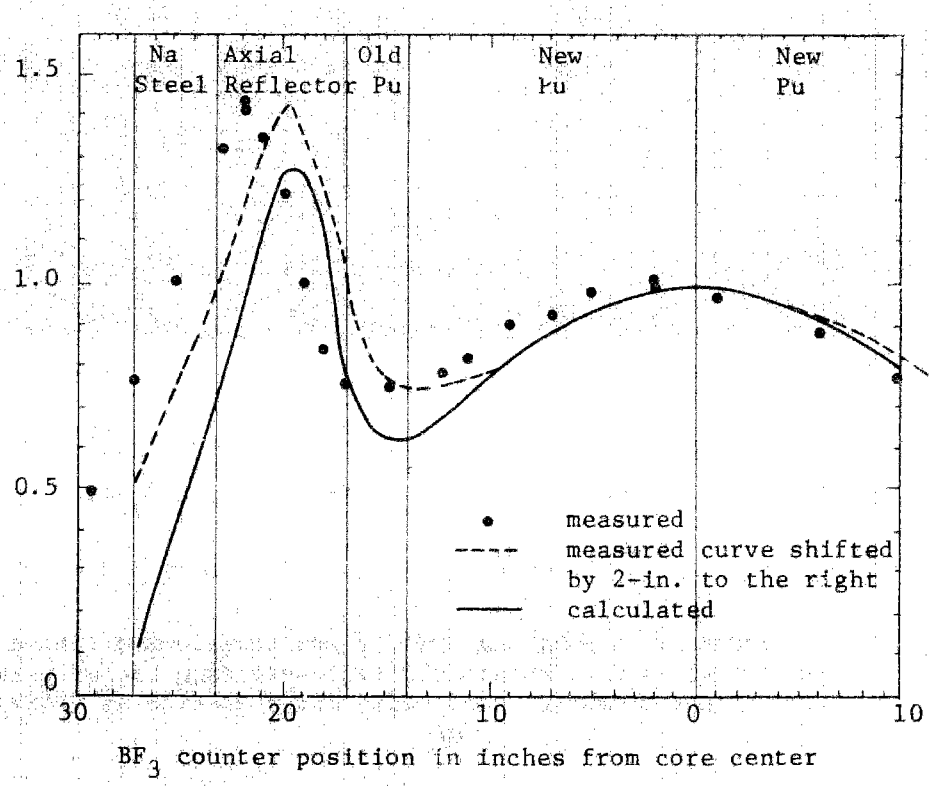

Fig. 7.1.5 BF_3 Counter Axial Traverse in ZPR-III Assembly 47 Ldg. 15

7.1.4 Central sample reactivity

The calculated conversion factor from the central perturbation cross section (barn) to the reactivity worth per 10^{24} atoms is 6.053×10^{-4}. This value, however, can have several percent of deviation because of the differences in the loaded mass between the calculational and the actual system and of the transformation into an equivalent homogeneous system including the heterogeneity effect. The calculated values of the material perturbation cross sections at the core center are shown in Table 7.1.7. The self-shielding factor of resonance, except for Ta, was obtained for core dilution.

Table 7.1.7 Central Perturbation Cross Sections in ZPR-III Assembly 47

Element	σ_P, barns	Element	σ_P, barns
Pu-239	3.668	Aℓ	-14.5 (-3)
Pu-240	0.467	Cr	-17.6 (-3)
Pu-241	6.157	Mn	-95.1 (-3)
U-235	2.968	Fe	-18.8 (-3)
U-238	-0.234	Ni	-29.5 (-3)
U-233	4.708	B-10	-3.441
Be	+10.71 (-3)	B-11	-2.86 (-3)
C	-1.34 (-3)	Nb	-0.386
O	-3.48 (-3)	Mo	-0.211
Na	+0.740(-3)	Ta*	-1.042

*) A sample of Ta weighing 1004.0g was transformed into a spherical form to obtain the self-shielding factor with the excess potential scattering cross section as $S/4NV_0$.

Table 7.1.8 shows the comparison of the measured and calculated values of the central material reactivity worth. A brief description of the sample material composition is given in Table 7.1.8 (Supplement). From Table 7.1.8, we can find the following things.

(i) As for the fissile element, C/E = 1.2 - 1.3. This is presumably to be regarded as an example of the central reactivity discrepancy.

(ii) C/E of absorbers such as B-10, Mn, Mo and Ta is about 2. In the case of Ta, the sample size was considered for S/4V in calculating the self-shielding factor of resonance. But result suggests that it is also necessary to take into consideration a spatial flux depression in the case of a soft spectrum as this core.

(iii) C/E of BeO was so high as 2.4 presumably because of the discrepancy between the component worths of Be and O and the offsetting of one another. For example, in calculation the reactivity worth of BeO 1 kg comprised Be: +15.45 Ih and O: -5.02 Ih. However, if the reactivity worth of Be is corrected by E/C = 33.2/42.9 of the reactivity worth of independent metal Be, the Be component becomes 12.0 Ih and accordingly the BeO reactivity worth becomes +6.9 Ih, considerably approaching the measured value.

(iv) The predicted value of the sodium reactivity worth is reversed in sign and greatly deviated. The calculated

value of the central perturbation cross section is +0.074 mb and the corresponding measured value is approximately -0.55 mb. As is clear from the calculated values of the components of the central perturbation cross section in Table 7.1.9, the discrepancy between the calculated values and the measured values was presumably due to the difference in the elastic slowing down term. The results of calculation are likely to change sentively depending particularly on how to treat the slowing down from the giant resonance region of sodium of 2.8 KeV. And we also probably cannot ignore the heterogeneity effect of cell. A further study will be needed for the improvement of this disagreement.

Table 7.1.8 Central Material Worths in ZPR-III Assy. 47. Comparison of Calculation with Experiment

Material	Material Weight gr	Material Worth, Ih/Kg Measured	Calculated	C/E
Pu	69, 138, 207	450∿470	533	1.2
Pu-U-Mo	80, 160, 240	52∿59	71.5	1.3
93% EU	72, 144, 216	328∿335	421	1.27
0.2% DU	2460 (b)	-21.5±0.1	-34.4	1.6
Enr. B_4C	32.4 (a)	-4300±125	-7730	1.8
SUS	1026.1 (b)	-10.8±0.2	-13.1	1.2
BeO	361.3 (b)	+4.4±0.6	+10.4	2.4
$A\ell_2O_3$	224.2 (c)	-15.2±0.9	-14.0	0.9
Fe_2O_3	341.0 (c)	-11.7±0.6	-10.9	0.93

Material	Material Weight gr	Material Worth, Ih/Kg Measured	Calculated	C/E
Be	240.7 (b)	+33.2±0.8	+42.9	1.3
C	196.4 (b)	-9.7±1.0	-4.03	0.4
Na	91.2 (c)	-8.4±3.0	+1.16	
Aℓ	350.5 (b)	-15.0±2.6	-19.4	1.3
Cr	439.2 (c)	-10.7±0.5	-12.2	1.15
Mn	597.3 (c)	-21.3±0.3	-62.5	2.9
Fe	1028.0(b)	-9.4±0.2	-12.1	1.3
Ni	1150.4(b)	-13.8±0.2	-18.1	1.3
Mo	1279.8(b)	-38.0±0.2	-79.4	2.1
Ta	1004.0(c)	-103.2±2.0	-208	2.0

Sample Size: a) 1/4 x 2 x 2 b) 2 x 2 x 2 c) T_{Wo} 1 x 2 x 2 inches

(Supplement) Compositions of Central Samples

Pu: 95.06 W/O ^{239}Pu, 4.55 W/O ^{240}Pu, 0.39 W/O ^{241}Pu

Pu-U-Mo: 17.86 W/O ^{239}Pu + ^{241}Pu, 1.64 W/O ^{240}Pu, 78.0 W/O depl U, 2.5 W/O Mo

Enriched U: 93.0 W/O ^{235}U

Enriched B_4C: 62.33 W/O ^{10}B, 7.01 W/O ^{11}B, 30.66 W/O C

SUS: 69.7 W/O Fe, 17.0 W/O Cr, 10.4 W/O Ni, 1.1 W/O Mn

Table 7.1.9 Central Perturbation Cross Section of Sodium in ZPR-III Assembly 47. (in millibarns)

Group	Energy Interval	Net	Absorption	Elastic Moderation	Inelastic Moderation
1	10.5 - 4.0 MeV	-1.79	-0.28	-0.18	-1.33
2	4.0 - 1.4	-4.58	-0.02	-1.79	-2.77
3	1.4 - 0.4	-2.64	-0.06	-1.82	-0.76
4	0.4 - 0.1	-2.46	-0.17	-2.29	0
5	100 - 21.5 KeV	-0.18	-0.16	-0.02	
6	21.5 - 10.0	+1.46	-0.06	+1.51	
7	10.0 - 4.65	+2.25	-0.10	+2.35	
8	4.65 - 2.15	+5.65	-0.76	+6.41	
9	2.15 - 1.0	+2.41	-0.27	+2.68	
10	1000 - 465 eV	+0.27	-0.09	+0.36	
11	465 - 215	+0.17	-0.04	+0.22	
12	215 - 100	+0.20	-0.02	+0.23	
13	100 - 0.215	-0.02	-0.02	0	
	Sum	+0.0740	-2.047	+7.651	-4.864

Note: 2 - dimensional 13-group diffusion perturbation calculation using NNS-5 set. Self-shielding factor was calculated for core dilution.

7.1.5 Sample Doppler reactivity

Two sample rods, 1.27 mm in diameter and 15.24 cm in length were positioned 12 cm apart from one another across the midplane at the center of Assembly 47 and measurements were made by the hot-to-cold method at four different temperatures, i.e. 300°K, 500°K, 800°K and 1100°K. There were four kinds of samples and they were 70% T.D oxide.

Table 7.1.10 Atomic Compositions of Doppler Samples (10^{22} atoms/cc)

	$^{239}PuO_2$	8:1 U-Pu Oxide	Natural UO_2	Enriched UO_2
Pu-239	1.47	0.153		
Pu-241	0.04	0.012		
U-235		0.010	0.01	1.54
U-238		1.327	1.56	0.04
O	3.02	3.012	3.14	3.16
Total Mass (g)	263.8	261.8	274.4	275.8

As for the natural UO_2 sample, measurements were made under three different circumstances, i.e. the normal core, Na-voided core and in boron sleeve. Since there are no sufficient data available about the circumstances, except for the normal core, they were omitted in the present analysises.

Calculations were made by use of the two-dimensional 13-group R-Z diffusion perturbation approximation and the regions of

R = 0-2.51 cm and Z = 5.09-20.37 cm were taken for the central sample position. The self-shielding factor of resonance of the sample was calculated for $\sigma_0 = 1.35\ S/4NV_0 = 0.532/N$ barns. The calculated and measured values are shown in Table 7.1.11 and Figs. 7.1.6 through 7.1.7. From the results, the following can be said.

(i) As for $^{235}UO_2$, $C/E \approx 2$. And from the results of analysis of similar experiments carried out on ZPR-III Assembly 4Z, it was found that $C/E \sim 2$ when NNS-5 set was used and $C/E \sim 4$ when ABBN set was used and $C/E \sim 4$ by the calculation made by C.E. Till. Such overestimation seems to be a rather general tendency.

(ii) The possibility of improvement of the disagreement between the calculated and measured values for PuO_2 is not foreseeable at the present time. The disagreement is not so important because the degree of dilution is so high in the actual reactor.

(iii) As for Nat. UO_2 and 8: 1U-Pu oxide samples, the calculated and measured values obtained at temperatures of 300 - 1100K were considerably well in agreement, i.e. C/E = 1.1. About the same value of the C/E ratio was obtained in the analysis of sample Doppler experiments on such other critical assemblies as ZPR-III-4Z, ZPR-3-48, ZPPR-2, FCA-III-1, FCA-III-2-S, FCA-V-1 and FCA-V-2, and this was a characteristic of NNS-5 set. However, there were some problems about the temperature dependence, i.e. there was

a tendency to overestimate the Doppler reactivity for small temperature differences. This tendency was also observed in the analysis of FCA-V-1 assembly.

Table 7.1.11 Central Sample Doppler Reactivity in ZPR-III Assembly 47

(Ih/Kg of Metal)

Temperature Change	Pu Sample		8:1 U/Pu Sample		Nat. UO_2 Sample		Enr. UO_2 Sample	
	Exp.	Calc.	Exp.	Calc.	Exp.	Calc.	Exp.	Calc.
300°K-500°K	-0.213 ±0.077	+0.328	-0.797 ±0.095	-1.02	-0.926	-1.111	+0.378 ±0.025	+0.770
				(1.28)		(1.20)		(2.04)
300°K-800°K	-0.546 ±0.084	+0.765	-1.645 ±0.052	-1.93	-1.903	-2.134	+0.833 ±0.056	+1.460
				(1.17)		(1.12)		(1.75)
300°K-1100°K	-0.044 ±0.077	+1.120	-2.264 ±0.061	-2.56	-2.567	-2.831	+1.901 ±0.043	+1.885
				(1.13)		(1.10)		
300°K-1800°K		+1.693		-3.49		-3.873		+2.469

The number in parentheses is C/E value.

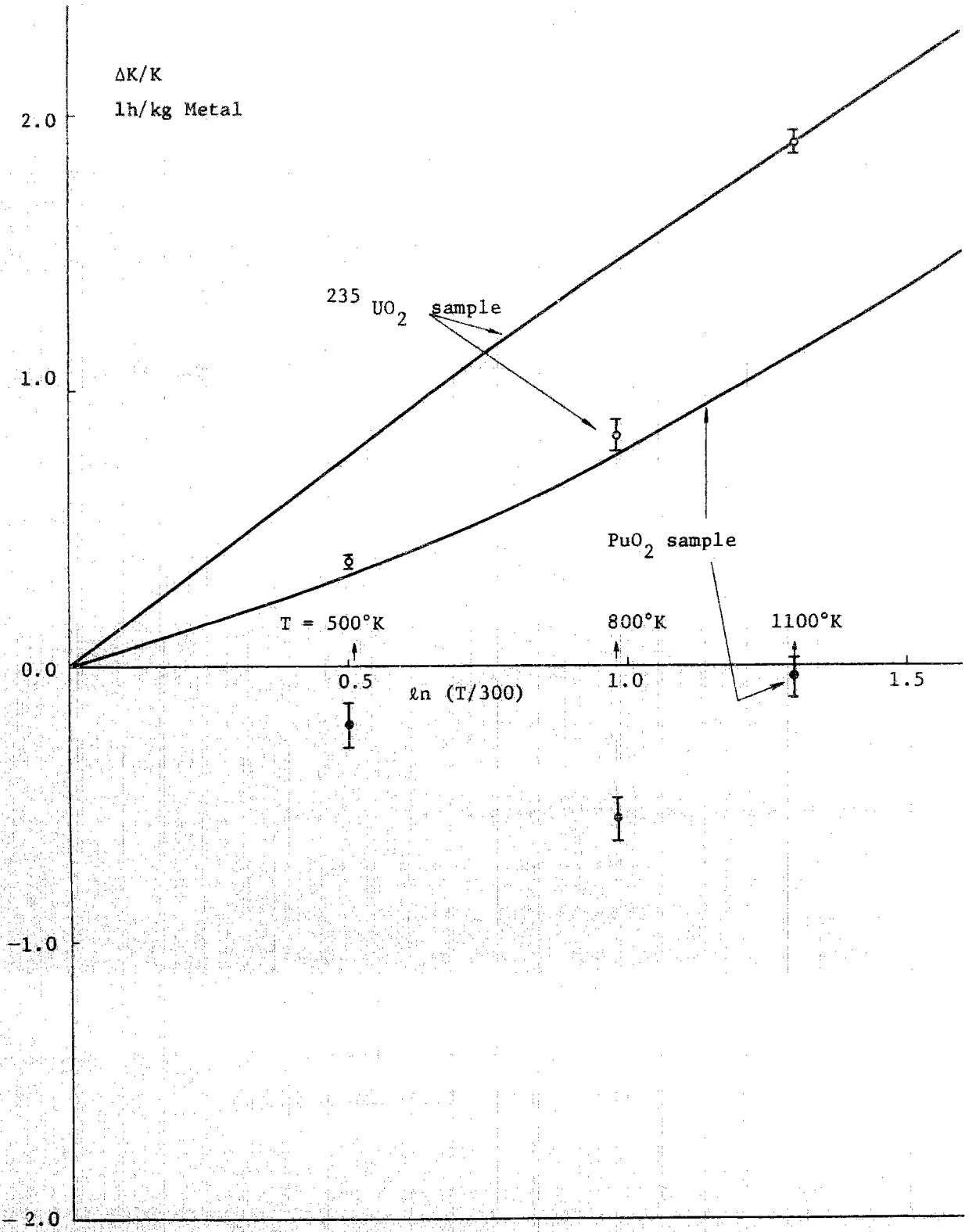

Fig. 7.1.6. $^{235}UO_2$ and PuO_2 Sample Doppler Reactivity at Core Center of ZPR-III Assembly 47, Ldg. 15

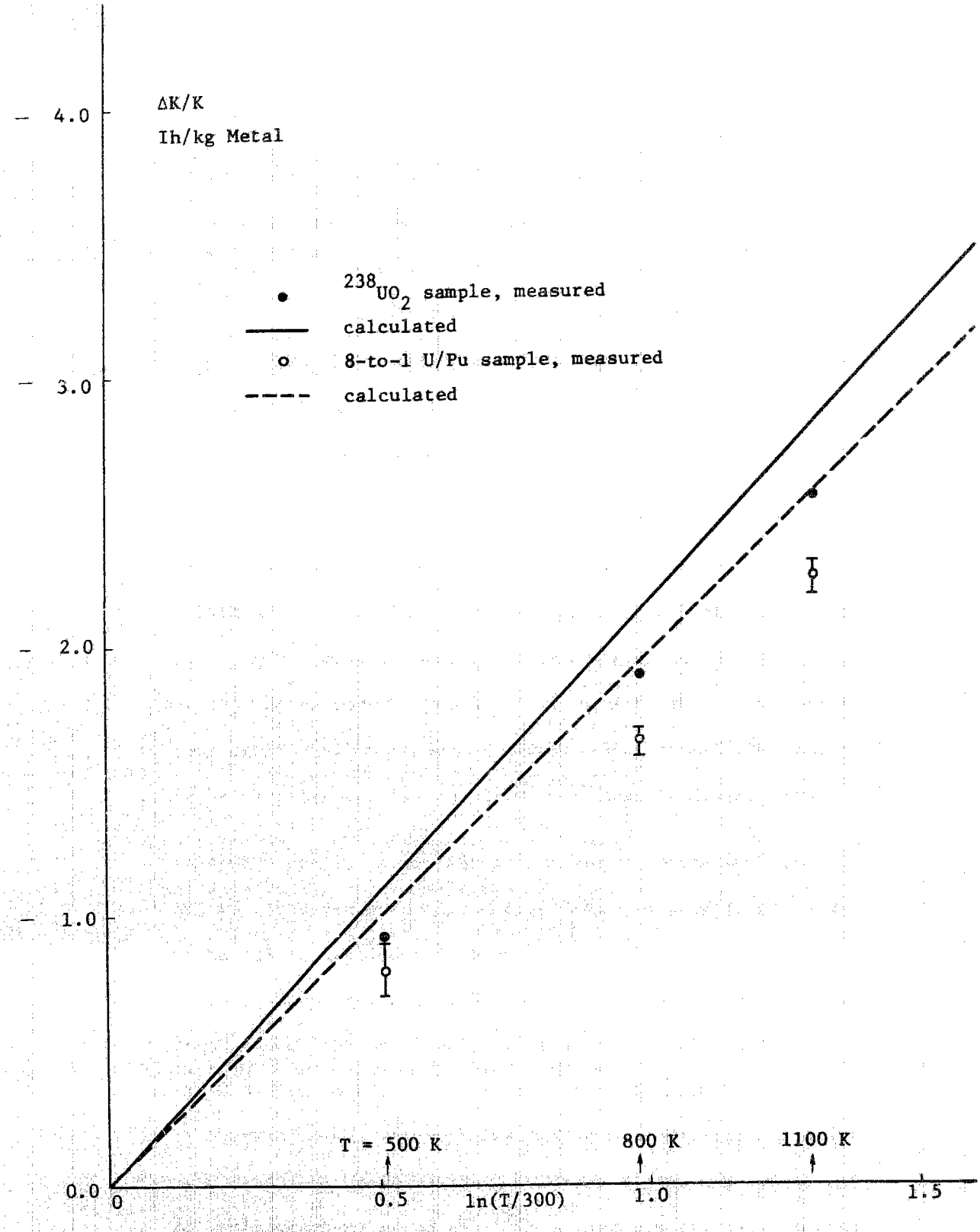

Fig. 7.1.7. $^{238}UO_2$ and 8-to-1 U/Pu Sample Doppler Reactivity at Core Center of ZPR-III Assembly 47, Ldg. 15.

7.2 Analysis of FCA-V

The central sample Doppler experiments were also carried out on FCA-V core which was constructed as a mockup assembly for "JOYO". The analysis of experiments on the general nuclear characteristics including the Doppler experiments on FCA-V is described in detail in "Evaluation of JOYO Nuclear Design Method (I), (III)[10]" (undertaken by Tokyo Shibaura Electric Co., Ltd. in 1971 and 1972). So, only the necessary points will be discussed here.

7.2.1 Calculational system and method

The sample Doppler experiments in FCA were carried out on V-1 and V-2 assemblies. The analysis was made on the standard spherical system and the two-dimensional system. Fig. 7.2.1 shows the two-dimensional calculational system which was used in the calculation. The atomic number densities of the assemblies are shown in Table 7.2.1.

Calculations were carried out at the center of the standard spherical core by use of 25-group diffusion perturbation first approximation. As for the value of the self-shielding factor of resonance, we used the value corresponding to the core composition. As for V-1 assembly, we calculated U-238 Doppler reactivity distribution on 2 axis at the center by R-Z 6-group diffusion perturbation method and obtained the correction factor for the sample length. In relation on the effective excess potential scattering σ_0^{28} = 75 barns (corresponding to

UO_2 rod of 1 cmϕ, $N^{28} = 0.02 \times 10^{24}$), the Doppler reactivity distribution was well represented in the form of ΔK (300° ∿ 1100°K) = const. x $\cos^2$ (0.036Z), Z in cm. From this result, it was found that the correction factor by which the central Doppler reactivity worth was to be multiplied was 0.976 in the case of a sample of 15 cm in length.

The same calculational method and the correction factor were applicable to V-2 assembly, too. As for the self-shielding factor of resonance, we took not only the value corresponding to core composition but also the value for $\sigma_P^* = \sigma_{PU} + 2\sigma_{P_0} + 1.35\ S/4NV_0$. The measured and calculated values are shown in Table 7.2.2.

7.3 Determination of C/E

As seen from Table 7.2.2, the C/E value considerably fluctuated according to the experiments but we determined the C/E as follows by taking the average of nat.UO_2 sample Doppler reactivities (300°K - 1100°K) of V-1 and V-2.

$$C/E = 1.07 \pm 0.2 \text{ (NNS-5)}$$
$$= 0.66 \pm 0.05 \text{ (ABBN)}$$

ABBN showd a better temperature dependence.

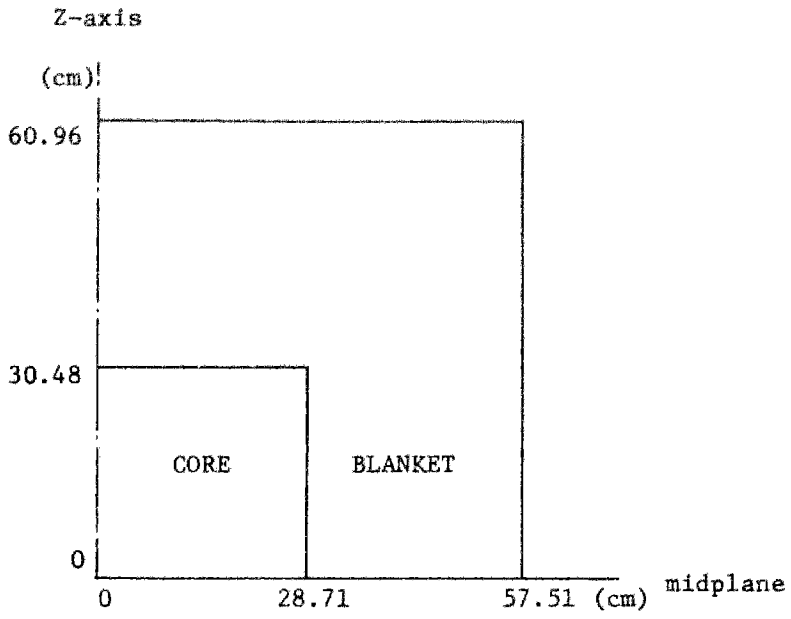

Assembly V-1

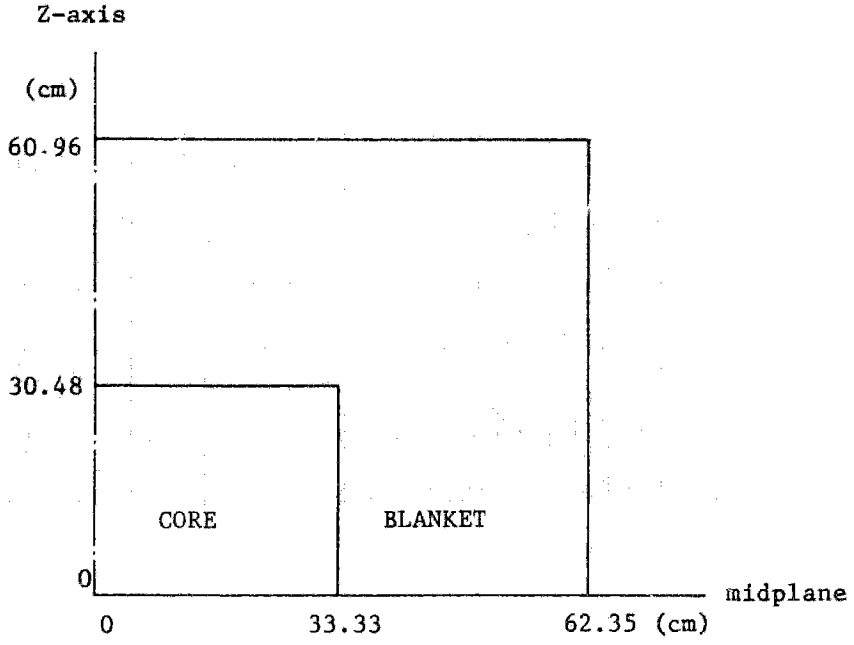

Assembly V-2

Fig. 7.2.1 Standard geometries for two dimensional RZ calculation of FCA assemblies V-1 and 2.

Table 7.2.1 Atomic Number Densities of FCA Assemblies V-1 and V-2

(10^{22} atoms/cc)

	Assembly V-1		Assembly V-2	
	Core	Blanket	Core	Blanket
Pu-239	0.10446		0.10458	
Pu-240	0.009427		0.009325	
Pu-241	0.001124		0.001069	
U-235	0.1960	0.02891	0.1470	0.02891
U-238	0.77812	3.9890	0.58359	3.9890
O	1.64758		1.3101	
Na	0.60431		0.81341	
Aℓ	1.10650		0.88295	
Cr	0.30535	0.1827	0.32734	0.1827
Fe	1.09705	0.6652	1.1950	0.6652
Ni	0.14275	0.07964	0.15345	0.07964

Table 7.2.2 Comparison of Theoretical and Experimental Doppler Reactivity Vorths

Assembly V-1 (in 10^{-5} $\Delta k/k/UO_2$ mol)				Assembly V-2 (in 10^{-6} $\Delta k/k$)			
		Calculation				Calculation	
	Measurement	NNS-5	ABBN		Measurement	NNS-5	ABBN
Nat UO_2				Nat UO_2			
Cold worth	-3.68±0.02	-4.25 (1.15)	-4.27 (1.16)	Cold worth	-103±1	-88.8(0.86) (0.92)*	-92.0(0.89) (0.99)*
300°∿600°K	-0.179±0.004	-0.250(1.40)	-0.146(0.82)	300°∿500°K			
300°∿850°K	-0.273±0.004	-0.352(1.29)	-0.218(0.80)	300°∿800°K			
300°∿1100°K	-0.353±0.004	-0.418(1.18)	-0.271(0.77)	300°∿1100°K	-10.65±0.13	-9.89(0.93) (0.95)*	-6.79(0.64) (0.68)*
				90% EUO_2			
				Cold worth	+1867±5	+2382(1.28) (1.27)*	+2274(1.22) (1.22)*
				300°∿500°K			
				300°∿800°K			
				300°∿1100°K	+0.9±0.3	+1.35(1.50)*	+2.53(2.81)*

Note: C/E values are presented in parentheses

* Results of 6G RZ perturbation. Others are results of 25G spherical calculation with central perturbation corrected by factor of sample length effect.

7.4 Analysis of ZPPR-2

The axial distribution of Doppler sample reactivity was measured in ZPPR-2 and the results were analyzed by use of RZ diffusion perturbation approximation. The sample was Nat.UO_2, 12 inches in length. The results of the analysis are shown in the table below.

Table Doppler Worth Ih/Kg U^{238}

Temp. Interval	Z = 0 cm		Z = 30.5 cm		Z = 61.0 cm	
	Exp.	C/E	Exp.	C/E	Exp.	C/E
Cold worth	-6.61	1.26	-2.68	1.64	-0.43	0.76
300∿500	-0.224	1.11	-0.140	1.10	-0.032	0.67
300∿800	-0.462	1.08	-0.312	0.96	-0.039	1.08
300∿1100	-0.622	1.02	-0.423	0.94	-0.060	0.96

Note: 1% $\Delta k/k$ = 973.8 Ih (Keepin)

VIII. Estimation of Doppler Reactivity Effect of "JOYO"

8.1 Assumption of Paralellism

In the case of Nat.UO_2 and 8 : 1 U-Pu oxide samples in ZPR-3-47, C/E at 300°K - 1100°K was approximately 1.1. However, in view of the C/E values at other temperatures, the C/E of the sample Doppler reactivity coefficient in this assembly is presumed to be somewhat higher than 1.1. Taking into consideration that NNS-5 tends to overestimate Doppler reactivity at lower temperatures, we averaged the C/E values excepting those at 300°K - 500°K and obtained the following value.

$$C/E = 1.13 \pm 0.04 \text{ (NNS-5)}.$$

In the case of SEFOR, the C/E value was roughly as follows.

$$C/E = 0.92 \pm 0.20 \text{ (Power = 0)}$$

$$= 1.15 \begin{matrix} + 0.10 \\ - 0.20 \end{matrix} \text{ (Power > 0)} \qquad \text{(NNS-5)}$$

When power = 0, the contribution of the reactivity effect due to thermal expansion was particularly large and uncertainty was so much larger. When power is > 0, it would be natural to assume that uncertainty on the negative side becomes slightly larger if the uncertainty of the reactivity scale is taken into consideration. If uncertainties are taken into consideration as above, there seems to be not much significant differences in C/E value between when power = 0 and when power > 0. And consequently we think that the following value may be used in general.

$$C/E = 1.15 \begin{matrix} +0.10 \\ -0.20 \end{matrix}$$

Since C/E is 1.13 ± 0.04 in ZPR-3-47 which is SEFOR mockup core, it may be safely assumed that there is a considerably stable consistency between the above value and the C/E value of SEFOR. If it is allowed to assume the pralellism between the relationship between ZPR-3-47 and SEFOR and that between FCA-V and JOYO, the value in JOYO is supposed to be estimated with a considerably high degree of accuracy from C/E in FCA-V by use of the following equation.

$$E_{JOYO} = C_{JOYO} \frac{E_{FCA}}{C_{FCA}}.$$

Although it is difficult to strictly prove the validity of the assumption of paralellism, as the first step in exterpolating an unmeasured system the above assumption may be used without causing any serious error. The design values of JOYO, which were obtained on the basis of such way of thinking, will be shown in the following section.

8.2 Design Values of "JOYO"

According to the "JOYO" Nuclear Design (II) Nuclear Design Calculations (JOYO-371), the conclusions about the Doppler reactivity of the initial core of "JOYO" are as follows.

(1) The design values are given in Table 8.2.1. These design values were obtained by correcting the calculated values by use of the C/E ratio of 1.07 ± 0.25 which was obtained from the measurement and analysis of the central nat UO_2 Doppler sample reactivity in "JOYO" mockup core FCA V-1 and V-2 assemblies. The uncertainty of C/E ratio in the

blanket was estimated at ±35%. From the same measurements, the temperature dependence of the Doppler reactivity was assumed to be T dK/dT = constant.

(2) 90% of the Doppler reactivity was due to that of U-238.

(3) Fig. 8.2.1 shows the radial temperature distributions for JOYO core at 100MWT and the Doppler reactivity coefficient (per one channel). The core Doppler reactivity weighted by the temperature distributions was 0.185% ΔK/K from the standard temperature 370°C and it was 0.179 ΔK/K when the core average temperature of 1242°C was used. So, the use of the core average temperature brings about a better approximation. As for the temperature distributions in the fuel pin, it is sufficient to use the average temperature in the pin.

Table 8.2.1 Design Value of Isothermal Doppler Reactivity of JOYO

$(-T\frac{dk}{dT}$ in $10^{-3}\ \frac{\Delta k}{k})$

	As-Calculated direct perturbation		Calculation (corrected)[a]	Uncertainty
All control and safety rods withdrawn:				
Core	2.07	2.09	1.93	±25%
Radial blanket	1.78	2.04	1.66	±35%
Axial blanket	0.69	0.73	0.64	±35%
All control rods inserted:				
Core	1.30		1.21	±25%
Radial blanket	1.75		1.64	±35%
Axial blanket	0.56		0.52	±35%

a) Corrected by using Exp't/Calc = 0.93 from central Doppler sample reactivities measured in FCA Assemblies V-1 and V-2 for temperature range 300°K-1100°K.

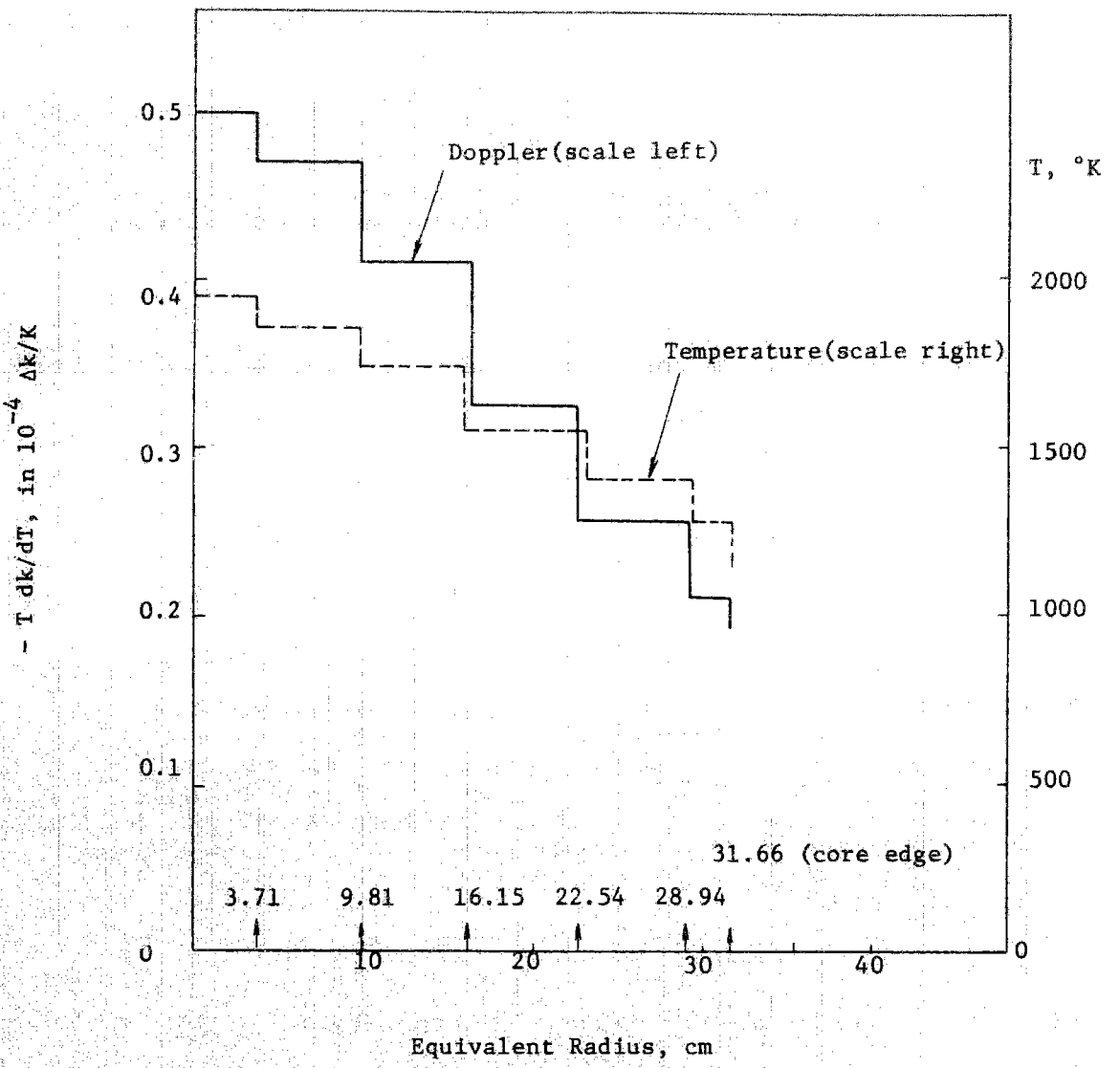

Fig. 8.2.1 Radial Distributions of Temperature and Doppler Reactivity Coefficient per Channel for JOYO Core at 100 MWT.

IX. Conclusion

In this study, we devoted our efforts mainly to the analysis of the first core of SEFOR while also making analysis of its mockup core, ZPR-3-47. When the Doppler reactivity coefficient alone is considered, C/E showed a high degree of stability in the analysis of the reactivity worth of the central Doppler sample in ZPR-3-47 and also in the analysis of the Doppler reactivity of the entire core of SEFOR, thus making it clear that C/E has a value of about $1.14^{+0.10}_{-0.20}$ in both cases if NNS-5 is used for the nuclear constants set. Assuming that this was also applicable to other fast reactors, the Doppler reactivity coefficient of JOYO was estimated from FCA-V in the simplest form. However, the validity of the above assumption has not yet been proved. This is problem left to be solved in the future. We consider it is useful as aid in solving this problem to carry out the analysis of the second core of SEFOR (its spectrum is harder than that of the first core) to find the general range of the C/E values.

As stated above, we made the analysis of the first core of SEFOR and determined the C/E value. The fact that thus obtained value is roughly in agreement with the C/E value of SEFOR mockup core is considered to be one of evidence to prove the validity of the design values of JOYO.

The fact that the C/E value of the Doppler sample reactivity distribution of ZPPR-2 had such a considerably stable value as C/E

0.97 ± 0.05 also may be used as an effective evidence in estimating the Doppler reactivity coefficient of a larger reactor from the experimental and analytical values of Doppler reactivity in the critical assembly.

X. Acknowledgement

We are grateful to Mr. Kinjo and Mr. Higashihara of the Power Reactor and Nuclear Fuel Development Corporation for collecting a great deal of information including the measurement data and various data required for our analytical studies and for their kind discussions with us with regard to the actual operations.

XI. References

(1) Compilation of Fast Critical Experiments Vol. 1 ∿ 6. Tokyo Shibaura-Electric Co., Ltd. J201 72-33-1 ∿ 3, J201 73-07-1 ∿ 2 (1972 ∿ 1973)

(2) P. F. Palmedo, Compilation of Fast Reactor Experiments Vol. 1, 2. BNL15746 (1971)

(3) Y. Matsuno et al., Compilation of Fast Critical Experiments (SEFOR) J201 72-15 (1972)

(4) L. D. Noble et al., Results of SEFOR Zero Power Experiments GEAP-13588 (1970)

(5) Y. Fukai, Private Communication (unpublished)

(6) K. D. Lathrop, LA-3373 DTF-IV

(7) Keepin, G. R., Physics of Nuclear Kinetics, Addisson-Wesley (1964)

(8) R. W. Smith, Proceedings of the 15th EACRP Meeting (1972)

(9) M. S. Krick, A. E. Evans, NSE 47, 311-318 (1972)

(10) Iijima and others, "Joyo" Evaluation of Nuclear Design Method (III) Toshiba (1972)